京都大学学術情報リポジトリ
KURENAI 紅
Kyoto University Research Information Repository

京都大学
KYOTO UNIVERSITY

Title	Anatomical and mechanical features of palm fibrovascular bundles(Dissertation_全文)
Author(s)	Zhai, Shengcheng
Citation	Kyoto University (京都大学)
Issue Date	2013-09-24
URL	http://dx.doi.org/10.14989/doctor.k17904
Right	許諾条件により要旨・本文は2014-09-24に公開
Type	Thesis or Dissertation
Textversion	ETD

Kyoto University

Anatomical and mechanical features of palm fibrovascular bundles

ZHAI SHENGCHENG

2013

CONTENTS

Chapter 1

General introduction

1.1 Palmae

PALMAE – The palm family has about 184 genera and 2400 species (Dransfield *et al*. 2008; Pei *et al*. 1991), and most species of this family grow in tropical and subtropical area, especially in tropical Asian and America. Some species also distribute in Africa. In China, there are 28 genus and more than 100 species, including common cultivated species. Palm trees are high-value and increasing common components of landscapes wherever they can be grown. Large, older specimens are in great demand and command a premium price. They are usually dug and removed from existing landscape sites or from a commercial nursery field, transported, and replanted at another site, creating an instant mature landscape.

In the monocotyledons, which are usually herbaceous and without secondary thickening, the stem structure normally differs from that of dicotyledons. A few monocotyledons are trees, like PALMAE (palms) some of which may rise to 45m. In palms, secondary thickening may occur though in some of them no secondary tissue is formed, increase in the diameter of the trunk being brought about by cell enlargement. In others, although there is no cambial region, cell division and cell enlargement occur in the ground tissue, while the fibers forming sheaths around the vascular bundles also increase in the size (Tomlinson 1990). Thickening of the trunk may also be due, in part, to increase in the size of existing intercellular spaces and the formation of new spaces. The ground tissue may become very hard. These unusual ways of increasing the size of the trunk are remarkable, and of all dendroid plants having non-typical structure, the palms are the most used as timber. They serve for constructional work, as whole trunks in house-building and piling, although the denser, outer part of the trunk may be cleft

into pieces suitable for flooring and beams. The vascular strands are often a different colour from the ground tissue and on a longitudinal surface have the appearance of quills, hence the name, porcupine wood, by which palm wood is sometimes known. It is because of this appearance and also because the wood takes a good finish, that it is also used at times for walking-sticks and umbrella handles, and for marquetry work.

1.1.1 *Trachycarpus fortunei* – Important palm in Asia

Trachycarpus fortunei is classified as subfamily of CORYPHOIDEAE Griff., tribe of CORYPHEAE Mart., sub tribe of THRINACINAE Becc., and its genus is *Trachycarpus* H. Wendl. (Pei *et al*. 1991).

棕-*Zong* is repeatedly mentioned in the 山海經[1]-*Shan hai jing*. 郭璞-*Guo pu* described it as a tree growing to a height of 30 feet; it is branchless. The leaves are at the end of a common stalk and form a circle [*the author means to describe a fan-shaped palm-leaf*]. The bark of the trunk forms joints and is useful for making ropes [*the author speaks of the sheaths of the bases of the leaves, which cover the trunk*]. It is also called 栟櫚-*Bing lv*.

The 說文[2]-*Shuo wen* likewise identified the 棕-*Zong* with the 栟櫚-*Bing lv*. The tree here spoken of is a palm, the *Trachycarpus fortunei* (windmill Palm), which is very common in Middle and Southern China. The coir furnished by it is largely manufactured into cloaks and hats.

T. fortunei is closely allied to the Japanese *T. excelsa*. Perhaps it is the same (Bretschneider 1882). *T. excelsa* (大崖棕) is originally growing in Italy and France according to Zhong (2004). *T. fortunei* is domestic species in China and it mainly

[1] 山海經 *Shan hai jing* – a Chinese classic text that is at least 2,200 years old. It is largely a fabled geographical and cultural account of pre-Qin China as well as a collection of mythology. The book is about 31,000 words long, and is divided into eighteen sections. It describes over 550 mountains and 300 channels. (From *WIKIPEDIA – Shan hai jing*)

[2] 說文 *Shuo wen* (*Shuo wen jie zi*)– an early 2nd century CE Chinese dictionary from the Han Dynasty. It was the first to analyze the structure of the characters and to give the rationale behind them (sometimes also the etymology of the words represented by them), as well as the first to use the principle of organization by sections with shared components, called radicals (*bùshǒu* 部首, lit. "section headers"). (From *WIKIPEDIA – Shuo wen jie zi*)

distributes at south of China, which is humid temperate climate. This species also distributes in Japan. According to Satake *et al*. (1989), there is only *T. fortunei* growing in Japan and they do not mention *T. excelsa*. So the species widely distributing in China and Japan is same and it is *T. fortunei*, which is also called as windmill palm.

This windmill palm is very tolerant to wind and salt. It spread from Fujian Province in east of China, to west China like Sichuan and Yunnan Province, and its distribution almost arrive north of Guangxi and Guangdong Province. The north line of windmill Palm is Shanxi, Gansu Province. It flourishes in Sichuan, Yunnan, Guizhou, Hunan, and Hubei Province (Zheng 2004) (Fig. 1.1).

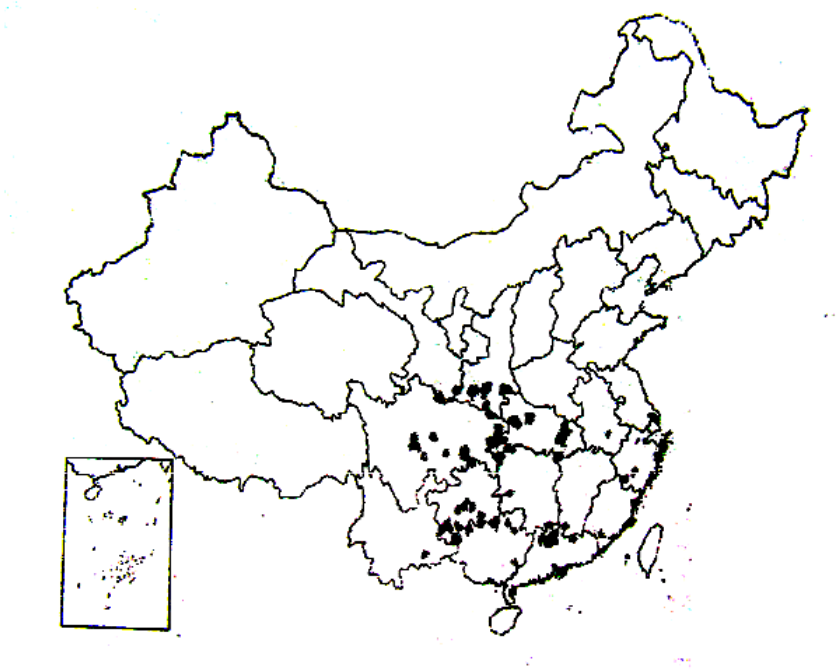

Figure 1.1 The distribution of *Trachycarpus fortunei* in China. *T. fortunei* is a widely distributing species of PALMEA in China. It can spread from Yunnan province to Shaanxi province.

The Chinese Pharmacopeia (中藥大圖典 – *Zhong Yao Da Tu Dian* 1977) lists a number of medicinal uses for various parts of the windmill palm, but under the name *T. wagnerianus*. Other references, however, correctly identify the widely cultivated and utilized species as *T. fortunei*. It appears that virtually every part of this palm has been used for one purpose or another by the Chinese and other peoples of the Orient (Essig & Dong1987).

Palms are economically important because they include major plantation crops, like oil-palm, coconut, and date-palm, but also numerous species which have minor economic importance are sources of cane, oil, wax, starch, fiber, sugar, and alcohol, and are of tremendous importance, without entering into anything, but local commerce, as sources of food, building, and weaving material, thatch, fiber, wax, oil, sugar, salt, alcoholic beverages, masticatories, and stimulants. They are symbolic of several cultures and have religious significance in many communities.

They have considerable aesthetic value, are used in magic and folk-medicine, and are an essential ecological associate of many primitive tribes. They have become increasingly important in commercial horticulture because of their elegant and predictable shapes. There is an extensive semi-popular literature dealing with them and a society devoted to their cultivation and study.

Fiber from *T. fortunei* has been of major importance in China and is mentioned in a number of historical accounts. Wilson (1913) mentioned that leaf-base fiber of *T. fortunei* was baled and exported down the Yangtze River from Sichuan Province "in quantity." He and others imply that the quality and for making ropes, mats, mattresses, and brushes. Figure 1.2 and 1.3 shows the products made by fibers from *T. fortunei*. It seems people succeed the traditional technique to use these fiber materials.

Figure 1.2 Display of a traditional raincoat 蓑衣-*Suoyi*, made of palm leave sheath fibers. (Photo by author at the Jiangxinzhou Folk Museum, Nanjing)

Figure 1.3 Palm-mattress for traditional style bed in in a palm-mattress shop, Yanzhou city, China.

In Taiwan, as well as in the mainland, rough raincoats were made of it. These were used in Taiwan as recently as 30 years ago and still are in some remote areas of mainland China. Grisard & Vanden-Berghe (1889) and Beccari (1905) reported similar uses. Segments of the fibrous leaf blade have been used to plait fans, hats, chairs, and sofas and to thatch roofs (Essig & Dong 1987).

From Takashima Island – 鷹島 excavated site in Japan, researchers found palm rope of *T. fortunei* in sunken ship of the Yuan dynasty (end of 13 century), which keep its original shape after hundreds of years in ocean. When excavated the archaeological site of Zhenghe treasure shipping (鄭和寶船 – *Zhenghe Baochuan*) in China, researchers found big palm rope of *T. fortunei* from the Ming dynasty. By checking ancient text, like 本草綱目[3] – *Bencao gangmu*, it showed that ancient people thought the palm fiber was a quite good material for making rope and it can be used for hundreds of years without decay. The question is why palm fiber can stay for so long period?

[3] 本草綱目(*Bencao gangmu*) – a dictionary of Chinese herbs, written by Li Shi Zhen (1518 - 1593). It consists of 52 volumes, with more than 1.9 million characters and more than one thousand and one hundred pictures. The book lists 1,892 medical material of herbs, animals and mineral with 11,096 formulae being used in the past. The book has been translated into more than 60 languages. (Sited from: http://alternativehealing.org , which is translated and explained by Joe Hing kwok Chu).

1.1.2 Fibrovascular bundles in leaf sheath

Palm leaf consists of three distinct parts, the rachis bearing the leaflets, a long or short petiole, and the basal leaf-sheath. The leaf at its insertion always completely encircles the stem, but above this the sheath may be either open or closed. When open it is gradually confluent with the petiole and in large fan-palms, e.g. *Corypha* and *Sabal*, and members of the Borassoid group, it often splits in a median vertical plane apparently owing to expansion of the stem. The leaf may be abscissed cleanly to leave a smooth leaf-scar and trunk, as in those Arecoid palm with distinct crown-shafts. According to Tomlinson (1961) there is an incipient abscission zone in some palms. Otherwise the leaf is not abscissed but wither gradually to leave an irregular stump, the surface of the stem then being rough as in *Copernicia*, *Elaeis*, and *Phoenix*. Where the leaf is not abscissed the persistent leaf-base may remain woody as in the Borassoid palms, but often its soft ground tissues decay to leave a reticulate mass of fibrous and vascular bundles as in *Raphia*, and especially in Trachycarpus. Rarely the leaf-base shreds to leave sharp spines as in *Zombia*. In scandent genera the tubular sheaths are very long, persistent, and tightly enclose the stem.

The leaf sheath of many palms shreds into its constituent fibrovascular bundles when old (Tomlinson 1961), or these ‘fibers’ may be isolated artificially. These ‘fibers’ are very coarse but are widely used for ropes, cables, coarse cloth, and matting, and particularly for sweeping brushes. The commonest sources for these fibers are species of the genera *Arenga*, *Caryota*, *Raphia*, *Trachycarpus*, etc. Figure 1.4 shows palms from these genera, which produce abundant of fibrovascular bundles from leaf sheath. Those of Arenga in Java and Sumatra were once the commonest roofing material. Less commonly the fibers from the upper part of the petiole and rachis are extracted, but they are weaker, although less coarse, than the basal fibers.

Figure 1.4 Palm species with abundant source of fibers from leaf sheath.

1.2 Vascular development of palms

Tomlinson (1990) set up a vascular template, which represents a quantitative plot a major bundle to each of the developing leaf primordial in the crown of *Rhapis*, shown in Figure 1.5. The diagram is an abstraction in that the leaves are represented in a single plane, rather than the 2/5 phyllotactic spiral of the actual crown. Furthermore, the bundles themselves are represented in a single plane, rather than the shallow helix they describe within the developing crown. The helical configuration is represented by the transverse projection of representative bundles in Figure 1.6.

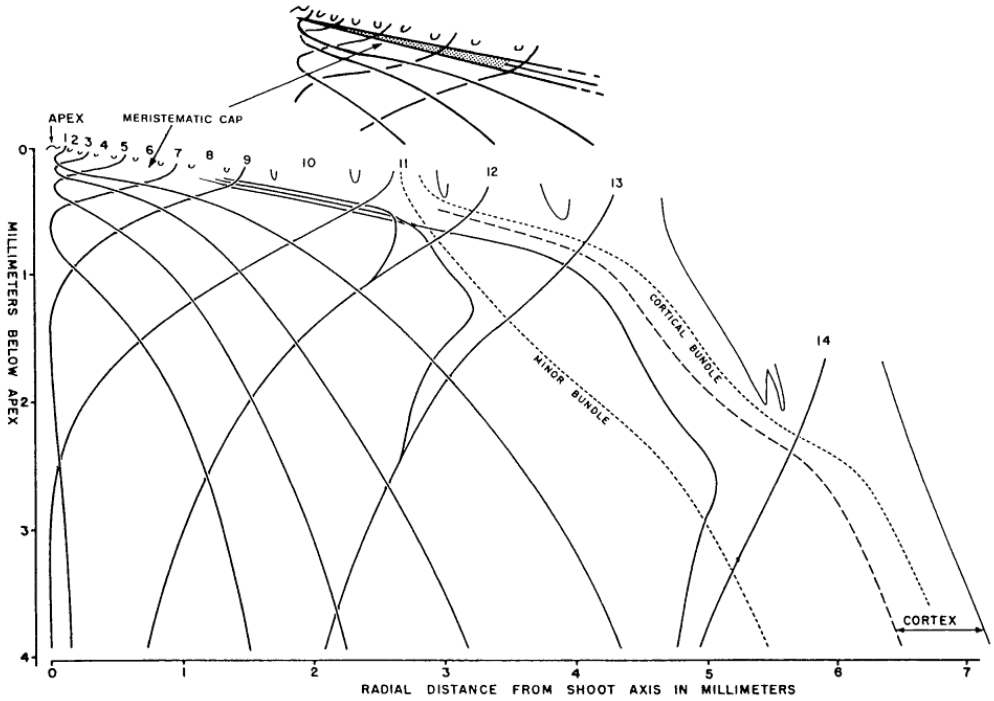

Figure 1.5 *Rhapis excelsa*. Diagrammatic radial longitudinal section of bundle distribution in the crown of the aerial vegetative axis. All dorsal sides of leaf insertions are rotated into a single radial plane so that major leaf traces can be compared. The helical path of the bundles is also not represented. Major traces are shown to leaves P1, P3, …. and P14. Solid lines represent plots of major bundles; dotted lines are plots of a minor bundle (in central cylinder) and a cortical bundle (in cortex). The dashed line represents the topographic boundary between cortex and central cylinder. Inset shows the approximate limits of the meristematic cap (Tomlinson 1990).

Figure 1.5 itself contains all the information necessary to understand the developmental process for the vascular system of a palm. It represents only very few bundles, but since constant principles determine bundle differentiation the bundle connection at each successive leaf position can represent development, if extrapolated as a dynamic process. The fundamental structural principle of branching of the axial system that gives rise to a leaf trace and a continuing axial bundle (a descriptive convention) can now be translated into a developmental statement if the vascular configuration of bundles supplying successively older leaves is interpreted dynamically.

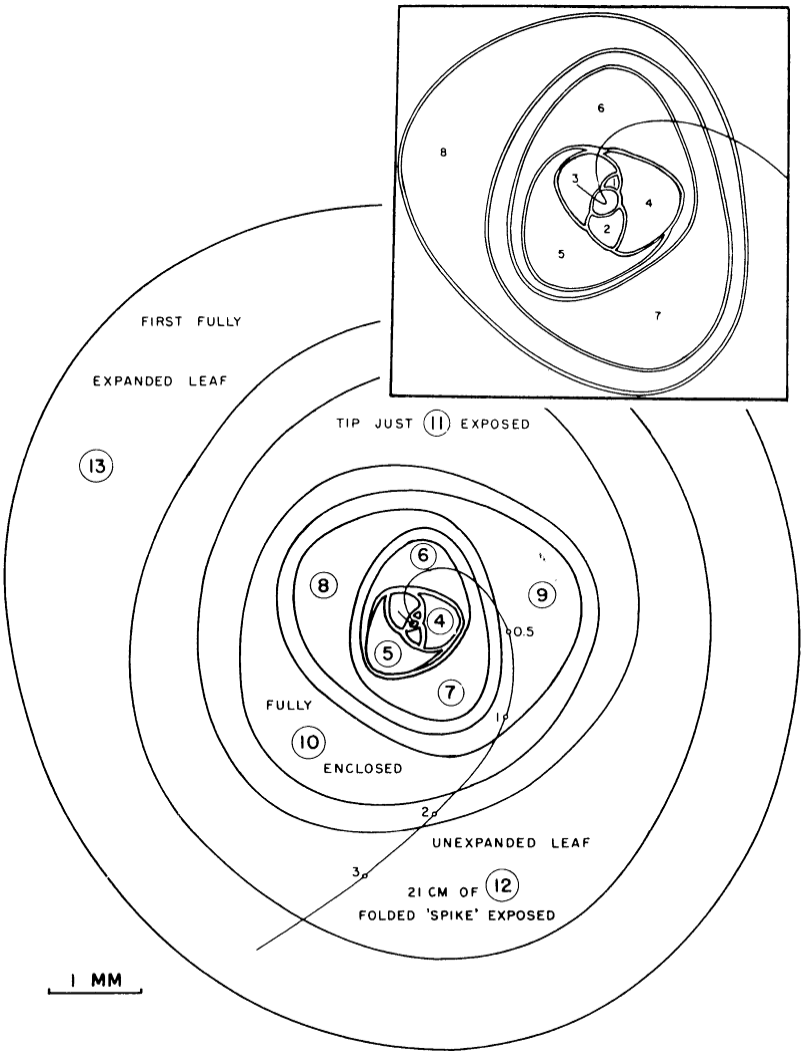

Figure 1.6 *Rhapis excelsa*. Path of a single vascular bundle projected onto a transverse plane, i.e. a section through the crown of the vegetative aerial axis. The bundle shown is a major trace to leaf P3 (inset detail). Numbers along the spiral are distances below the apex in millimetres. Leaves 2-5 are cut above their encircling attachment (Tomlinson 1990).

The system has been presented thus far in a simplified version in which principles of development are illustrated by single bundles. This is appropriate because the whole vascular system can thus be seen as the continuous repetition of a basic process, expressed by each vascular bundle. The plots of bundle increase in successive leaves approximately a sigmoid curve, so that the number of bundles rises from one in the youngest primordium, to over 1000 in the mature leaf, over about 15 plastochrones. The

majority of these bundles are cortical bundles since they differentiate outside the meristematic cap. About 100 bundles link within the central cylinder. Total bundle number and stem diameter are clearly correlated with each other, and these in turn to leaf number, leaf size, and bundle number per leaf.

Then, after accepting all the conventions used in the representation of the bundle course in the crown, Tomlinson (1990) thought the growth model of palm tree may be depicted in the totally schematic diagram of Figure 1.7. Three growth centres are needed to provide the growth model: the leaf primordium (X), the meristematic cap (Y), and an existing leaf trace (Z). Vascular differentiation can be envisaged as the development of 'lines of force' like a magnetic field. In the axial (central) vascular system, linkage occurs initially between the leaf trace (Z), in the region of its departure into the leaf base, and the meristematic cap (Y). This provides the uncommitted axial bundle whose linkage is only completed via the leaf base (X) at a later stage. Thus, in Figure 1.7 the linkage step Z-Y occurs in the trace at position leaf n, the later linkage Y-Z when the leaf is in position leaf n+*k*. The value of *k* varies according to the age of the leaf at the time of full connection.

Why this procedure is made seemingly so complex when a continuous acropetal differentiation of bundles would seem to be a simpler mechanism? The cortical bundles supply the answer; they differentiate basipetally under the influence of pole A, but since they are too remote from pole Z. Because at this stage tissues are reaching maturation, the A-B connection is a weak one. The apparent basipetal (basally directed) differentiation in palms, as in most monocotyledons, must relate to the intercalary meristem and basipetal and maturation of the leaf. The right-hand diagram in Figure 1.7 shows the sequence of events for bundles those are associated with seven successive leaves, using the plotting conventions of Figure 1.5.

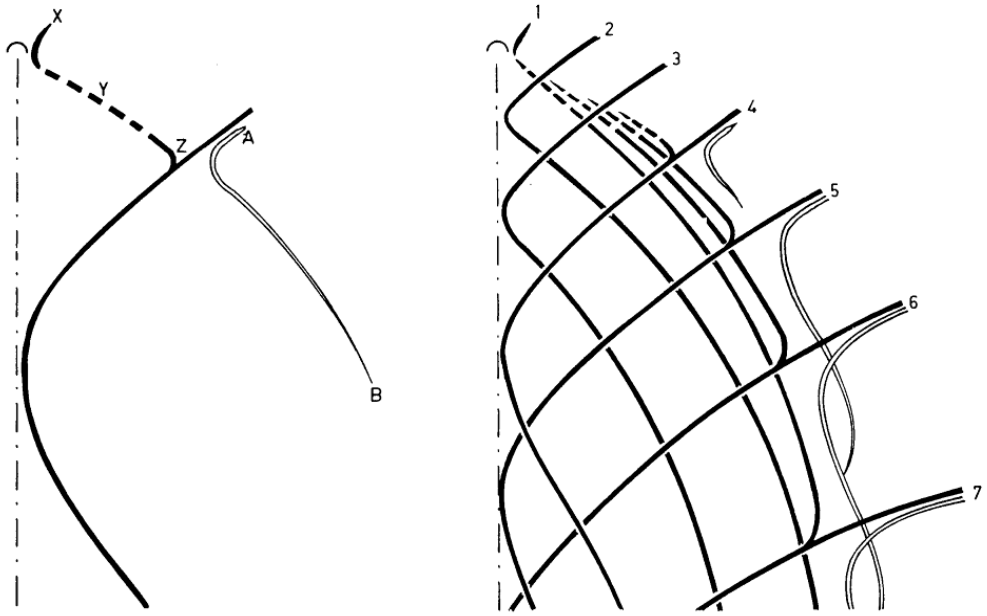

Figure 1.7 The principle of vascular development in monocotyledonous stems (after Zimmermann and Tomlinson, 1971). Solid lines represent bundles of the inner system (central cylinder), open lines represent bundles of the outer system (cortex) (from Zimmermann and Tomlinson, 1971). An axial bundle is generated at Z as a branch from an outgoing leaf trace and continues to grow distally in continuity with the meristematic cap Y (dashed line). Axial bundles generated in this way them maintain the cap. The initially distally uncommitted axial bundle eventually makes contact with a leaf primordium at X to complete the cycle of development. The region X, Y, and Z may be thought of morphogenetic poles between which vascular contacts are made in the order Z – Y, Y – X. A and B represent poles in the leaf base (A) and the cortical region (B) that also serve as morphogenetic poles in linking A and B. A is topographically located below the meristematic cap and cannot make a distal (A – Y) linkage (Tomlinson 1990).

1.3 Cell wall structure of woody cell

As the growing cell approaches its full size the deposition of the much stiffer secondary wall takes place (Fig. 1.8). This wall may be thin or extremely thick, and it is deposited on the primary wall in layers. Three main layers are usually recognized, a thin outer wall, which is the oldest, and of course, comes next to the primary wall; a thicker middle layer and a thin inner layer which forms the wall surface bounding the cell cavity or, in the living cell, the protoplasm. These several layers are now conveniently designated P, the primary wall, and S_1, S_2, and S_3, respectively the outer, middle and

inner layers of the secondary wall. Sometimes yet another layer is deposited, not regularly over the cell, but in the form of thin, spiral bands, which give the spiral thickening found in some cells. Such spiral thickening and sometimes, indeed, the whole of S_3, has been termed the tertiary wall, but there is no justification for this usage and the term should be avoided. There is every reason for regarding the S_3 as the innermost and youngest layer of the secondary wall.

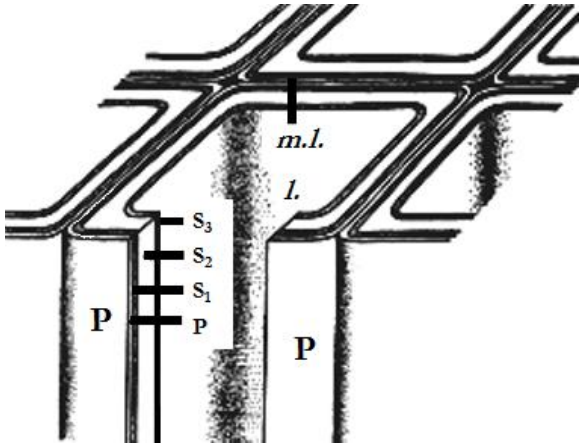

Figure 1.8 Diagram of the layers of the cell wall of a woody cell. The middle lamella is shown in black, followed by the primary wall, the outer layer (S_1) of the secondary wall, the middle layer (S_2) of the secondary wall and the inner layer (S_3) of the secondary wall, which surrounds the lumen of the cell. *m.l.*, middle lamella; *P.*, primary wall; S_1, S_2, S_3, successive layers of the secondary wall; *l.*, lumen of cell (Jane 1970).

The middle lamella is at first composed largely of pectic, and the primary wall consists mainly of cellulose and pectic. The secondary wall, at its inception, consists of cellulose, or of cellulose and related compounds. Thus, to begin with, the cell wall is not woody or lignified. Lignin, a complex substance whose chemical composition has yet to be fully determined, is deposited later, among the substances which formed the original wall. The middle lamella and primary wall become strongly lignified, and the primary wall often becomes indurated with mineral substances as well. Lignin is also deposited in the secondary wall, but here, even in the fully differentiated cell, it is relatively less dense than in the primary wall and the middle lamella.

The secondary wall is not deposited evenly over the whole of the primary wall, for

it is usually interrupted over the primary pit-fields, or elsewhere over the primary wall, and consequently pit-like structures are built up in the wall in these regions. These pits may remain of equal size from their base or floor, at the middle lamella or primary wall, to their mouth or aperture at the inner surface of the secondary wall.

It was by means of the technique of polarization microscopy that an understanding of the layering or stratification of the wood cell wall was first obtained (Jane 1970; Bailey and Vestal 1937; Clarke 1938; Bailey and Berkeley 1942; Wardrop and Preston 1947&1951), as shown in Figure 1.9.

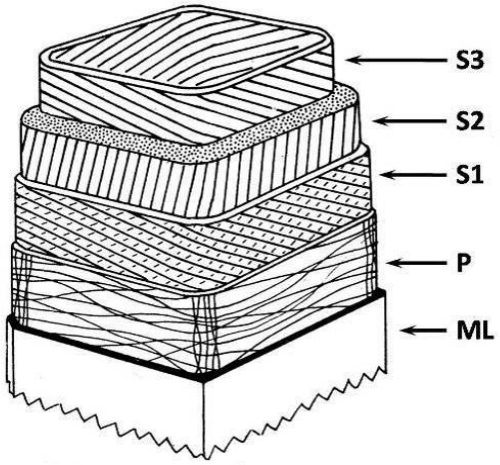

Figure 1.9 Diagram of part of a fiber or tracheid to show the usual orientation of the microfibrils in the various layers of the wall. There are no microfibrils in the middle lamella. In P they are sparse, and their orientation is rather irregular, but generally approximating to the transverse plane, except that some may be nearly axial (Jane 1970).

In the primary wall the pitch of the helices of the micelles is low, i.e. they lie nearly transversely. This is also the case in S_1, and often in S_3, but in S_2 the micelles are arranged in much steeper helices, more nearly parallel to the long axis of the cell. The orientation of the micelles in any one layer, so far as this can be deduced from the extinction directions determined by the polarizing microscope, is however, only an average one. Even within a single layer of the wall, the micelles do not all have precisely the same orientation, for there is considerable angular dispersion of their axes about the mean, as given by the extinction positions. Preston (1949) found this angular dispersion to be especially high in S_1. When a cell wall is viewed at right-angles to its

surface, as seen for instance, in face view in a longitudinal section, so that the various layers are superimposed in the light path, the observed extinction directions will represent averages for all the layers. They usually approximate closely to the directions given by the S_2 alone (Preston 1965).

Development of the electron microscope has provided another method for investigating the structure of cell walls and since this instrument has become more widely available it has been used extensively for this purpose and has confirmed and extended the data obtained by the use of the older, more indirect techniques which have just been considered.

Parameswaran & Liese (1976) studied the fine structure of thick-walled bamboo fibers and demonstrated the polylamellate nature of fiber's cell wall (Fig. 1.10). Its composition is such that narrow lamellae regularly alternate with broader ones, whereby the width of the broad lamellae appears to vary. The microfibrillar orientation in these two types of lamellae has a crisscross arrangement, the narrow lamellae showing a fibrillar angle of 80-90° to the cell axis, while in the broad ones the fibrils are almost parallel to this axis.

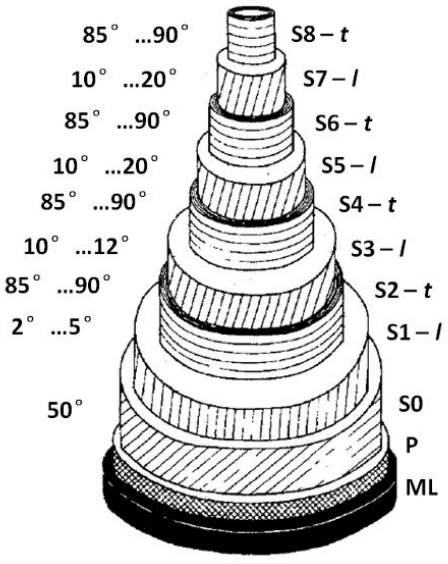

Figure 1.10 Model of the polylamellate structure of a thick – walled bamboo fiber. Figures on the left indicate fibril angle, letters on the right terminology of wall lamellae (Parameswaran & Liese 1976).

As regards the terminology of the different layers or lamellae within the thick-walled bamboo fiber, Tono and Ono (1962) designated the narrow layers as S_1., S_2., S_3., S_4., and the broad regions as S_1, S_2, S_3, S_4, whereby T is the last layer bordering the lumen. Preston (1974) numbers the layers consecutively beginning from the middle lamella: S_1, S_2, S_3, S_4 and S_5 in a fiber wall with three briefringent layers. This system appears logical when compared with the secondary wall layer terminology applied to a wood tracheid with its S_1, S_2 and T or S_3. However, in view of the constantly occurring change in the fibrillar orientation in the diverse alternating lamellae as well as the absence of a tertiary wall layer, the following nomenclature is proposed. Beginning from the outermost lamella at the middle lamella: primary wall (P), the secondary wall transition lamella S_0 (S zero, not always present), S_1-*l*, S_2-*t*, S_3-*l*, S_4-*t*, S_5-*l*, S_6-*t* etc. The affixes *l* and *t* stand for the almost longitudinal and transverse orientation of the cellulose fibrils in the respective lamellae.

Thus, the alternating lamellae, which are mostly broad and narrow with longitudinal and transverse microfibrillar orientation, can be described and designated simultaneously with particular reference to the polylamellate bamboo fiber wall without confusing the issue with the wood tracheid wall terminology. This concept is embodied in a fiber wall model in Fig. 1.10.

In palm 'wood', the amount of secondary wall deposited in fibers is also variable. Although certain palm species, such as *Sabal palmetto*, tend to have cells with extremely thick secondary walls in a given organ (Fig. 1.11), the age of the fibers also seems to determine the amount of secondary wall deposited (Parthasarathy & Klotz 1976). The secondary walls in old fibers usually display a characteristic multilayered structure under both normal and polarized light. Secondary walls of vascular fibers are usually lignified; but non – vascular fibers in leaves are normally unlignified (Tomlinson 1961).

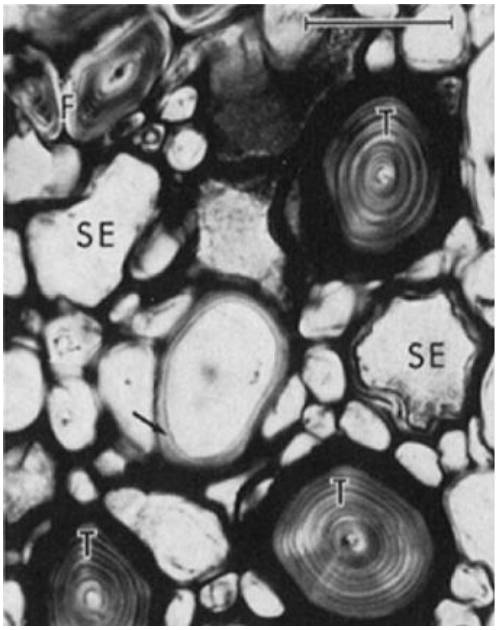

Figure 1.11 *Sabal palmetto*. Transverse section of the metaphloem of a presumably nonfunctioning vascular bundle in the basal part of a stem. The tylosoids have developed very thick secondary walls that are characteristically multilayered (T). Arrow indicates a tylosoid that has developed only a thin secondary wall. F: vascular fiber, SE: sieve element. Scale bar is 0.02mm (Parthasarathy and Klotz 1976).

1.4 Personal motivation and objectives

PALMEA is an important family of monocotyledon and palm plays an essential role in daily life of millions of people in tropical and subtropical regions. The properties and commercial utilization of palms are influenced by its structural characters. Until now researchers put most of their attention on the structural biology of commercial palm and there are many publications on oil palm (*Elaeis guineensis*) and coconut palm (*Cocos nucifera*). Tomlinson *et al*. (1961, 1990, 2011) did great research on the stem anatomy of palms. However, the morphological, chemical, mechanical properties of fibrovascular bundles from palms, specially the palms widely distribute over the world, has not been studied well. For example, *Trachycarpus fortunei* grows in large parts of world where few other palms do; it could serve there as a local source of fiber, wax, etc. From ancient time people already use its leaf sheath fiber for making rope and the rope shows nice decay resistance. In tropical area people use palm trunks for building

construction (Essig & Dong 1987). The fibrovascular bundles from windmill palm are durable for wet-dry cycling condition. However, there is less research to clarify the morphological structure of fibers and its functional implications.

In the monocotyledons, which are usually herbaceous and without secondary thickening, the stem structure normally differs from that of dicotyledons. There is no clearly defined pith or cortex, but a parenchymatous ground tissue in which numerous vascular bundles are situated. In a transverse section these bundles may appear to be scattered throughout the stem, although they are more numerous in the more peripheral part. A few monocotyledons are trees, like PALMAE (palms), there are many dendroid species, some of which may rise to 45m. Bamboo is also monocots; fibers in bamboo showed multiple layering in the secondary wall. While for wood tracheid/fiber, usually there are only three layers, namely S_1, S_2 and S_3, in the secondary wall. It is interesting for us to know the cell wall structure of palm fibers, in which less of research has been done until now.

This thesis is organized as follows:

In Chapter 1, the general introduction about palm family, important palm species, vascular bundles in palm stem and leaf, and cell wall structure of woody fibers.

In Chapter 2, the materials and methods used in this research were described in detail.

In Chapter 3, the morphological development of leaf sheath in windmill palm was first investigated. The fibrovascular bundles in each sheet of leaf sheath were well organized with proper directions. Along one leaf sheath, the contents of cellulose and hemicellulose decreased, while lignin increased from bottom to top of leaf sheath.

In Chapter 4, fibers in leaf fibrovascular bundles from windmill palm showed two-layered secondary cell wall structure. Together with large MFA and high lignin content, this set of knowledge could help explain the high durability and stability of windmill palm fibers.

In Chapter 5, it is confirmed that the two-layered structure of the secondary wall was specific character in palm leaf fibers, which different from other monocotyledons, such as bamboo and rattan, and wood.

In Chapter 6, different types of fibrovascular bundles in one leaf sheath of windmill palm were studied. The mechanical properties and MFA varied among different types, which might be related to the biomechanical movements of leaf sheath.

In Chapter 7, the study on anatomical, chemical and mechanical characteristics of fibrovascular bundles extended to different palm genus. The result indicated the large MFAs of palm fibers in combination with high lignin contents, result in limited elastic deformation, long-term plastic deformation, and relatively low tensile strength of palm fibrovascular bundles.

1.5 References

Bailey, I. W. & Berkeley, E. E. (1942). The significance of X – rays in studying the orientation of cellulose in the secondary wall of tracheids. Amer. J. Bot. 29: 231-241.

Bailey, I. W. & Vestal, N. R. (1937). The significance of certain wood – destroying fungi in the study of the enzymatic hydrolysis of cellulose. J. Arnold Arbor. 18: 196-205.

Beccari, O. (1905). Le Palme del genere "Trachycarpus." Webbia 1: 41-68.

Bretschneider E. (1882). Notes on Chinese Botany from Native and Western Sources. Botanicon Sinicum. London. p387.

Clarke, S. H. (1938). Fine structure of the plant cell wall. Nature, Lond. 142,899.

Dransfield, J., Uhl, N.W., Asmussen, C.B., Baker, W.J., Harley, M.M., Lewis, C.E. (2008) Genera Palmarum. The evolution and classification of palms. Kew Publishing, Royal Botanic Gardens, Kew, UK.

Essig, F. B., Dong, Y. (1987) The Many Uses of Trachycarpus fortunei (Arecaceae) in China [J]. Economic Botany. 41(3): 411-417.

Grisard, J., Vanden-Berghe, M. (1889) Les palmiers utiles et leur allies. J. Rothschild, Paris.

Jane, F. W. (1970) The structure of wood (2nd Edition). Adam & Charles Black. London.

Parameswaran, N., Liese, W. (1976) On the fine structure of bamboo fibres. Wood Sci.

Technol. 10: 231-246.

Parthasarathy, M.V., Klotz, L.H. (1976) Palm 'Wood' I: Anatomical Aspects. Wood Science and Technology. 10: 215-229.

Pei, S., Chen, S., Tong, S. (1991) Tomus 13(1): Angiospermae—Monocotyledoneae, Palme, Flora of Reipublicae Popularis Sinicae. Science Press, Beijing. [In Chinese]

Preston, R. D. (1949) The organisation of the cell wall in relation to the structure of fibres. In Preston, J.M., Fibre Science, 218-247. Manchester.

Preston, R. D. (1965) Interdisciplinary approaches to wood structure. In W.A. Côté (ed.), Cellular ultrastructure of woody plants. Syracuse University Press.

Preston, R.D. (1974) The physical biology of plant cell walls. Chapman and Hall, London.

Satake, G., Watari, S., Hara, H., Tominari, T. (1989) Wild Plants in Japan - Woody Plants II. Heibonsha Press. Japan.

Tono, T., Ono, K. (1962) Researches on the morphological structure and the physical properties of bamboo fibers for paper making. I. Relation between the behaviour of swelling and the morphological structure. J. Jap. Wood Res. Soc. 8: 238-244.

Tono, T., Ono, K. (1962) Researches on the morphological structure and the physical properties of bamboo fibers for paper making. II. The layered structure and its morphological transformation by acid treatment. J. Jap. Wood Res. Soc. 8: 245-249.

Tomlinson, P.B. (1961) Anatomy of the monocotyledons. Ⅱ. PALMAE. Oxford University Press, London.

Tomlinson, P.B. (1990) The structural biology of palms. Clarendon Press, Oxford.

Tomlinson, P.B., Horn, J.W., Fisher, J.B. (2011) The anatomy of palms. Oxford University press, New York.

Wardrop, A. B., Preston, R. D. (1947) Organisation of the Cell Walls of Tracheids and Wood Fibres. Nature. 160: 911-913

Wardrop, A. B., Preston, R. D. (1951) The submicroscopic organization of the cell wall in conifer tracheids and wood fibers. J. Exp. Bot. 2:20-30.

Wilson, E. H. (1913) A naturalist in western China. Doubleday, New York.

Zheng Wan-jun. (2004). Atlas of Chinese Tree. China Forestry Press. Beijing. [In Chinese]

Zhong, R. (2004) A Collection of Illustrative Plates for Palmarceou Introduction. Anhui Science & Technology Press. China. [In Chinese]

Chapter 2

Experimentals

2.1 Materials and sample preparations

2.1.1 Materials

2.1.1.1 Various samples from windmill palm

Figure 2.1 shows the samples from a typical windmill palm. Usually, the fibrovascular bundles from mature leaf sheath are used for various experiments, such as ultrastructural observation of cell wall in fibers, mechanical and chemical properties tests, X-ray diffraction analysis, etc. The leaf stalk and stem are used for general anatomy of fibrovascular bundles. Three windmill palm trees (*Trachycarpus fortunei*) were collected in Nanjing, China. One of which was from the suburbs of Nanjing and the other two were from the botanical experimental field in Nanjing Forestry University. The trunks of palms were about a half meter tall. The leaf sheath of these palms were peeled off and each leaf sheath collected was numbered from core to exterior.

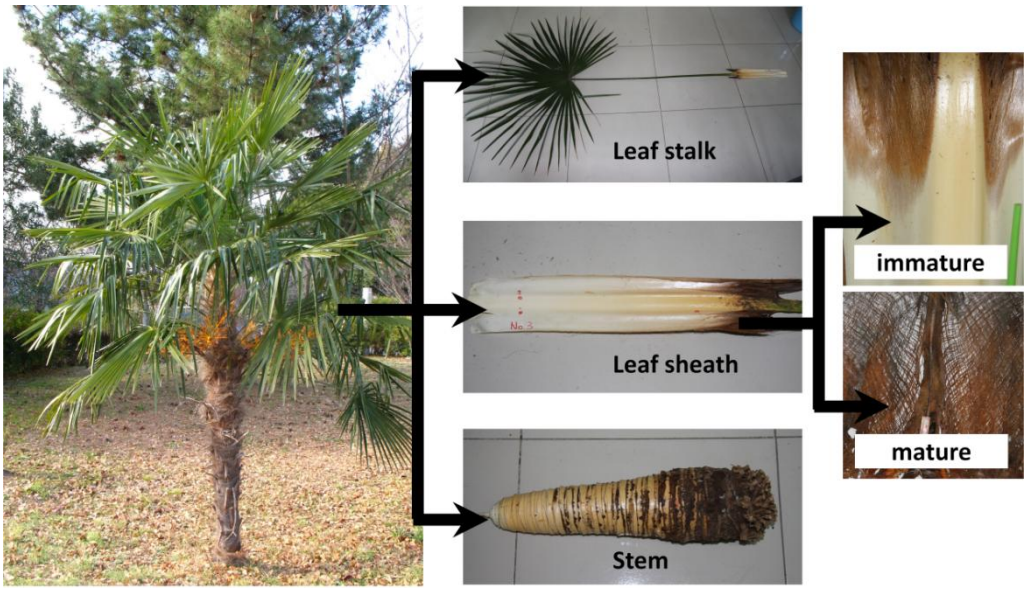

Figure 2.1 Three parts used for various experiments from windmill palm.

It is noted that each leaf sheath is composed of outer, middle, and inner layers, and, each layer contains fibrovascular bundles of different diameters, orientations, and locations. The fibrovascular bundles with the largest diameter are observed in the middle layer, those with a middle-sized diameter are observed in the outer layer, and those with the smallest diameter are observed in the inner layer (Fig. 2.2). Tomlinson (1964) illustrated the arrangement of these fibrovascular bundles/strands in a small sample of leaf sheath in coconut palm as shown in Figure 2.3. It was described as the ventral tissue of the coconut leaf base is 3-stranded, not 2-stranded as a manmade fabric. Therefore, in the palm tissue distinction has to be made not only between 'warp' and 'weft' but also between a third system, 'filling', although it is appreciated that the last two terms are synonymous in the textile trade. Tomlinson mentioned that the other differences between the palm and an artificial fabric are reside on the absence of interweaving between warp and weft, and the failure of warp and weft to run perpendicularly to each other (Fig. 2.3).

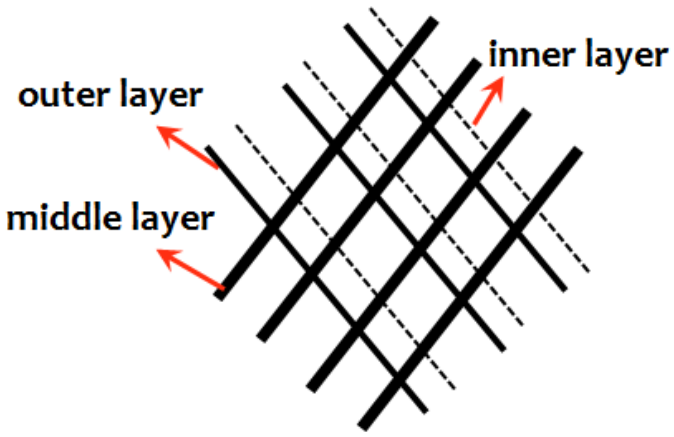

Figure 2.2 Model of fibrovascular bundles' variance in one sheet of leaf sheath. The layers of fibrovascular bundles are defined by difference of diameter, orientation and location of fibrovascular bundles (Zhai *et al*. 2012).

Figure 2.3 Diagrammatic representation in perspective of strand systems in a small part of leaf sheath from *Cocos nucifera* (Tomlinson 1964).

2.1.1.2 Fibrovascular bundles from leaf sheath among different palms

In general, after the soft ground tissues of leaf-sheath are breakdown, a reticulate mass of fibrovascular bundles are left covering around the whole palm stem (Tomlinson 1961, 1990). The remained fibrovascular bundles are easily hand-collected from palm stem surface in different place in China (Fig. 2.4).

Figure 2.4 Distribution of sampling place in China.

Seventeen species belonging to 14 palm genera and one more species from *Arenga* genus, which produced fibrovascular bundles from leaf-sheath, were selected for the study: *Butia capitata* (Mart.) Becc. (*bca*), *Cocos nucifera* L. (*cnu*), *Syagrus*

romanzoffiana (Cham.) Glassman. (*sro*), *Elaeis guineensis* Jacq. (*egu*), *Medemia nobilis* (Hildebrandt & H. Wendl.) Gall. (*mno*), *Phoenix dactylifera* L. (*pda*), *Phoenix roebelenii* O' Brien (*pro*), *Arenga engleri* Becc. (*aen*), *Arenga* sp. (*asp*), *Caryota maxima* Blume ex Mart. (*cma*), *Caryota monostachya* Becc. (*cmo*), *Caryota urens* L. (*cur*), *Corypha umbraculifera* L. (*cum*), *Sabal umbraculifera* Mart. (*sum*), *Washingtonia filifera* (Linden ex André) H. Wendl. ex de Bary. (*wfi*), *Livistona chinensis* (Jacq.) R.Br. ex Mart. (*lch*), *Trachycarpus fortunei* (Hook.) H. Wendl. (*tfo*), and *Rhapis excelsa* (Thunb.) Herry (*rex*) (Fig. 2.5).

The fibrovascular bundles of these species were collected from the surfaces of palm trees at Beijing Botanical Garden, Kunming Botanical Garden, Shenzhen Botanical Garden, Nanjing Botanical Garden, and Taipei Botanical Garden in China. The fibrovascular bundles were rinsed in running tap water to remove dust from their surface. These samples were air-dried prior to use in further experiments. Figure 2.6 shows parts of fibrovascular bundles from different palms; the color differences might have relation with extractives and lignin contents.

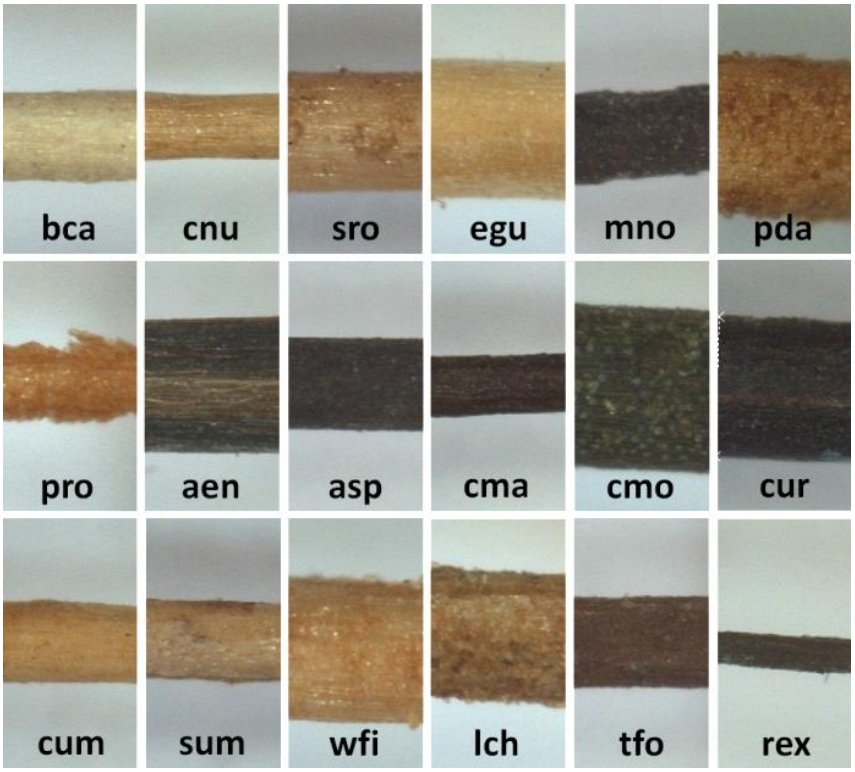

Figure 2.5 Parts of fibrovascular bundles from different palms. The magnifications are inconstant.

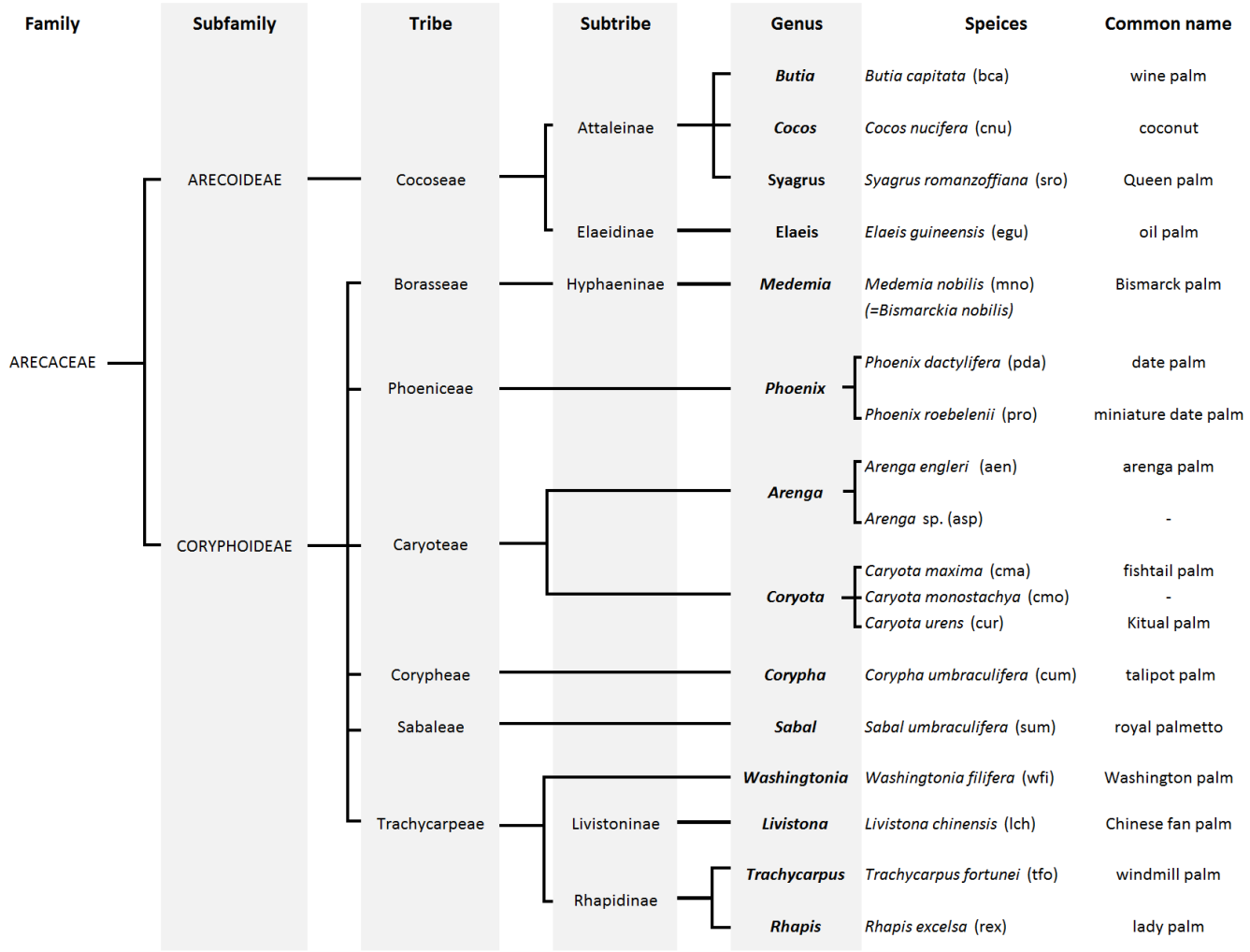

Figure 2.4 Phylogenetic classification of palms used in this research, redrawn from Dransfield *et al*. (2008) and Tomlinson *et al*. (2011).

2.1.2 Sample preparations for microscopy

The anatomical observations were carried out on 1) stem, 2) leaf stalk, 3) leaf sheath, and 4) fibrovascular bundles from different species. The young leaf stalks were soft; they need to be embedded by using paraffin method. The leaf sheathes and stem parts (also knot parts) have hard fibrovascular bundles inside, to get nice tangential section of leaf sheath and transverse section of stem part, they were embedded by using celloidin method. One the other hand, the single fibrovascular bundles of different species were tiny, so that they were embedded by methacrylate or Epon812 resin and used for making semi-thin and ultra-thin sections. Table 2.1 lists the detail information of embedding methods used for different samples (Glauert 1986).

Table 2.1 Embedding methods used for different samples.

Samples	Embedding methods				N.A.
	Paraffin	Celloidin	Epoxy	Methacrylate	
Leaf stalk (small blocks)					
Immature	○				
Mature					○
Leaf sheath					
Immature (small pieces)		○			
Mature (fibrovascular bundles)			○	○	
Stem (small blocks)		○	○		○

○ *Paraffin embedding*

Young leaf stalks were fixed by F.A.A solution (Formalin- Acetic acid- Alcohol) following graded ethanol dehydration, and embedded in paraffin. Serial sections of the embedded samples were obtained by a rotary microtome (Leica RM2245), while the sections of mature leaf stalks were obtained by a Leitz Wetzlar sliding microtome. Both types of sections were double-stained by safranin and fast green after removing paraffin by xylene. The sections were mounted by balsam neutral gum on glass slides.

○ *Celloidin embedding*

For the young palm trunk, which is soft, and the leaf sheaths, which are quite thin, it was not easy to make thin sections from them. Samples from leaf sheaths and knot parts were embedded in celloidin for making sections. The samples were cut into 5mm blocks and were treated as follows: Firstly, all specimens were dehydrated by graded ethanol series; secondly, tissues were transferred into ether-absolute ethyl alcohol (1:1) overnight; thirdly, all specimens were passed through a 2, 4, 6, 8 and 10 % celloidin series at intervals of 2 days, using water-bath at 60°C; finally, the celloidin embedded specimens were mounted on hardwood blocks with 10% celloidin, then harden in chloroform for 12 hours. Specimens can be stored in chloroform until needed. Sections (20-30 μm in thickness) were obtained by a sliding microtome. The mixture of ether - absolute ethyl alcohol (1:1) was used for removing the celloidin in sections. The sections were mounted by balsam neutral gum on glass slides.

○ *Epon812 resin embedding (Semithin and utralthin sectioning)*

5 to 10 palm fibrovascular bundles from leaf sheath were tightly binded together by cotton thread (Fig. 2.6).

Figure 2.6 Cotton thread binded fibrovascular bundles for embedding.

Small tissue parts of palm trunk's knot also were taken. All specimens were dehydrated by graded ethanol series, followed by absolute ethyl alcohol with propylene oxide (1:1), and propylene oxide only. Then, the specimens were embedded with Epoxy resin. From these resin-embedded specimens, semi-thin sections (1-2 μm in thickness) were cut using a semi-thin microtome (Leica, RM2145, Germany). Some of the transverse sections were stained with safranin in order to observe the lignified tissue more clearly. The sections were observed under transmitted- and polarized-light microscopes (Ortoplan, Leitz Wetzlar, Germany). After confirming the position of the fiber cap in each fibrovascular bundle under the light microscope, ultra-thin transverse sections (50-80 nm) were prepared by an ultra-microtome (Ultra-cut E. Reichert-Jung, Capovani Brothers Inc. USA) equipped with a diamond knife. The ultra-thin sections were then mounted on the copper grids preliminary supported by Formvar film and reinforced with carbon. Ultra-thin sections were stained with uranyl acetate and lead citrate.

○ *Methacrylate resin embedding and de-embedding (Utralthin sectioning)*

Fibrovascular bundles were tightly bound together by a cotton thread after being washed, and cut into 5mm long pieces. Some of the fibrovascular bundles were pretreated with acidified sodium chlorite, following the Wise procedure, which was modified by Kerr and Goring (1975) for simultaneous lignin removal. After fixation with 1% osmium tetroxide followed by washing with distilled water, the specimens were dehydrated with a graded ethanol series and embedded in methacrylate resin (*n*-butyl methacrylate: methyl-methacrylate 8:2, benzoyl peroxide 1-2%). The hardness of embedding blocks increases with the proportion of methyl-methacrylate.

Ultra-thin transverse sections (70 nm) were prepared by an ultra-microtome (Ultra-cut E. Reichert-Jung, Capovani Brothers Inc. USA) equipped with a diamond knife.; then mounted on the copper grids preliminary supported by Formvar film and reinforced with carbon. The sections were stained with uranyl acetate after the removal of methacrylate resin with acetone.

Oblique ultra-thin sections, tilted to 8 to 10° to the fiber axis, were prepared, following a method similar to that used for preparing transverse sections with and

without Pt-Pd shadowing.

2.2 Experiments

2.2.1 Morphological observation

2.2.1.1 Light microscopy

Sections (10 – 20 μm) obtained from paraffin and celloidin samples were observed by a light microscope (Olympus BX51, Japan) equipped with a digital camera (Olympus DP73, Japan).

Note: Above experiments appeared at Chapter 3 & 6.

Sections (1 – 3 μm), cut from Epoxy and methacrylate resin, were observed under transmitted- and polarized-light microscopes (Ortoplan, Leitz Wetzlar, Germany). These microscopes equipped with a LCD Olympus video camera (model DP70) were used to resolve images.

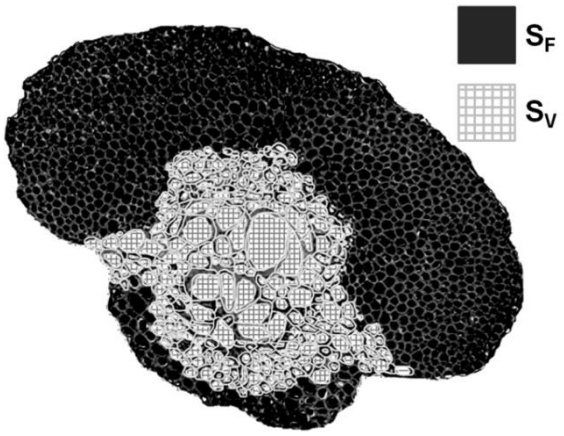

Figure 2.7 Illustration showing areas of S_F and S_V in a fibrovascular bundle from palm leaf sheath.

S_F = transverse sectional area occupied by fibers in a fibrovascular bundle,

S_V = transverse sectional area occupied by vessels and a phloem tissue in a fibrovascular bundle.

The images were used for quantitative analysis by using image analysis software *ImageJ* in order to obtain such basic data on palm fibrovascular bundles as the amount of transverse sectional area occupied by fiber in a fibrovascular bundle (S_F), transverse sectional area occupied by vessels and a phloem tissue in a fibrovascular bundle (S_V)

(Fig. 2.7), number of single fiber in a fibrovascular bundle, single fiber wall thickness and diameter.

Note: Above experiments partially appeared at Chapter 4, 5, 6 & 7.

The dimensions of fibers including length, diameter, cell-wall thickness, and lumen diameter were also got by light microscopy. Thirty fibrovascular bundles from each palm species were macerated at 60°C for 24 h in a solution of acetic acid and hydrogen peroxide (1:1 ratio) (Franklin 1954). After maceration, all specimens were washed with distilled water for neutralization, and were shaken gently in the distilled water until individual fibers were separated from the fibrovascular bundles. The fibers were then stained with 1% safranin solution to observe the lignified tissue. The dimensions of 30 fibers were measured, and average values with standard deviations were calculated for each palm species. An ANOVA was performed to test for significant differences ($P < 0.05$) in fiber dimensions among palm species.

Three derived values were also calculated using fiber dimensions:

1. Slenderness ratio = Fiber length/Fiber diameter
2. Flexibility coefficient = (Fiber lumen diameter/Fiber diameter) × 100%
3. Runkel ratio = (Fiber cell-wall thickness/Fiber lumen diameter) × 2

The fiber dimensions and derived values were compared with published data to assess the suitability of the palms for pulping and other utilizations.

Note: Above experiments appeared at Chapter 7.

2.2.1.2 Transmission electron microscopy

All ultrathin sections were examined using a transmission electron microscope (TEM, 2000EX II**,** JEOL Co. Ltd, Tokyo, Japan) at an acceleration voltage of 100 kV. All images were recorded digitally by a MegaView G2 CCD camera, and used for the measurement of cell wall thickness with public domain software *ImageJ* (National Institutes of Health, USA).

Note: Above experiments appeared at Chapter 4 & 5.

2.2.1.3 Scanning electron microscopy

Fibrovascular bundles from windmill palm were split longitudinally with a sharp razor blade after being freeze dried. The split specimens were glued onto a specimen holder, and sputtered with Pt approximately 10 nm thick, using a JFC-1600 auto fine coater (JEOL Co. Ltd, Tokyo, Japan). The specimens were examined using a field emission scanning electron microscope (FE-SEM, JSM-6700F, JEOL Co. Ltd, Tokyo, Japan) at an acceleration voltage of 1.5 kV and working distance of 6-8 mm.

Fibrovascular bundles from windmill palm after tensile strength test were also observed by SEM for the fracture surface.

Note: Above experiments appeared at Chapter 4 & 6.

2.2.2 MFA analysis

2.2.2.1 X-ray diffraction analysis

Typical fibrovascular bundles were taken from leaf sheath of different palms for X-ray diffraction analysis. The X-ray diffraction diagrams were obtained using a Bruker Hi-Star detector using CuKα radiation (= 1.5418 Å) produced by a rotating anode X-ray generator at tube voltage 45 kV and tube current 90 mA (MAC Science M18XHF). The distance between the specimen and the detector was 15 cm. The data were processed, merged, and scaled using the SAINT program (Bruker) (Watanabe *et al.* 2002). All measurements were performed in triplicate. The files were converted into 16-bit image files by *FIT2D* (European Synchrotron Radiation Facility, France). Using image analysis software *ImageJ* (v.1.46r), the MFA was determined based on azimuthal intensity distribution of 200 reflections of cellulose I_β (Sugiyama *et al*. 1991).

For fibrovascular bundles from windmill palm, the X-ray diffraction diagrams were obtained by using a vacuum camera mounted on a Rigaku RU-200BH rotating anode X-ray generator. The main experimental conditions were Cu Kα radiation (λ=1.54Å), tube voltage 50kV, tube current 100mA. X-ray diffraction patterns were recorded on Fuji Imaging Plates (BAS-IP SR 127). From the obtained X-ray diffraction pattern, using image analysis software *ImageJ*, the mean MFA of palm fibers was

determined based on azimuthal intensity distribution of cellulose 200 reflections. Secondary, equatorial profiles were obtained by radial integration of the diagram, where the Gaussian functions were fitted to crystalline peaks. The relative crystallinity index (CrI) was determined from the ratio of the separated peak area to the total area.

Assuming a cylindrical spiral with an angle of θ, it can be calculated that (Preston 1952, 1974):

$$\cos\theta \cos\varphi = \sin\alpha \ ;$$

where θ is the Bragg angle for the 200 reflection, with a value 11.4°. φ is the observed angle from X-ray diffraction diagrams, and α is the real MFA value.

Note: Above experiments appeared at Chapter 4 & 6.

2.2.2.2 Polarized light microscopic analysis

To overcome the difficulty of cutting the fibers longitudinally, and to leave only a single wall, 900-nm semi-thin sections with an oblique angle of 5° were prepared. Five fibrovascular bundles were selected, from which 10 fibers in each bundle were observed using PLM. *Apparent* MFA does not correspond to *real* MFA when using oblique sections. The relationship between *apparent* MFA and *real* MFA is diagrammatically shown in Figure 2.8a.

The microfibrils lay at the AB position on the longitudinal section. After tilting with a θ angle (∠CAE), the microfibrils of a cut section lay at the AD position, where AE is perpendicular to CE. Hence, the *real* MFA is ∠BAC (α), while *apparent* MFA is ∠DAE (α′). It is also known that DE is equal to BC. Furthermore, in a right-angled triangle ∆AEC, AE = AC cosθ. Accordingly, the relationship between *real* MFA and *apparent* MFA can be presented as follows:

$$\tan\alpha = \cos\theta \tan\alpha'$$

Apparent MFA is larger than *real* MFA. For instance, if the oblique angle was approximately 5°, the oblique error might be negligible, as the value of cosθ is very close to 1. To explain microfibrils orientation in detail, the definition of S- and Z-helix based on the degree of MFA (α) is shown in Figure 2.8b. If microfibrils orient in an S-helix, the degree of MFA will be over 90°. On the other hand, when microfibrils

orient in a Z-helix, MFA will be less than 90°.

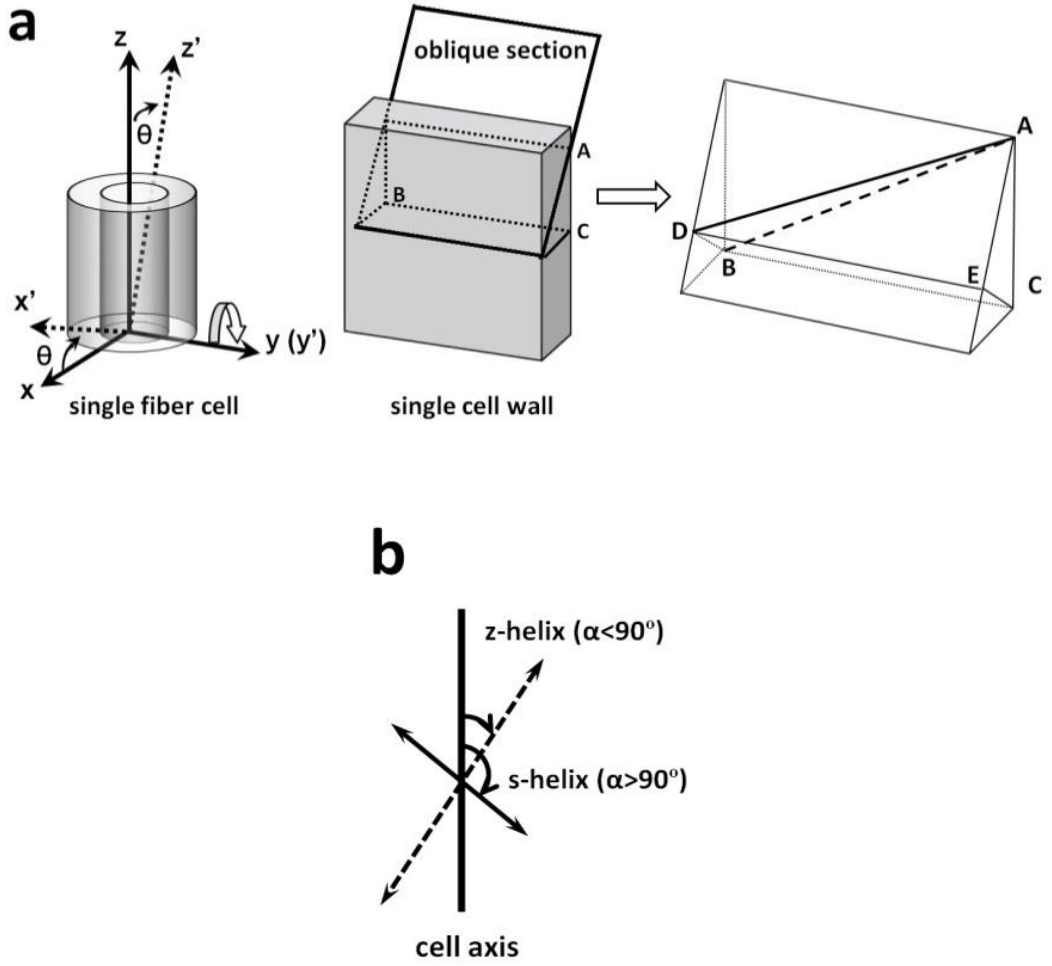

Figure 2.8 Illustration of the relationship between *real* MFA and the *apparent* MFA. --a: An orthogonal co-ordinate system (x, y, z) is set. The (x, y, z) axis was rotated by θ degree (∠CAE) around the y-axis to give the (x', y', z')-axes. The oblique section was located in the y'－z' plane. The oblique section is partially enlarged for displaying the microfibril localization. AB is the cellulose microfiber localization at the longitudinal section of a cell wall. The *real* MFA is ∠BAC = α to the cell axis. On the oblique section, the angle between AD and the cell axis is visible using polarized light microscopy, which is the *apparent* MFA (∠DAE = α') that we sought to measure. --b: Definition of Microfibrils orientation (z-helix or s-helix) related with MFA (α). The double arrow lines indicate microfibrils.

To determine the reliability of the MFA obtained from PLM, these results were

compared against the MFA of windmill palm fibers obtained by X-ray diffraction diagrams.

Note: Above experiments appeared at Chapter 4.

2.2.3 Chemical composition studies

2.2.3.1 Qualitative analysis - FTIR spectroscopy

Samples obtained by the delignification procedure above and untreated samples for examining the changes before and after chemical treatment were frozen-dried overnight and then used for analysis of ATR-FTIR. The palm fibrovascular bundle samples were pressed uniformly against the diamond surface using a spring-loaded anvil. The IR spectra (4000 - 400cm^{-1}) were obtained on a Spectrum One system (Perkin Elmer, Universal ATR Sampling Accessory, USA) at a resolution of 4 cm^{-1}. Five replicate spectra of samples with various reaction intervals were recorded. Good-quality ATR spectra were obtained based on the smoothness of the baseline and resolution, according to previous publication (Pandey & Pitman 2003, 2004; Pandey & Nagveni 2007). All spectra were baseline corrected, smoothened, and normalized for qualitative comparison among the samples. Peaks were assigned according to former researchers (Harrington *et al*. 1964; Pandey & Pitman 2003, 2004). The peak height for lignin associated bands was rationed against the height of C-H stretching absorption around 2920cm^{-1} to provide relative changes of lignin (Fig. 2.9). A similar method of measuring was used by Rodrigues *et al*. (1998) for determining lignin content of *Eucalyptus globulus* wood.

For calculating relative content of lignin (RC_{lignin}), the following equation was used.

$$RC_{lignin} = H_{1510} / H_{2920}$$

$$H_{2920} = A_{2920} - A_b - [(A_a - A_b) \times (2920 - b)/(a - b)]$$

$$H_{1510} = A_{1510} - A_c - [(A_d - A_c) \times (c - 1510)/(c - d)]$$

where A_i indicates the absorbance value of the wave i cm^{-1}. a, b, c and d is wave number around 3000, 2650, 1550 and 1490. H_{2920} is the relative absorbance value around 2920 cm^{-1} of C-H stretching vibration and H_{1510} is the relative absorbance value around 1510 cm^{-1} of aromatic skeletal in lignin.

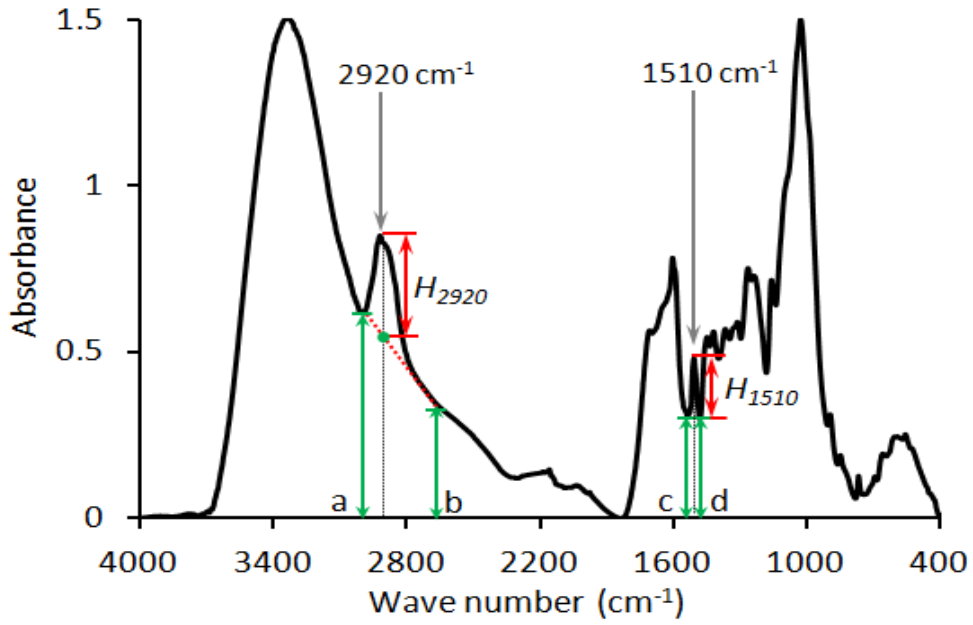

Figure 2.9 IR spectrum of windmill palm fibrovascular bundles as an example. The peak of 2920 cm^{-1} indicates a prominent C-H stretching absorption and the peak of 1510 cm^{-1} for aromatic skeleton in lignin.

Note: Above experiments appeared at Chapter 3 & 4.

2.2.3.2 Quantitative analysis – Tappi standard for Klason lignin

Individual fibrovascular bundles were separated from the leaf sheaths of the windmill palm. The fibrovascular bundles were extracted for 6 h in ethanol-benzene at a ratio of 1:2 (v/v) in a Soxhlet apparatus, according to the TAPPI standard T264 (TAPPI 1997). A fibrovascular bundle includes not only fibers, but also vessels and phloem tissue. Additionally, according to our former report, the transverse sectional area occupied by fibers in a fibrovascular bundle is always over 50%. The content of the Klason lignin (acid-insoluble lignin) was determined using the TAPPI standard T-222 (TAPPI 1998). De-waxed palm fibrovascular bundles were extracted by using Sulfuric acid (72% w/w) as a reagent. The residue was used to determine Klason lignin. To obtain an accurate result for Klason lignin content, it has been suggested that the ash content of acid-insoluble residue should be measured. Hence, the residues were transferred to a crucible, which was placed in a muffle furnace at 575 ± 25°C for 5 h to

obtain ash content data (Sluiter *et al*. 2011).

Note: Above experiments appeared at Chapter 4 & 7.

2.2.4 Mechanical property studies

All fibrovascular bundles were air-dried to a moisture content ranging from 8% to 10% by weight. After cutting the fibrovascular bundles into 20–25 mm lengths, the bundles were fixed on paper frames with 10-mm gauge length (Fig. 2.10) by medium-viscosity epoxy adhesives (Aron Alpha EX2020, Toagosei America, Inc., Japan), according to the preparation procedure mentioned in the ASTM D 3379-75 standard (1978). The diameter of each fibrovascular bundle was measured using a digital optical microscope (Micro Square, DS-3USV, RAS Machine Tool Technologies, Inc., USA) at 10 randomly selected points. The transverse sectional area of each fibrovascular bundle was determined using the circle equation based on the mean value of measured diameter.

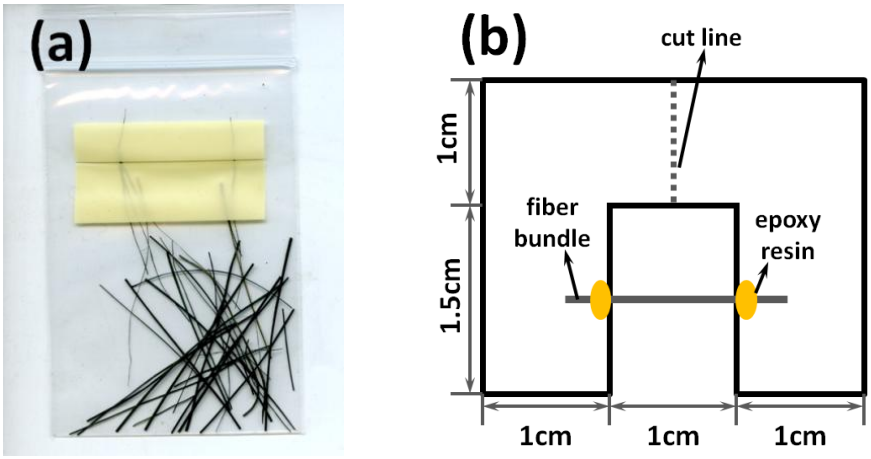

Figure 2.10 Illustration of fibrovascular bundles **(a)** and its supporting paper frame used for tensile strength test **(b)**. A fibrovascular bundle is fixed on the paper frame by an epoxy adhesive. The supporting paper will be pulled apart right after the paper is cut in its middle part indicated by dotted line.

Figure 2.11 Specimens under 60% relative humidity and 20°C condition.

Prior to mechanical testing, specimens were conditioned at 60% relative humidity and 20°C for 1 month (Fig. 2.11). Following the ASTM D-882 standard, the mechanical properties of fibrovascular bundles were determined using a universal testing machine (Instron 4411) with a crosshead speed of 1 mm/min. Before testing, the middle part of the supporting paper was cut. Thirty fibrovascular bundles from each palm species were tested in order to perform statistical analyses. The data were assessed by ANOVA to test for significant differences ($P < 0.05$).

Note: Above experiments appeared at Chapter 6 & 7.

2.3 References

American Society for Testing and Materials. (1978) ASTM D 3379-75 standard test method for tensile strength and Young's modulus for high-modulus single-filament materials. ASTM, Philadelphia, 847-852

Dransfield, J., Uhl, N.W., Asmussen, C.B., Baker, W.J., Harley, M.M., Lewis, C.E. (2008) Genera Palmarum. The evolution and classification of palms. Kew Publishing, Royal Botanic Gardens, Kew, UK.

Franklin, G.L. 1954. A rapid method for softening wood for anatomical analysis. Tropical woods. 88: 35-36.

Glauert, A. M. (1986) Fixation, dehydration and embedding of biological specimens. Practical Methods in Electron Microscopy. Volume 3, Part I. (Glauert A.M. ed.).

Elsevier North-Holland Biomedical Press, AE Amsterdam, The Netherlands.

Harrington, K.J., Higgins, H.G., Michell, A.J. (1964) Infrared spectra of *Eucalypus regnans* F. Muell. and *Pinus radiata* D. Don. Holzforschung. 18: 108-113.

Kerr, A. J., Goring, D. A. I. (1975) Ultrastrucutral arrangement of the wood cell wall. Cellul. Chem. Technol. 9: 563-573.

Pandey, K.K., Nagveni, H.C. (2007) Rapid characterisation of brown and white rot degraded chir pine and rubberwood by FTIR spectroscop. Holz Roh Werkst. 65: 477-481.

Pandey, K.K., Pitman, A.J. (2003) FTIR studies of the changes in wood chemistry following decay by brown-rot and white-rot fungi. Int. Biodeter. Biodegr. 52(3): 151-160.

Pandey, K.K., Pitman, A.J. (2004) Examination of the lignin content in a softwood and a hardwood decayed by a brown-rot fungus with the acetyl bromide method and Fourier transform infrared spectroscopy. J. Polym. Sci., Part A: Polym. Chem. 42(10): 2340-2346.

Preston, R.D. (1952) The molecular architecture of plant cell walls. Chapman and Hall, London.

Preston, R.D. (1974) The physical biology of plant cell walls. Chapman and Hall, London.

Sluiter, A., Hames, B., Ruiz, R., Scarlata, C., Sluiter, J., Templeton, D., Crocker, D. (2011) Determination of Structural Carbohydrates and Lignin in Biomass. National Renewable Energy Laboratory, Golden, CO, USA.

Sugiyama, J., Vuong, R., Chanzy, H. (1991) Electron diffraction study on the two crystalline phases occuring in native cellulose from an algal cell wall. Macromolecules. 24: 4168-4175.

TAPPI Standard T 222. (1998) Acid insoluble lignin in wood and pulp.

TAPPI Standard T 264. (1997) Preparation of wood for chemical analysis.

Tomlinson, P.B. (1961) Anatomy of the monocotyledons. II. PALMAE. Oxford University Press, London.

Tomlinson, P.B. (1964) The vascular skeleton of coconut leaf base. Phytomorphology.

14: 218-230.

Tomlinson, P.B. (1990) The structural biology of palms. Clarendon Press, Oxford.

Tomlinson, P.B., Horn, J.W., Fisher, J.B. (2011) The anatomy of palms. Oxford University press, New York.

Watanabe, A., Yoshimura, T. Mikami, B. Hayashi, H. Kagamiyama, H., Esaki, N.. (2002) Reaction mechanism of alanine racemase from Bacillus stearothermophilus. J. Biol. Chem. 277(21): 19166-19172.

Chapter 3

General anatomy of leaf and stem in windmill palm

3.1 Morphological development of leaf sheath

The windmill palm stem are usually surrounded by leaf sheath (Tomlinson *et al*. 1961; 1990). All leaf sheaths were peeled off from palm stems and each leaf sheath collected was sequentially numbered from core to exterior. The lower leaf sheaths of a palm tree were aged and with dark brown color as shown in Figure 3.1 a, while the upper and younger leaf sheath had gradually changed the color from dark brown to white vertically along the leaf sheath from top to bottom (Fig. 3.1 b). For younger leaf sheath, the bottom part showed living tissue and the top part sheet or assembly of mature fiber bundles only (Fig. 3.1 c). In between top and bottom, there was a transition area with light brown color. In this transition area, parenchyma cells already devitalized and still attached on vascular bundles loosely.

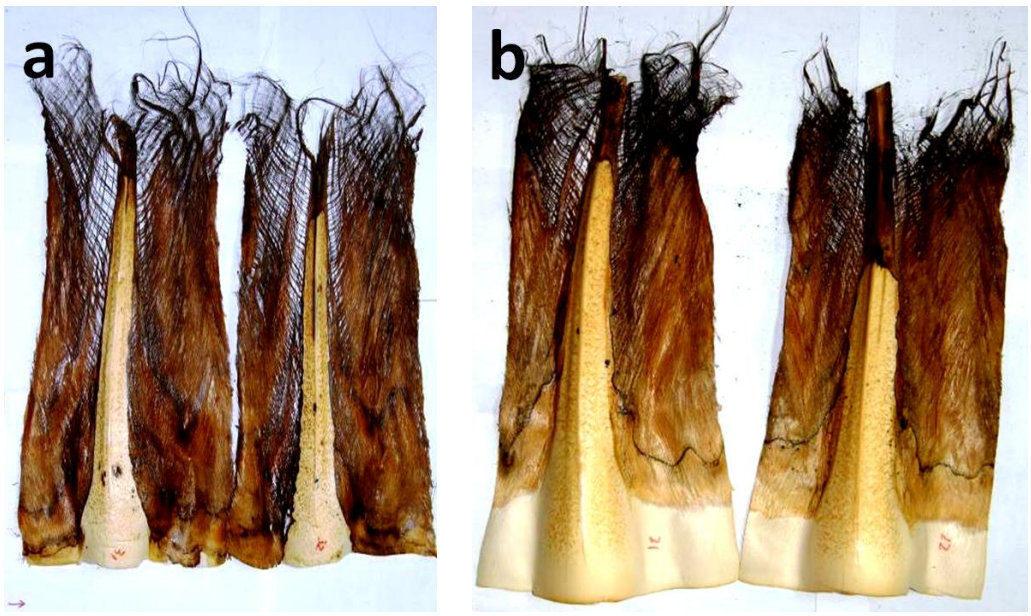

Figure 3.1 Leafs from windmill palm. **a:** Leaf No. 31 & 32, which show dark brown color over all sheath and detached fibers. **b:** Leaf No. 21 & 22, which show changing color from bottom to top part. **c:** Transition parts (a twig pointed area) between living and non-living tissues in leaf sheath of leaf No.18.

Series of leaf sheaths were measured from outside to inside (or from upper to lower part) of the palm stem. The measured index included the circumference length (*a*), the height of living tissue (b) and height of leaf sheath (c), also the crossed angle of vascular bundles (Fig. 3.2).

The height of leaf sheath had almost no change from top to bottom of the stem. From knot No.8 to No. 56, the highest leaf sheath was 40.3 cm, while the lowest one was 30.8cm with a mean height of 35.7 cm among 49 pieces of leaf sheaths. According to the measure, the circumference length of leaf sheath was the circumference length of palm stem. The uppermost leaf sheath, which could be measured, was no.5 with 3.6 cm in girth. While No.56 leaf sheath, which was the lowermost leaf sheath, was measured as 37.0 cm in girth. The living tissue area of leaf sheath was highest in the knot No.8. In this stage, a leaf sheath was all made of living tissue. The living tissue remained up to leaf sheath No.32. All leaf sheaths lower than No.32 turned to brown color, indicating that the tissue part was matured, leaving all vascular bundles separated from devitalized parenchyma tissues.

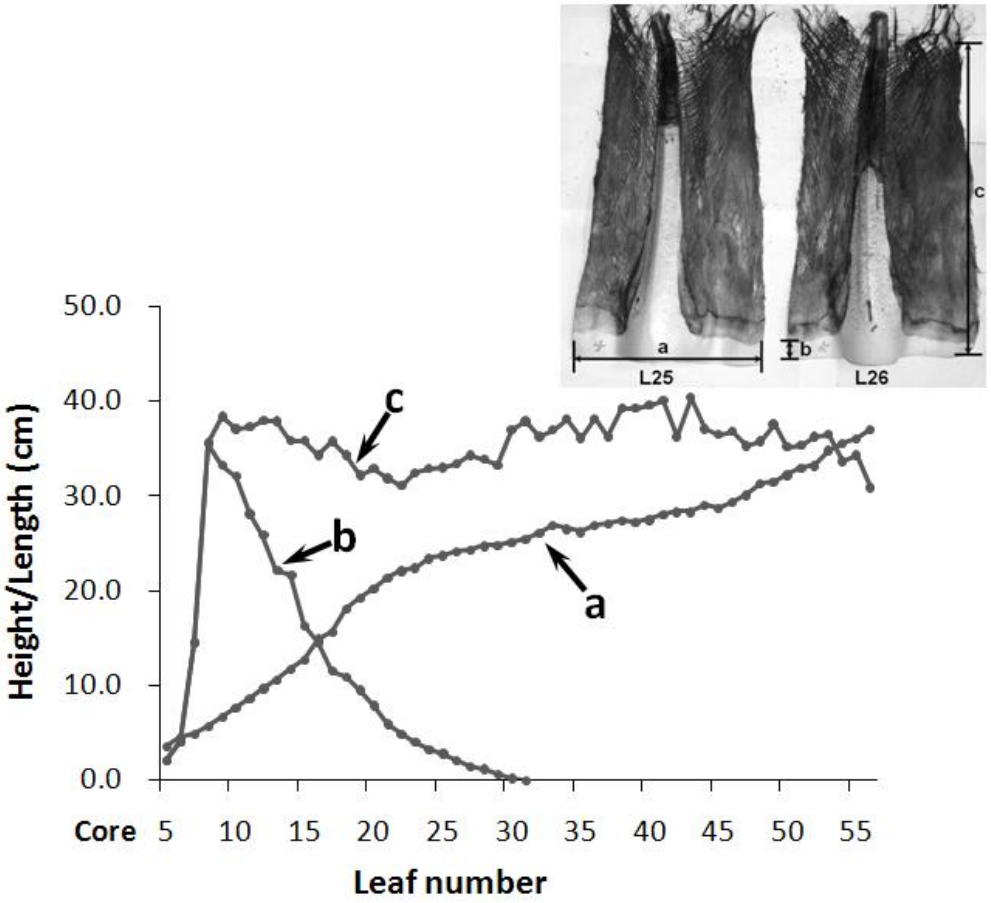

Figure 3.2 The diagram describes the growth tendency of one palm. **a:** The circumference length of leaf sheath (also means the circumference length of palm trunk); **b:** The height of living tissue in one leaf sheath; **c:** height of leaf sheath.

When observe living tissue closer, vascular bundles with crossed structure was visualized as shown in Figure 3.3. The evidence was further confirmed by the observation of the longitudinal section parallel to a living tissue under a light microscope (Fig. 3.4). The results for the measurements of crossed angle and its relation with stem width are shown in Figure 3.5. The figure shows a consistent increase of the angle with the growing of a palm. By applying a linear regression analysis, a linear relationship between crossed angle of vascular bundles (y) and palm stem girth (x) was obtained.

Figure 3.3 Leaf sheath with crossed structure. Under the surface cell of leaf sheath, the crossed pattern of fiber bundles can be seen clearly. The knot height of palm is about 1cm.

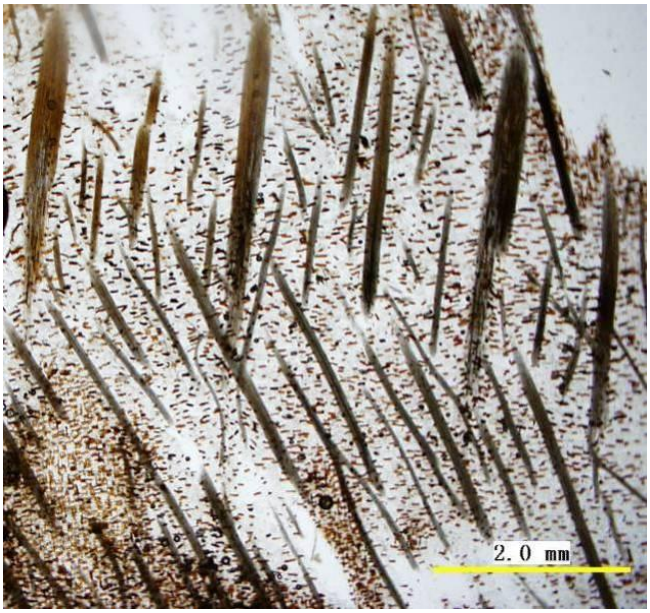

Figure 3.4 Well oriented fibrovascular bundles of leaf sheath observed under light microscope. Bar=2.0mm.

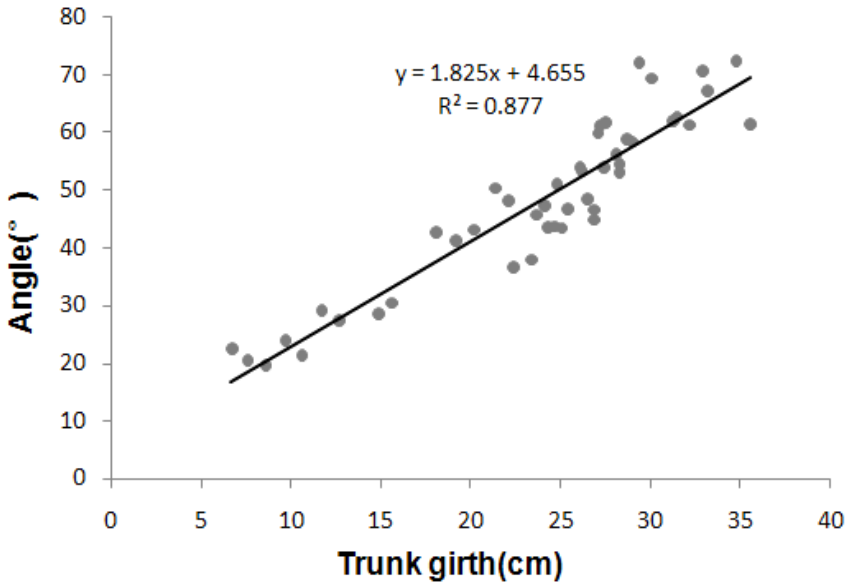

Figure 3.5 The diagram presents the relation between the crossed angle of fibrovascular bundles in leaf sheath and the trunk girth. These two variables have a linear relationship with R – squared value of 0.877, which indicates good linear reliability. (R – Squared value is the square of the correlation coefficient. Value close to 1 indicates excellent linear reliability.)

It is hypothesized that a change of color in an immature leaf sheath from white to dark brown (as shown in Fig.3.3) indicated a change of metabolism in parenchyma tissues, which had happened in advance of parenchyma disintegration to make vascular bundles mature and to be separated. To test the change of chemical contents in immature leaf sheathes, the spectral analysis using ATR-FTIR was carried out in different parts of the leaf sheath during its development as shown in Figure 3.6.

The Figure 3.6a shows a transitional region of leaf sheath during its development from an immature to a mature state. Six different areas vertically aligned along an immature leaf sheath were selected for the test. The areas of number 1 to 3 belongs to the white region, the area of number 4 to the transitional region and those of numbers 5 and 6 to the dark colored region. The dark colored region in the upper left part of Figure 3.6 (a) indicates that living parenchyma tissues are disintegrating, followed by development of mature leaf sheathes. Figure 3.6 (b) shows a spectrum that was recorded

for the bottom point of a tested leaf sheath (Fig. 3.6 a). At around 1730 cm^{-1} it is noted a peak for unconjugated C=O in hemicelluloses (1), 1510 cm^{-1} for aromatic skeletal in lignin (2) and 898 cm^{-1} for C-H deformation in celluloses (3). These typical peaks were chosen for identifying the existence of hemicelluloses, lignin and cellulose.

By testing several leaf sheathes which contain the transitional region, a ratio between the typical peak height to the standard peak height was obtained for qualitative comparison among the specimens. It was found that the relative contents of cellulose and hemicelluloses decreased gradually, while lignin increased relatively to the decrease of these polysaccharides as fibers become matured and separated (Fig. 3.6 c).

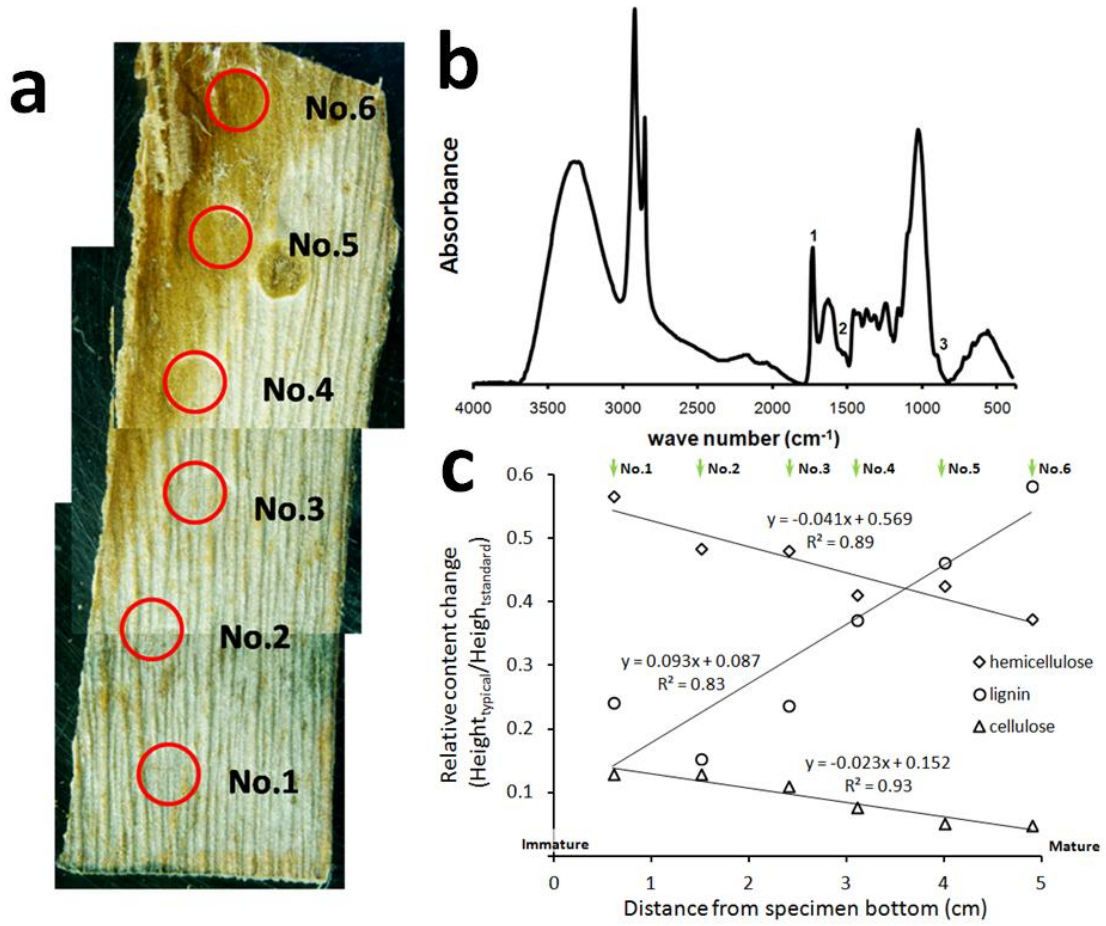

Figure 3.6 Leaf sheath specimen for FTIR test which shows gradual change of color from bottom to up and the change of chemical contents.

The FTIR spectrum of matured fibrovascular bundles from leaf sheath in *T. fortunei* is shown in Figure 3.7 and main characteristic bands of palm fibers are shown in Table 3.1. From Figure 3.7, it is noted that after delignification, intensities of absorption bands resulting from lignin at 1650, 1596, 1510, 1462, 1425, 1268 and 1244 cm^{-1} decreased or disappeared. The band at 770 cm^{-1}, which people thought calcium oxalate components have an absorption peak, also disappeared via delignification processing.

For further comparison, band 2922 cm^{-1} was selected as the standard band. Because C-H stretching absorption around there and all woody plants have this band of approximate content. Around 1730 cm^{-1} can see peak for unconjugated C=O in hemicelluloses, 1510 cm^{-1} for aromatic skeletal in lignin and 898cm^{-1} for C-H deformation in cellulose. These typical peaks were chosen for identifying the presence of hemicelluloses, lignin and cellulose. The values used for getting relative intensities are ratios based on peak heights.

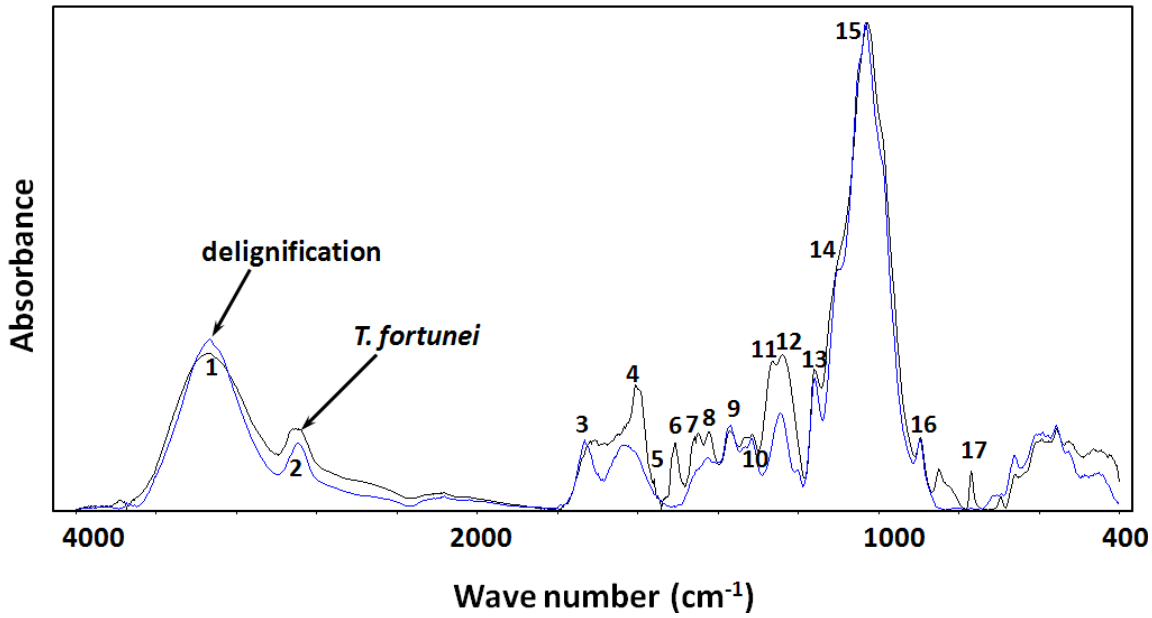

Figure 3.7 FTIR spectra of *T. fortunei* fibrovascular bundles and delignified fibrovascular bundles.

Table 3.1 Main characteristic absorptions of palm fibrovascular bundles numbered in Fig. 3.8 (Rodrigues *et al*. 1998; Pandey & Pitman 2003, 2004; Mohebby 2005).

No.	Functional groups	Wave number (cm^{-1})
1	hydrogen bonded stretching (O-H)	3400
2	stretching in methyl and methylene groups	2922
3	unconjugated C=O in xylans (hemicellulose)	1730
4	absorbed O-H in lignin	1650
5	conjugated C-O in lignin	1596
6	aromatic skeletal in lignin	1510
7	C-H deformation in lignin and carbohydrates	1462
8		1425
9	C-H deformation in cellulose and hemicellulose	1372
10	C-H vibration in cellulose and C-O vibration in syringyl derivatives	1330
11	guaiacyl ring breathing, C-O stretch in lignin and for C-O linkage in guaiacyl aromatic methoxyl groups	1268
12	syringyl ring and C-O stretch in lignin and xylan	1244
13	C-O-C vibration in cellulose and hemicellulose	1158
14	aromatic skeletal and C-O strentch	1122
15	C-O stretch in cellulose and hemicellulose	1048
16	C-H deformation in cellulose	898
17	calcium oxalate components have an absorption peak at this band	770

3.2 Structure of stem, leaf stalk and leaf sheath in windmill palm

3.2.1 Stem anatomy of windmill palm

Figure 3.8a shows a cross sectional view of a palm stem. As described by Tomlinson (1990), vascular bundles next to cortex were smaller and numerous and those in inner part were larger and fewer; however, a zone occupied with small vascular bundles was observed in the middle of inner zone mostly with large vascular bundles. The fact is quite different from bamboo (Fig. 3.8b) which does not show such a distribution of smaller vascular bundles in inner part of the stem but distribute only at the peripheral zone (Liese, 1998). Furthermore, there are two distinct microscopic features can be observed in cross sectional view of the palm stem: one is an even distribution of many parenchyma cells filled with resin and the other the vascular bundles mostly surrounded by parenchyma cells that contain silica bodies (Fig. 3.9) (Prychid *et al*. 2003).

3.2.2 Leaf stalk anatomy of windmill palm

Figure 3.10a shows a cross sectional view of mature leaf stalk, which already well developed and surrounded with circular leaf sheath. The vascular bundles are stained with safranin, which showed the vascular bundle already lignified strongly. Using the young leaf stalk for double staining (Safranin and Fast Green), the vascular bundles were stained lightly with safranin (Fig. 3.10b). While leaf sheath is connected with leaf stalk, so the chemical changing of vascular bundles during its developing should be similar. In order to know the change of some chemical components during development of leaf sheath in *T. fortunei*. FTIR test was done; this has been described in the former part of this Chapter.

3.2.3 Leaf sheath anatomy of windmill palm

Figure 3.11 shows a cross sectional image of immature leaf sheath. The distribution of vascular bundles can be divided into three layers which showed bigger size in the middle and smaller one in both outside and inside. This character also was confirmed in many pieces of mature leaf sheath taken from different height of a palm.

After leaf sheath becoming matured, parenchyma cells were decomposed and detached from vascular bundles, resulting in their complete separation each other (Fig. 3.12).

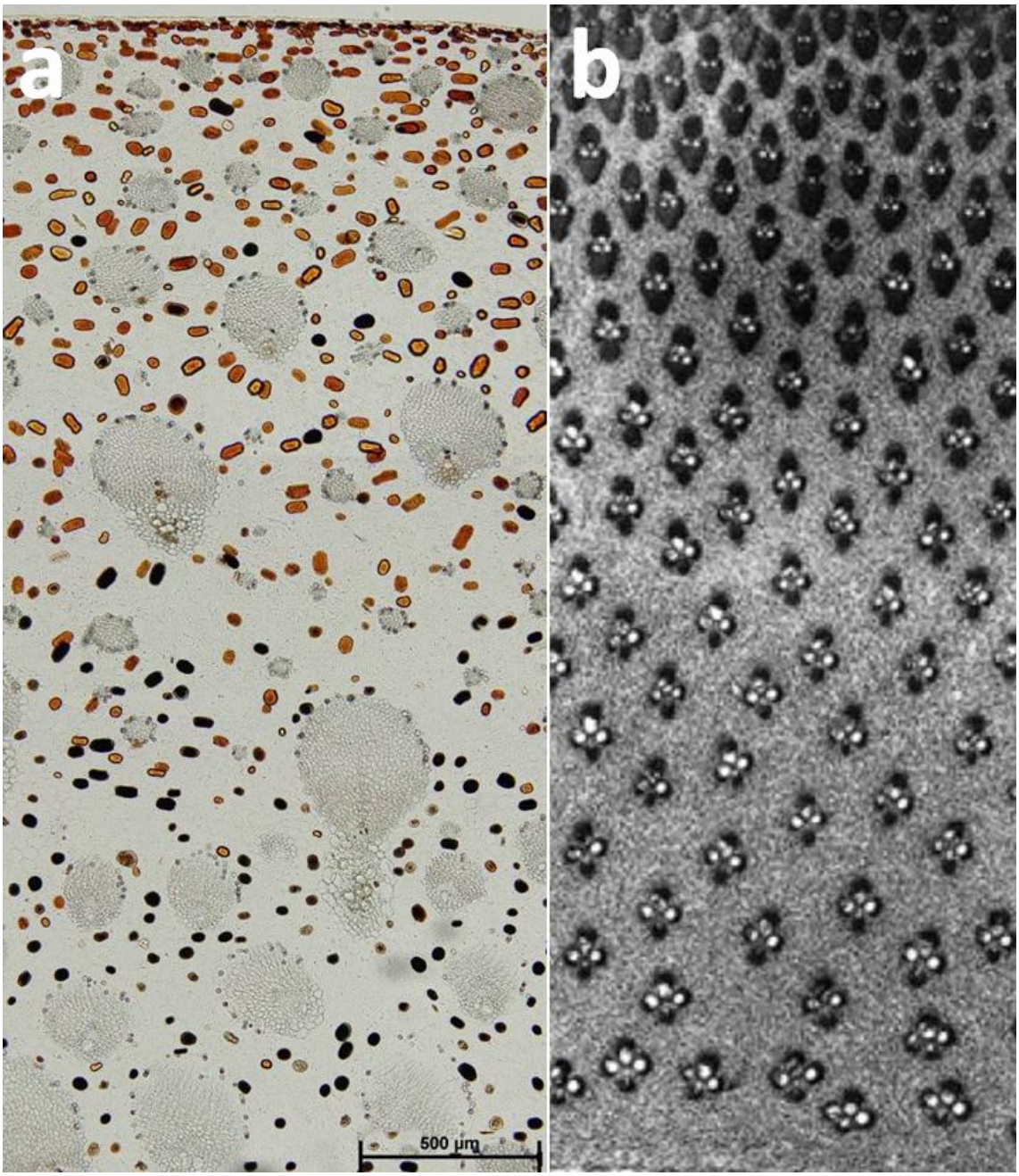

Figure 3.8 (a) Transverse section of *T. fortunei* stem around No. 20 knot (same to No. 20 leaf). **(b)** A typical transverse section of a culm wall with vascular bundles of the monopodial bamboo *Phyllostachys edulis* embedded in the ground parenchyma cells reported by Liese (1998). Scale was not shown in original report.

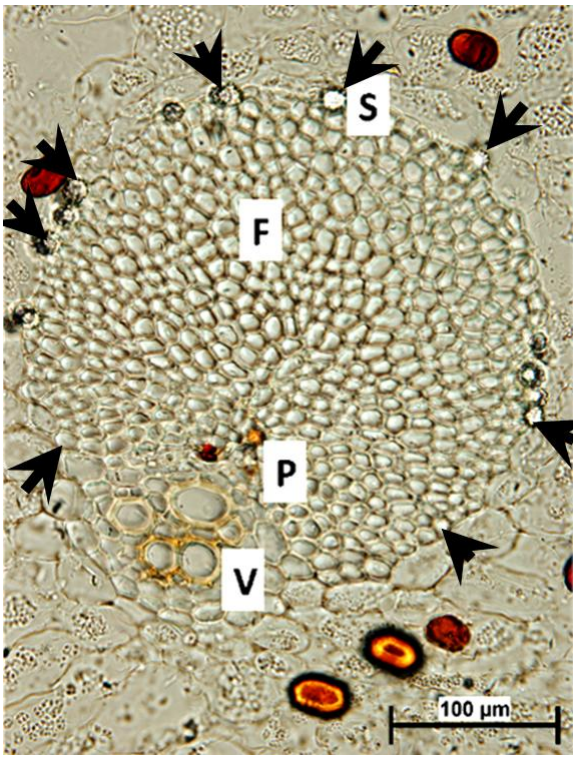

Figure 3.9 Transverse section of single vascular bundle surrounded by parenchyma cells (*T. fortunei*). F: Fibers; P: Phloem; V: Vessel; S: Silica body. Bar=100µm. Arrows point to the silica bodies.

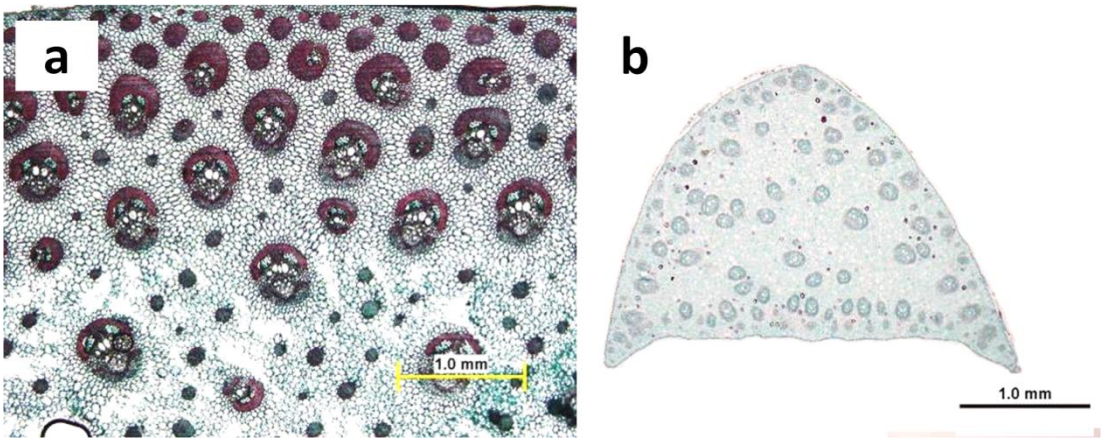

Figure 3.10 Double stained transverse sections of mature **(a)** and immature **(b)** leaf stalk of *T. fortunei*. Bar=1.0mm.

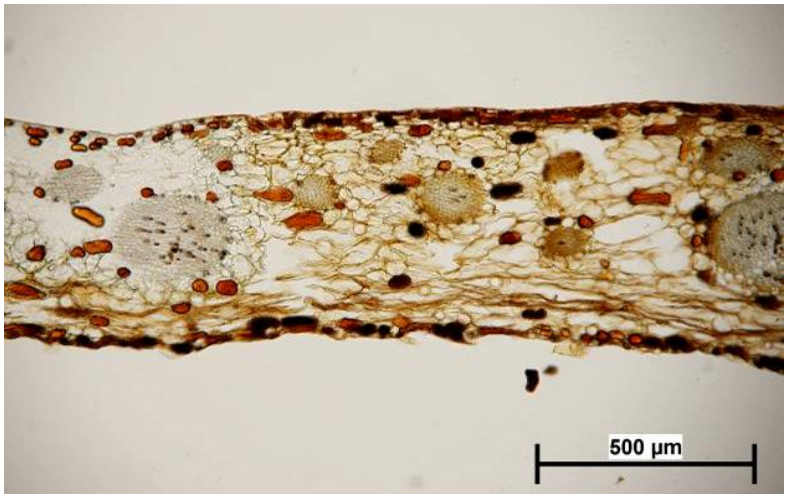

Figure 3.11 Transverse section of No. 18 leaf sheath of *T. fortunei* showing the distribution of vascular bundles in different size. Bar=500µm.

Figure 3.12 One small piece of mature leaf sheath taken from a windmill palm tree. This leaf already fell from tree and all leaf has no living tissue. The remains of parenchyma can be seem, which still surround the fibers, and the fibers separated from each other.

3.3 Summary

Series of leaf sheaths were examined from outside to inside (or from upper to lower part) of palm stem. The measured items included the circumference length (*a*), the height of living tissue (b) and height of leaf sheath (c), also the crossed angle of vascular bundles. The height of leaf sheath almost had no change from top to bottom of the stem. From knot No.8 to No. 56, the highest leaf sheath was 40.3cm, while the lowest one was 30.8cm with a mean height of 35.7cm among 49 pieces of leaf sheaths. According to the measurement, the circumference length of leaf sheath was same with circumference length of palm stem. The bottom part showed living tissue and the top part a sheet or assembly of mature fiber bundles only. In between top and bottom, there was a transition area with light brown color. In this transition area, parenchyma already died but still attached to vascular bundles loosely. By observing the vascular bundles embedded in living tissue of the leaf sheath, vascular bundles with crossed structure were visualized. The evidence was further confirmed by the microscopic observation of the longitudinal section parallel to a living tissue. It is noted that large vascular bundles are all oriented in the same direction.

Along the axial direction of living leaf sheath, the transformation of chemical contents in leaf sheath from bottom to top part was estimated by FTIR analysis. As fiber becoming matured and separated, the contents of cellulose and hemicellulose tended to decrease gradually, while lignin increased.

3.4 References

Liese, W. (1998) The anatomy of bamboo culms. INBAR technical report. Technical report. International Network for Bamboo and Rattan.

Mohebby, B. (2005) Attenuated total reflection infrared spectroscopy of white-rot decayed beech wood. Int. Biodeter. Biodegr. 55(4): 247-251.

Pandey, K.K., Pitman, A.J. (2003) FTIR studies of the changes in wood chemistry following decay by brown-rot and white-rot fungi. Int. Biodeter. Biodegr. 52(3): 151-160.

Pandey, K.K., Pitman, A.J. (2004) Examination of the lignin content in a softwood and a

hardwood decayed by a brown-rot fungus with the acetyl bromide method and Fourier transform infrared spectroscopy. J. Polym. Sci., Part A: Polym. Chem. 42(10): 2340-2346.

Prychid, C.J., Rudall, P.J., Gregory, M. (2003) Systematics and biology of silica bodies in monocotyledons. The botanical review. 69(4): 377-440.

Rodrigues, J., Faix, O., Pereira, H. (1998) Determination of lignin content of *Eucalyptus globulus* wood using FTIR spectroscopy. Holzforschung. 52(1): 46-50.

Tomlinson, P.B. (1961) Anatomy of the monocotyledons. II. PALMAE. Oxford University Press, London.

Tomlinson, P.B. (1990) The structural biology of palms. Clarendon Press, Oxford.

Chapter 4

Cell wall characterization of leaf fibers from windmill palm and its functional implications

4.1 Introduction

Windmill palm (*Trachycarpus fortunei*) is widely distributed in China and Japan. Historically, this palm has provided a rich fiber source in the areas where it grows, for making thatched roofs, sofas, mats, mattresses, marine ropes, and traditional working tools. Wilson (1913), along with other researchers, indicated that the quality and utility of windmill palm fiber is comparable to that of the coconut coir. In addition, the windmill palm fibers are primarily collected from well-lignified leaf sheaths surrounding the stem. The *Bencao gangmu*, a Ming Dynasty (1368-1644) materia medica (Li 2008 - first edition published in 1578), showed that in the past, people were aware that windmill palm fibers were suitable for making ropes. Palm ropes could be used in wet conditions for hundreds of years without showing signs of decay. Furthermore, Zhai *et al*. (2012) described palm ropes excavated from archaeological sites, testifying the utilization of the windmill palm fibers in ancient times. In Japan, the windmill palm fiber is used to make *Tawashi*, a traditional brush, and *Houki*, a type of broom. These tools are used under a repeated cycling of wet (high moisture) and dry (low moisture) conditions which places severe stress on the fiber materials. It is worthwhile to investigate why windmill palm fibers show extraordinary properties under wet conditions.

The structure of xylem and phloem in palms has been described in many publications (Zimmermann & Tomlinson 1965; Parthasarathy 1974; Parthasarathy & Klotz 1976a, b, etc). Some authors examined structure-property relationships of coconut palm (Sudo 1980; Killmann 1983). Structural variability of vascular bundles and the

cell walls in rattan, *Calamus* spp., a climbing palm was described by Bhat *et al.* (1990). However, the cell wall structure of fibers in leaf sheaths has received little attention despite their commercial importance. In this study, author studied the cell wall structure of windmill palm fibers by transmission electron microscopy (TEM), field emission scanning electron microscopy (FE-SEM), and polarized light microscopy (PLM). At the same time, microfibril orientations in different layers of the cell wall and Klason lignin content were also investigated. The objective of the present study was not only to characterize the cell wall structure of windmill palm fiber, but also to try to understand the correlation between cell wall structure and the durability together with stability of palm fibers.

Former researchers indicated that the lignin in woody cell wall is involved in heavy electron-dense deposition after staining with potassium permanganate during TEM observation (Singh & Daniel 2001; Fromm *et al*. 2003; Lybeer & Koch 2005). The cellulose microfibrils orientation appears to be covered with lignin in different layers of the secondary wall. By acidified sodium chlorite treatment, the lignin content in the cell wall will be decreased and the microfibrils orientation in secondary wall will be clearly visible (Awano *et al*. 2002). To clarify the cellulose orientation in different cell wall layers of palm leaf fibers and to show cell wall layering with higher contrast by delignification treatment, the leaf fibers from windmill palm were stepwise delignified. The remains of fiber cell wall with different reaction intervals were examined by attenuated total reflectance Fourier transform infrared (ATR-FTIR) spectroscopic analysis for the chemical changes and TEM for the ultrastructure confirmation/determination, which was undertaken for the first time.

4.2 Cell wall structure of the windmill palm fibers

Usually, each leaf sheath is composed of an outer, middle, and inner layer, and, each layer contains fibrovascular bundles of different diameters, orientations, and locations (Zhai *et al*. 2012). The fibrovascular bundles in the middle layer were larger than those in the outer and inner layers of the leaf sheath. A fibrovascular bundle is composed of vascular tissue and fiber cap (Fig. 4.1a). The fibers in the fiber cap have

fairly thick cell walls (Fig. 4.1b). These fibers showed double rings of birefringence between crossed Nicols in semi-thin transverse sections (Fig. 4.1c). This fact was confirmed in a survey of the leaf sheath fibers in different heights of the palm. The secondary walls of the fibers contain at least two layers, an outer (S_1) and an inner one (S_2). It was noted that the S_1 near the middle lamellae showed a birefringence stronger than the S_2 near the lumen.

Figure 4.2 shows a longitudinally oblique section of the windmill palm fibers observed with PLM. It is noted that the S_2 shows strong birefringence, while the S_1 shows weak birefringence. Based on the performances of the birefringence, the microfibrils in the S_1 should have a flatter orientation to the fiber axis compared to those in the S_2. In other words, the MFA of the S_1 is larger than that of the S_2.

The electron microscopic observations were mainly restricted to the fiber walls within the fibrovascular bundles. Figure 4.3a presents the cell wall structure at the corner of three adjacent fibers. The outermost layer adjacent to the middle lamella appears thin and electron-dense, corresponding to the primary wall (P). The thickness of the primary wall is about 0.1 μm at the cell corner. The average thickness of S_1 and S_2 was measured as 0.65 μm (SD ± 0.12) and 1.28 μm (SD ± 0.30), respectively (Table 4.1). Furthermore, an S_3 in the palm fibers was absent in all electron micrographs, including observations by FE-SEM (Fig. 4.4). Figure 4.4a shows a lower magnification image of a palm fibrovascular bundle fractured in longitudinally. Most fibers showed the fractured plane of S_1. Figure 4.4b shows a higher magnification of the square inset in Fig. 4.4a. The arrows in the figure show different orientation of microfibrils in S_1 and S_2. These results obtained by both TEM and FE-SEM coincide with the PLM images showing that the secondary cell wall of windmill palm fibers comprises just two layers: S_1 (the outer layer) and S_2 (the inner layer).

In softwood and hardwood, the secondary cell wall of tracheids and fibers is composed of a three layered structure, S_1, S_2 and S_3. In contrast, both bamboo and rattan, which belong to the woody monocots, show a typical polylamellate structure (Parameswaran & Liese 1980; Bhat *et al.* 1990). According to our research, the cell wall structure of fibers from the leaf fibrovascular bundle in the windmill palm did not show

a polylamellate, but a two-layered structure (S_1 and S_2) in the secondary wall.

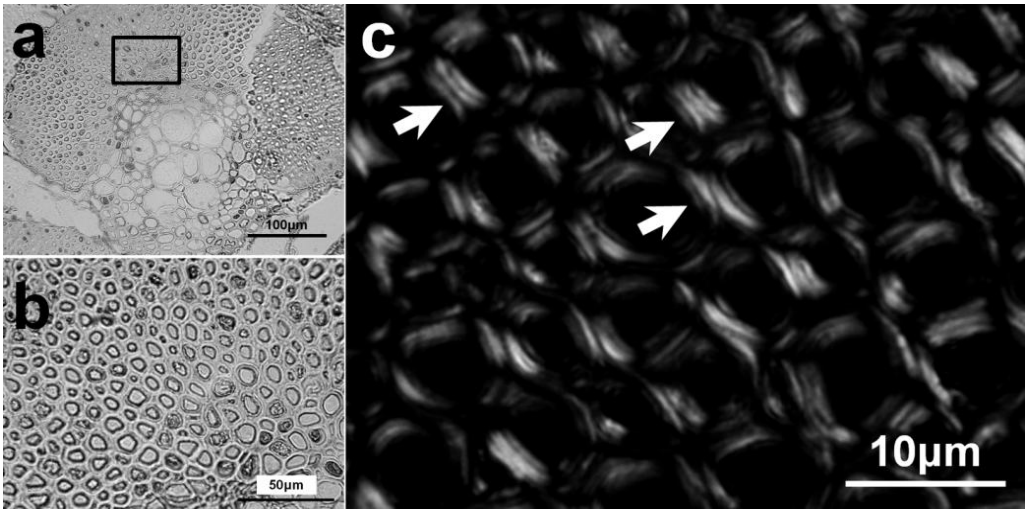

Figure 4.1 Micrographs obtained using a transmitted and polarized light microscope. **(a)** A complete fibrovascular bundle from a leaf sheath of windmill palm. **(b)** Enlargement of a part of the fiber cap in the fibrovascular bundle. **(c)** Double birefringence of the secondary wall in fibers of windmill palm. The layers near the middle lamellae show a birefringence stronger than that near the lumen (arrows) (Zhai *et al*. 2013).

Figure 4.2 Polarized light micrograph of a radial oblique section of fibers of the windmill palm with oblique angle 5°. S_1, S_2: outmost and inner layers of the secondary wall (Zhai *et al*. 2013).

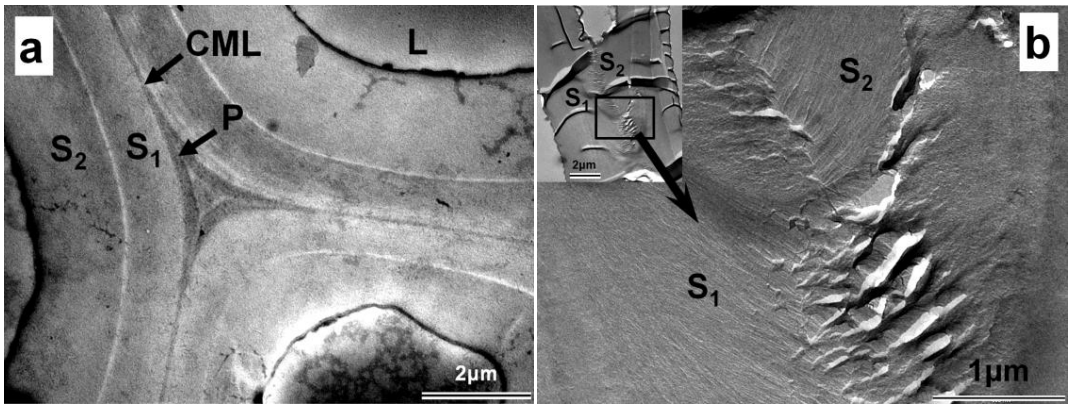

Figure 4.3 Electron micrographs of the windmill palm leaf fibers. **(a)** Transverse section of a two-layered secondary wall of windmill palm leaf fibers. **(b)** Enlargement of the fiber cell tip on the oblique section, demonstrating microfibril orientation in the two layers of the secondary wall. CML: compound middle lamella; L: lumen; P: primary wall; S_1, S_2: outmost and inner layers of the secondary wall (Zhai *et al*. 2013).

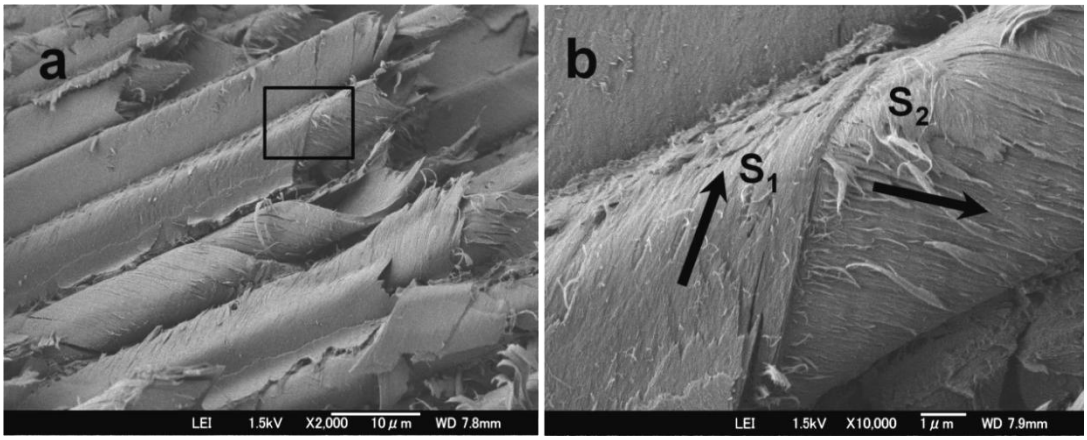

Figure 4.4 FE-SEM micrographs of the different layers of the cell walls in windmill palm leaf fibers. **(b)** Enlargement of the indicated area in **Fig. 4.4a**. The secondary wall of S_1 and S_2 is presented with clear cellulose fibrils orientations in a different layer of the secondary cell wall. The arrows indicated the direction that the microfibrils helically wind about cell lumen in cell wall (Zhai *et al*. 2013).

The S_1 layer of windmill palm fibers was thicker than in fibers/tracheids in other common plants (Table 4.1). The thickness ratio of S_1 to the whole cell wall in windmill palm fibers was 0.32, while that in *Pinus densiflora* (tracheid), *Picea abies* (tracheid), *Fagus crenata* (tracheid) and *Fagus crenata* (fiber-tracheid) it was 0.13, 0.06, 0.16 and 0.10, respectively. Consequently, the ratio of S_1 to the whole cell wall thickness in windmill palm fibers is substantially higher, making it a specific feature of these palm fibers.

4.3 Cellulose microfibril orientation and MFA in different layers

Figure 4.3b shows a TEM image obtained from an oblique ultra-thin section of a palm fiber. The low magnification image shows two different layers of the secondary wall, S_1 and S_2. An enlargement of the square inset shows both the smooth and rough surfaces of the fiber tip. If the diamond knife cuts with the microfibril orientation during sectioning, it would make a smooth surface. In contrast, if the knife cuts against the microfibril orientation, it would produce a rough surface. The opposite appearance of smooth and rough surfaces in S_1 and S_2 layers could be dependent on the different microfibril orientation in S_1 and S_2. The arrows in Figure 4.4b show the direction in which the microfibrils in S_1 and S_2 wind helically around the long axis of the cell. The figure clearly shows the microfibrils orientation of two individual layers crossed each other in a single wall. In consideration of the results obtained by PLM, TEM and FE-SEM, it is concluded that the microfibril orientation of the S_1 is in S or left-handed helix, and that of the S_2 is in Z or right-handed helix.

As shown in Table 4.2, the MFAs of S_1 and S_2 measured by PLM are 127.0° (SD ± 2.0) and 43.7° (SD ± 2.2), respectively. Our previous study (Zhai *et al*. 2012) showed that the mean MFA of windmill palm fibers obtained from X-ray diffraction diagrams was 39.5° (SD ± 2.4). Following the calculation described in the methods of the current study, the average MFA of all fibers in a fibrovascular bundle of windmill palm was 49.1° (SD ± 2.3) by X-ray diffraction method. Comparison of MFA for the secondary wall layers obtained from birefringence in PLM with that from the X-ray diagrams showed good agreement.

Table 4.2 lists the MFA of different plant species (mainly woods) as determined by the PLM, X-rays and TEM or FE-SEM. The X-ray values gave an average MFA of the whole fibrovascular bundles. In contrast, the PLM method gave MFA of the individual layers in a fiber wall. Comparing MFA of different plant species, it can be noted that the MFA of the S_1 layer of the windmill palm fibers was steeper than that of normal wood fibers and tracheids. For example, Tang (1973) measured MFA values of 80° for the S_1 layer in *Pinus virginiana*. Müller *et al.* (2002) studied the S_1 layer during secondary

Table 4.1 Comparison of cell wall thickness among different plant species. (Zhai *et al*. 2013)

Species	Cell type	Cell wall thickness (μm)				Ratio of S_1 to a whole cell wall	References
		P	S_1	S_2	S_3		
Trachycarpus fortunei	fiber	0.1	0.65 (± 0.12)	1.28 (± 0.30)	-	0.32	
Pinus densiflora	tracheid	0.06	0.31	1.93	0.17	0.13	Harada 1965a
Pinus radiata (compression wood) *	tracheid		0.67	4.48			Singh & Donaldson 1999
Pinus radiata *	tracheid		0.13	0.71	0.09		Donaldson & Frankland 2004
Fagus crenata	tracheid	0.07	0.24	0.99	0.17	0.16	Harada 1965b
	fiber-tracheid	0.07	0.51	4.32	0.10	0.10	
	axial parenchyma	0.06	0.35	0.78	0.37	0.22	
Picea abies	tracheid	0.11	0.30	3.99	0.04	0.07	Bodig & Jayne 1982
Picea abies (earlywood)	tracheid		0.12				Fengel & Stoll 1973
Picea abies (latewood)	tracheid		0.38				
Picea abies (earlywood) *	tracheid		0.33	5.11	0.11	0.06	Brändström *et al.* 2003

* data were measured from image on published papers.

Table 4.2 The MFA of different plant species as determined by the polarized light microscope and X-rays. (Zhai *et al*. 2013)

Species	Cell type	m.e.p*			X-rays	References
		S_1	S_2	S_3		
Trachycarpus fortunei	fiber	127.0° (± 2.0)	43.7° (± 2.2)	-	49.1°	
Pinus radiata	tracheid	-	-	-	22-46°	Wardrop 1951
Pinus virginiana	tracheid	78-80°	17-37°	73-77°	-	Tang 1973
Chamaecyparis obtusa	tracheid	23-26°	13-16°	20-21°	-	Kataoka *et al*. 1992 (measured by TEM micrographs)
Pinus densiflora	tracheid	22-23°	12-14°	23°	-	
Cryptomeria japonica	tracheid	19°	10-12°	20-21°	-	
Betula pendula	fiber	-	-	-	9.4-18.3°	Bonham & Barnett 2001
Eucalyptus delagatensis	fiber	-	-	-	8.5-20°	Evans & Ilic 2001
Abies sachalinensis	tracheid	-	3-14°	-	-	Abe & Funada 2005 (measured by FE-SEM micrographs)
Larix kaempferi	tracheid	-	9-21°	-	-	
Picea jezoensis	tracheid	-	17-32°	-	-	
Calamus merrillii	fiber				28.5°	Abasolo *et al.* 2000

* **m.e.p is the major extinction position** of a single cell wall, as measured with a polarized light microscope.

** data were the mean MFA of vascular bundles and parenchyma ground in bamboo culm.

wall formation in *Picea abies* using X-ray and electron micro-diffraction, and obtained MFA values of 70–90°. Furthermore, in compression wood tracheids, microfibril orientation is nearly transverse. This fact was further supported by Brändström (2004), who found that microfibril orientation of the S_1 layer in compression wood tracheids is almost always perpendicular to the fiber axis (90º) in *Picea abies* and shows less variation than normal wood tracheids.

The MFA of the S_2 layer of the windmill palm fibers was larger than that of normal wood fibers and rattan fibers. Table 4.2 lists the MFA in fibers/tracheid of selected softwood and hardwood species as well as bamboo and rattan, measured by PLM and X-ray diffraction. The average MFA of the S_2 layer in mature wood ranged between 3–37° to the fiber axis. MFAs of the S_2 layer were much larger in the juvenile wood of conifers, particularly at the base of the tree, contributing to the low stiffness of wood in the butt log (Cave & Walker 1994; Xu *et al*. 2004; Donaldson 2008). According to the authors, the stem flexibility of the juvenile tree is high compared to the mature tree. Given the increase in specific MOE, or decrease in MFA with age, researchers presume that flexible wood in the young tree is desirable to prevent wind damage (Telewski 1989, Barnett & Bonham 2004, McLean *et al.* 2011). Considering this evidence, it can be suggested that the high MFA of fibers from the leaf sheath of windmill palm is related to their high flexibility.

4.4 Ultrastructural changes of cell wall during delignification of windmill palm fibers

The lignin band at 1510 cm^{-1}, namely the aromatic skeletal vibration in lignin, was remarkably reduced by delignification in the ATR-FTIR transmission spectra (Rodrigues *et al*. 1998; Pandey & Pitman 2003, 2004; Mohebby 2005). By calculating the ratios of the relative intensities of lignin peaks at 1510 cm^{-1} against peaks at 2920 cm^{-1} (Fig. 4.5a), the changes on the relative content of lignin was clear and shown in Figure 4.5b. TEM photos of the fiber residues collected before and after various reaction times are shown in Figure 4.6.

In control sample, all layers of cell wall were little stained with uranyl acetate and

lead citrate (Fig. 4.6a). There was no strong contrast between S_1 and S_2 layers and the arrangement of microfibrils in each layer could not be observed clearly.

After 1 hour reaction, the S_1 and S_2 seemed to have more contrast to each other and the fibrillar texture could be visualized (Fig. 4.6b). The outermost layer of S_1 and innermost layer of S_2 appeared a little swollen and delignified. With high magnification observation, the dark and bright lines were observed. The dark lines were believed to be the deposition of staining materials in the spaces remained after delignification, whereas the bright lines could be cellulose microfibrils. Furthermore, the net-like structure in the cell corner (CC) and compound middle lamellae (CML) was distinct, suggesting that lignin was partially removed. By calculating the relative content of lignin analyzed by ART-FTIR spectra, 42.7% (SD±11.5%) of lignin was not removed and remained in the cell wall after 1 hour reaction (Fig. 4.5b).

With a reaction time of 3 hours, only 11.6% (SD±1.6%) of lignin was remained in the cell wall. The outer layer of S_1 was markedly separated from CML due to the progress of delignification (Fig. 4.6c). Observation with high magnification (Fig. 4.6d), the arrangement of microfibrils in secondary wall were clearly visible.

After treatment for more than 5 hours to overnight, 1.8% (SD±0.3%) of lignin was still remained in the cell walls. At this time, all fiber cells were completely separated with each other (Fig. 4.6e). All parts of cell wall including CML became electron-transparent, which means lignin was almost fully removed. It can be noted that two layers of secondary wall (S_1 and S_2) were distinguished to each other with very clear difference in the arrangement of microfibril (Fig. 4.6f). With delignification treatment, author can observe clearly S_1 and S_2 layers in the secondary wall with high contrast and the microfibril orientation also became visible. However, author has never found another layer, S_3, after the successive test of delignification in leaf fibers from windmill palm.

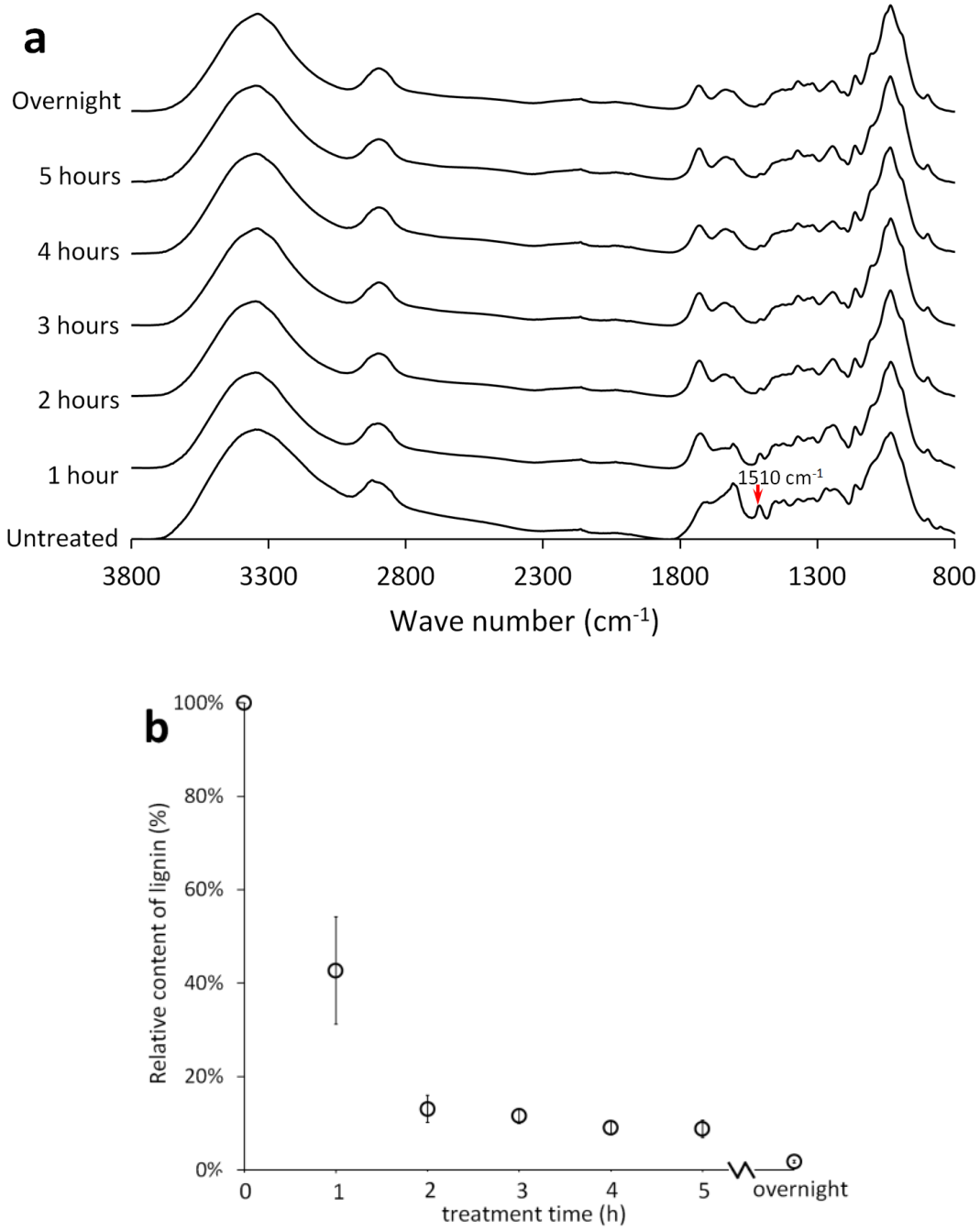

Figure 4.5 Change of IR spectrum and relative content of lignin in fiber residues after various reaction times of acidified sodium chlorite treatments (**Fig. 4.5a**). The peak at 1510 cm^{-1} represents lignin, which is for aromatic skeleton in lignin. The relative content of lignin in all treatment time was calculated from IR spectrum and shown in **Fig. 4.5b**. The circle indicates the mean value of five samples and the error bar shows the standard deviation.

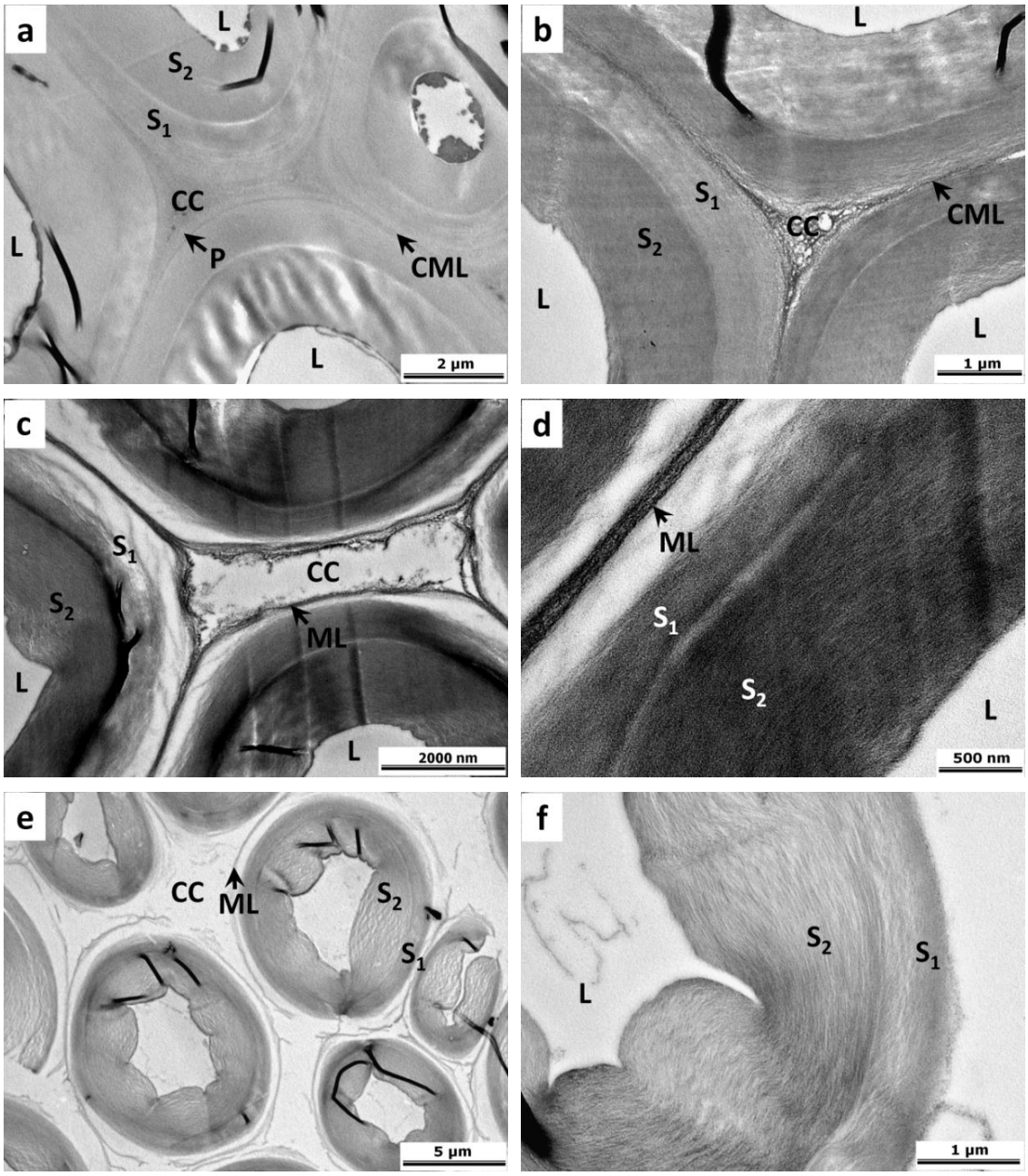

Figure 4.6 Transmission electron micrographs of transverse sections from windmill palm fiber collected after various reaction times. **(a)** control sample; **(b)** 1 hour reaction; **(c)** 3 hours reaction; **(d)** 3 hours reaction with high magnification; **(e)** overnight reaction; **(f)** overnight reaction with high magnification. CC: cell corner; CML: compound middle lamella; L: lumen; ML: middle lamella; P: primary wall; S_1, S_2: outer and inner layers of the secondary wall.

4.5 Klason lignin content of windmill palm fibers

Table 4.3 shows the Klason lignin content of fibrovascular bundles in windmill palm along with that in different other plant species. With 39.8% the Klason lignin content of windmill palm fiber was the highest among all. The lignin content in normal wood tissues was less than 30%. Thus, the lignin content in windmill palm was noticeably high compared to other plant species.

Table 4.3 Variation of Klason lignin content (wt.%) in different plant species. (Zhai *et al*. 2013)

Species	Klason lignin	References
Trachycarpus fortunei	39.8 (± 4.1)	
Quercus acutissima	21.1	Yamaguchi *et al*. 1994
Cinnamomum camphora	28.4	
Picea abies	26.9	Japan Wood Research Society 2010
Pinus sylvestris	27.3	
Abies balsamea compression wood*	38.9	Timell 1973
Picea mariana compression wood*	37.0	
Pinus resinosa compression wood*	38.8	
Larix laricina compression wood*	38.9	
Tsuga Canadensis compression wood*	39.3	
Cocos nucifera	31.9 (coir)	Van Dam *et al*. 2004
Elaeis guineensis	19.3 (stem)	Mansor & Ahmad 1990
Elaeis guineensis	27.1 (fiber)	Oi *et al*. 1994
Gossypium hirsutum (Cotton)	15.5	Ververis *et al*. 2004
Hibiscus cannabinus (Kenaf)	14.6	
Ampelocissus cavicaulis bast fiber	33.2 (±3.0)	Agu *et al.* 2012
Agave sisalana (Sisal)	12	Megiatto *et al.* 2007
Linum usitatissimum (Flax) mature fiber	6 (±1)	Gorshkova *et al.* 2000
Cannabis sativa (Hemp)	4.6	Gutiérrez *et al.* 2006
Corchorus capsularis (Jute)	13.3	del Río *et al.* 2009

* the data were lignin content rather than Klason lignin.

The chemical test in the present study gave new evidence that the fibrovascular bundles of the windmill palm showed a substantially higher lignin content than selected plant species such as softwoods, hardwoods, sisal, kenaf, jute, and hemp (Table 4.3). In plants, lignin plays a vital role, facilitating water transport and providing structural support by cementing cellulose microfibrils (Cateto *et al*. 2011). Previous researchers have mentioned that lignin has anti-biological reactions (Latham *et al*. 1978, 1979). After investigating 20 Japanese hardwoods, Yamaguchi *et al*. (1994) found that species with higher Klason lignin content had smaller enzymatic susceptibilities. Further, biodegradation experiments by white and brown rot fungi showed that compression woods which have greater concentration of lignin (ca. 40%) are more resistant to decay than normal wood, such as from *Abies balsamea*, *Picea mariana* and *Pinus strobes* (Blanchette *et al.* 1994; Timell 1973). In consideration of this evidence, it is suggested that the high Klason lignin content could give supports to the high durability of the fibrovascular bundles in windmill palm.

Furthermore, the high lignin content might be related to the mechanical behavior of windmill palm fibers. About mechanical properties, the behavior of cell walls under tensile stress is a complicated mixture of plastic and elastic deformation. Brett & Waldron (1996) mentioned that much stronger secondary walls of plant cells show only a limited ability to extend; elastic extension is small, but some plastic extension can occur. Cellulose tends to exhibit plastic rather than elastic deformation. While, Burgert (2006) showed that there was non-load bearing to the amorphous lignin during mechanical loading. The lignin might contribute to the elastic deformation, rather than plastic deformation of cell wall. As shown in our former paper (Zhai *et al.* 2012), the breaking strains of fibrovascular bundles from windmill palm was abnormally higher (40 to 55%) than sisal (3 to 7%), flax (3.3%), hemp (1.6%) and jute (1.5 to 1.8%). Although there is no statistical data for comparison, Table 3 shows the results of Klason lignin content in windmill palm (40%), sisal (12%), flax (6%), hemp (4.6%) and jute (13.3%). Eventually, the high lignin contents in windmill palm fibers could have a close relationship to the high breaking strains.

4.6 Implication of cell wall structure in fibers for palm plant biomechanics and stability

In plant cell wall, the parallel cellulose chains bind together by hydrogen bonds to form microfibrils. These high tensile strength crystalline microfibrils are the fundamental structure unit in plant cell walls and make the major contribution to the mechanical strength of the plant cell walls. The microfibrils in cell walls are encrusted by a gel matrix composed of hemicelluloses, lignin, and other carbohydrate polymers to form a bio-composite (Yu *et al*. 2008). The orientation of cellulose microfibrils is used by plants to dispose tissues in the growing phase for passive actuation of organs by humidity changes even after cell senescence. The underlying mechanism is the anisotropic deformation of cell walls upon swelling and shrinking due to the influx and efflux of water (Burgert & Fratzl 2009). Additionally, the mechanical properties of secondary cell walls depend to a large extent on the orientation of cellulose fibrils. Consequently, many materials used for structural applications are designed based on the structure of the wood cell wall. 'Spiral-winding method' (Yamauchi *et al*. 1997) is a kind of manufacturing processes for cylindrical industrial products including paper tubes and fiber reinforced plastics. The design of cylindrical LVL proposed by the above method was originated from the wood fiber cell wall structure.

Figure 4.7 presents cell wall models of conifer tracheids and palm fibers. The crossed pattern of microfibrils arrangement in longitudinal plane is a stable model to be resistant to shape deformation during environmental moisture changes. It is shown that two cells or two cell walls are cooperated with each other to maintain the stable structure of wood fiber/tracheid**.** This is because the S_1 layer is quite thin comparing with S_2 layer in wood fiber/tracheid. Fine crystalline cellulose microfibrils in S_2 layer are helically winded in Z-helix. Data from Harada (1965a; 1965b) showed that the thickness ratio of S_1: S_2 is 1:6. While in the palm fiber model, it can be notified that only one cell already have functional properties equivalent to two tracheids. In palm fiber cell wall, both S_1 and S_2 layers are thick and the cellulose microfibrils in S_1 layer trace an S-helix and those in S_2 a Z-helix. The thickness ratio of S_1: S_2 is 1:2. In windmill palm fiber, the cell wall structure with well ordered cellulose microfibrils has

positive effect on its stability during environment changing. The experimental data to clarify the mechanism of cell wall model from palm fiber will be a worthy topic for further exploration.

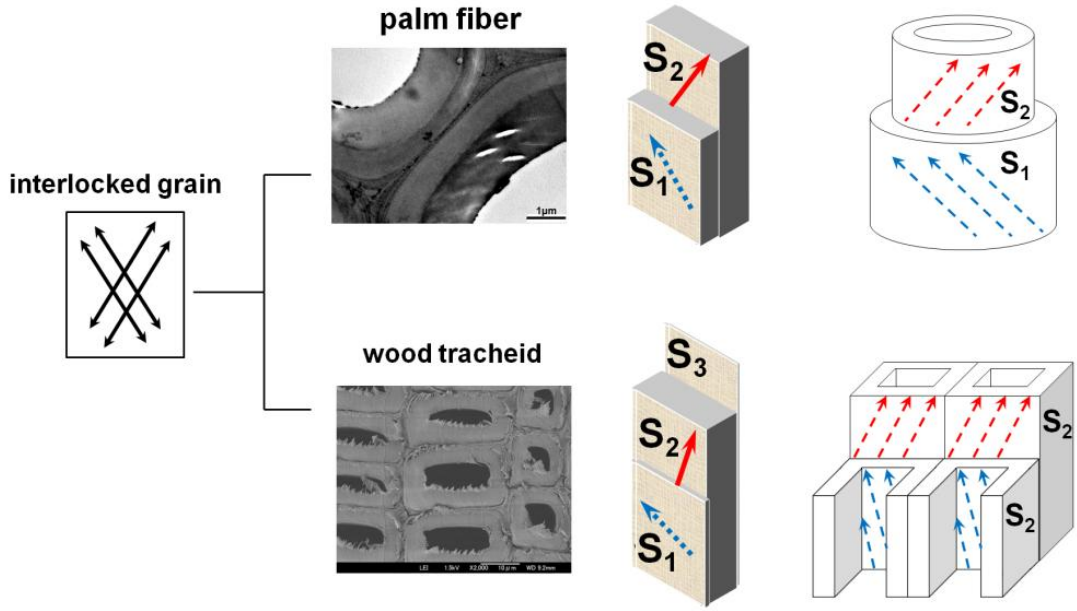

Figure 4.7 Diagram showing the cell wall models of palm fiber and tracheid (from Japanese cedar, *Cryptomeria japonica*), with cellulose microfibrils orientations in cell wall layers. The arrow lines indicate the microfibrils orientation. In single palm fiber, the cellulose microfibrils in S_1 layer trace an S helix and in S_2 is a Z helix, which makes crisscross structure in single cell. While, in conifer tracheid only S_2 layer shows a Z helix. This indicates two cell cooperation is necessary for making stable crisscross structure.

4.7 Summary

In daily life, palm fibers have been widely used to make different products such as *Tawashi* (a type of traditional-style brush used in Japan), *Houki* (brooms), and ropes with excellent durability/stability. By observing the ultra-structural and chemical features, the cell wall structure of windmill palm fibers appeared different from that of common fibers/tracheids of hardwoods and softwoods, and even from bamboo and rattan. In case of the windmill palm fiber, the secondary wall comprises just two layers (outer and inner ones) with a crossed orientation of cellulose microfibrils in a single cell

wall. The ratio of the S_1 to the whole cell wall thickness of the windmill palm fibers was much higher than that of fibers/tracheids in softwood and hardwood. The MFA of the S_1 layer of the windmill palm fibers was steeper and MFA of S_2 was larger compared to that of normal wood fibers and tracheids. Further, the fibrovascular bundles of windmill palm showed a high lignin content. These evidences could help to explain the high durability/stability and large elastic extension of windmill palm fibers.

4.8 References

Abasolo, W.P., Yoshida, M., Yamamoto, H., Okuyama, T. (2000) Microfibril angle determination of rattan fibers and its influence on the properties of the cane. Holzforschung. 54(4): 437-442.

Abe, H., Funada, R. (2005) Review - The orientation of cellulose microfibrils in the cell walls of tracheids in conifers. IAWA J. Vol. 26(2): 161-174.

Agu, C.V., Njoku, O.U., Chilaka, F.C., Okorie, S.A., Agbiogwu, D. (2012) Physico-chemical characterization of lignocellulosic fibre from *Ampelocissus cavicaulis*. Inter. J. Basic & App. Sci. 12(3): 68-77.

Awano, T., Takabe, K., Fujita, M. (2002) Xylan deposition on secondary wall of *Fagus crenata* fiber. Protoplasma. 219: 106-115.

Barnett, J.R., Bonham, V.A. (2004) Cellulose microfibril angle in the cell wall of wood fibres. Biol Rev. 79(2): 461-472.

Bhat, K.M., Liese, W., Schmitt, U. (1990) Structural variability of vascular bundles and cell wall in rattan stem. Wood Sci. Technol. 24(3): 211-224.

Blanchette, R. A., Obst, J. R., Timell, T. E. (1994) Biodegradation of compression wood and tension wood by white and brown rot fungi. Holzforschung. 48(1): 34-42.

Bodig, J., Jayne, B.A. (1982) Mechanics of wood and wood composites. Van Nostrand Reinhold, New York.

Bonham, V.A., Barnett, J. R. 2001. Fiber length and microfibril angle in silver birch (*Betula pendula* Roth). Holzforschung 55(2): 159-162.

Brändström, J. (2004) Microfibril angle of the S1 cell wall layer of Norway spruce compression wood tracheids. IAWA J. 25(4): 415-423.

Brändström, J., Bardage, S. L., Daniel, G., Nilsson, T. (2003) The structural organization of the S1 cell wall layer of Norway spruce tracheids. IAWA J., Vol. 24(1): 27-40.

Brett, C., Waldron, K. (1996) Physiology and biochemistry of plant cell walls (2nd Edition). Chapman & Hall, London.

Burgert, I. (2006) Exploring the micromechanical design of plant cell walls. Am. J. Bot. 93(10): 1391-1401.

Burgert, I., Fratzl, P. (2009) Plants control the properties and actuation of their organs through the orientation of cellulose fibrils in their cell walls. Integra Comp Biol 49(1): 69-79.

Cateto, C.A., Barreiro, M.F., Rodrigues, A.E., Belgacem, M.N. (2011) Kinetic study of the formation of lignin-based polyurethanes in bulk. React. Func. Polym. 71(8): 863-869.

Cave, I.D., Walker, J.C.F. (1994) Stiffness of wood in fast-grown plantation softwoods: The influence of microfibril angle. For. Prod. J. 44(5): 43-48.

del Río, J.C., Rencoret, J., Marques, G., Li, J., Gellerstedt, G., Jiménez-Barbero, J., Martínez, A.T., Gutiérrez, A. (2009) Structural characterization of the lignin from jute (*Corchorus capsularis*) fibers. J Agric Food Chem. 57(21): 10271-10281.

Donaldson, L. (2008) Microfibril angle: Measurement, variation and relationships – A review. IAWA J. 29(4): 345-386.

Donaldson, L., Frankland, A. (2004) Ultrastructure of iodine treated wood. Holzforschung. 58(3): 219-225.

Evans, R., Ilic, J. (2001) Rapid prediction of wood stiffness from microfibril angle and density. Forest Prod. J. 51(3): 53-57.

Fengel, D., Stoll, M. (1973) Variation in cell cross-sectional area, cell-wall thickness and wall layers of spruce tracheids within an annual ring. Holzforschung 27: 1-7.

Fromm, J., Rockel, B., Lautner, S., Windeisen, E., Wanner, G. (2003) Lignin distribution in wood cell walls determined by TEM and backscattered SEM techniques. J. Struct. Biol. 143: 77-84.

Gorshkova, T.A., Salnikov, V.V., Pogodina, N.M., Chemikosova, S.B., Yablokova, E.V.,

Ulanov, A.V. (2000) Composition and distribution of cell wall phenolic compounds in flax (*Linum usitatissimum* L.) stem tissues. Ann Bot. 85(4): 477-486.

Gutiérrez, A., Rodríguez, I. M., del Río, J.C. (2006) Chemical characterization of lignin and lipid fractions in industrial hemp bast fibers used for manufacturing high-quality paper pulps. J Agric Food Chem. 54: 2138-2144.

Harada, H. (1965a) Ultrastructure and Organization of Gymnosperm Cell Walls. In: Côté WA (ed) Cellular Ultrastructure of Woody Plants. Syracuse University Press, New York, pp. 215-233.

Harada, H. (1965b) Ultrastructure of Angiosperm Vessels and Ray Parenchyma. In: Côté WA (ed) Cellular Ultrastructure of Woody Plants. Syracuse University Press, New York, pp. 235-249.

Japan Wood Research Society. (2010) Wood Chemistry. Bun Eido, Tokyo. pp.164-165. [In Japanese]

Kataoka, Y., Saiki, H., Fujita, M. (1992) Arrangement and superimposition of cellulose microfibrils in the secondary walls of coniferous tracheids. Mokuzai Gakkaishi. 38(4): 327-335.

Killmann, W. (1983) Some physical properties of the coconut palm stem. Wood Sci. Technol. 17(3): 167-185.

Latham M.J., Brooker, B.E., Pettipher, G.L., Harris, P.J. (1978) Adhesion of *Bacteroides succinogenes* in pure culture and in the presence of *Ruminococcus flavefaciens* to cell wall in leaves of perennial ryegrass (*Lolium perene*). Appl. Environ. Microbiol. 35(6): 1166-1173.

Latham M.J., Hobbs, D.G., Harris, P.J. (1979) Adhesion of rumen bacteria to alkali-treated plant stems. Ann Rech Vet. 10: 244-245.

Li, S. (2008) Bencao gangmu (1578) – compendium of material medica. Science and Technology Publishing, Shanghai. [In Chinese]

Lybeer, B., Koch, G. (2005) Lignin distribution in the tropical bamboo species *Gigantochloa levis*. IAWA J. 26(4): 443-456.

Mansor H., Ahmad, A.R. (1990) Carbohydrates in the oil palm stem and their potential use. J. Trop. Forest Sci. 2(3): 220--226.

McLean, J.P., Zhang, T., Bardet, S., Beauchêne, J., Thibaut, A., Clair, B., Thibaut, B. (2011) The decreasing radial wood stiffness pattern of some tropical trees growing in the primary forest is reversed and increases when they are grown in a plantation. Ann. For. Sci. 68: 681-688.

Megiatto, J. D., Houreau, W., Gardrat, C., Frollini, E., Castellan, A. (2007) Sisal fibers: Surface chemical modification using reagent obtained from renewable source, characterization of hemicellulose and lignin as model study. J Agric Food Chem. 55(21): 8576-8584.

Mohebby, B. (2005) Attenuated total reflection infrared spectroscopy of white-rot decayed beech wood. Int. Biodeter. Biodegr. 55(4): 247-251.

Müller, M., Hori, R., Itoh, T., Sugiyama, J. (2002) X-ray microbeam and electron diffraction experiments on developing xylem cell walls. Biomacromolecules 3(1): 182-186.

Oi S., Matsuzaki, K., Tanaka, T., Iizuka, M., Taniguchi, M., Prasertsan, P. (1994) Effect of steam explosion treatment on enzymatic hydrolysis of palm cake and fiber as solid wastes and natural resources. J. Ferment. Bioeng. 77(3): 326-328.

Pandey, K.K., Pitman, A.J. (2003) FTIR studies of the changes in wood chemistry following decay by brown-rot and white-rot fungi. Int. Biodeter. Biodegr. 52(3): 151-160.

Pandey, K.K., Pitman, A.J. (2004) Examination of the lignin content in a softwood and a hardwood decayed by a brown-rot fungus with the acetyl bromide method and Fourier transform infrared spectroscopy. J. Polym. Sci., Part A: Polym. Chem. 42(10): 2340-2346.

Parameswaran, N., Liese, W. (1980) Ultrastructural aspects of bamboo cells. Cellulose Chem. Technol. 14: 587-609.

Parthasarathy, M.V. (1974) Ultrastructure of phloem in palms. I. Mature sieve elements and parenchyma elements. Protoplasma. 79: 59-91.

Parthasarathy, M.V., Klotz, L. H. (1976a) Palm ‘wood’ I. Anatomical aspects. Wood Sci. Technol. 10: 215-229.

Parthasarathy, M.V., Klotz, L. H. (1976b) Palm ‘wood’ II. Ultrastructural aspects of

sieve elements, tracheary elements and fibres. Wood Sci. Technol. 10: 247-271.

Rodrigues, J., Faix, O., Pereira, H. (1998) Determination of lignin content of *Eucalyptus globulus* wood using FTIR spectroscopy. Holzforschung. 52(1): 46-50.

Singh, A.P., Daniel, G. (2001) The S2 layer in the tracheid walls of *Picea abies* wood: Inhomogeneity in lignin distribution and cell wall microstructure. Holzforschung. 55(4): 373-378.

Singh, A. P., Donaldson, L. A. (1999) Ultrastructure of tracheid cell walls in radiata pine (*Pinus radiata*) mild compression wood. Can. J. Bot. 77(1): 32-40.

Sudo, S. (1980) Some anatomical properties and density of the stem of coconut palm (*Cocos nucifera*), with consideration for pulp quality. IAWA Bull. n.s. 1: 161-171.

Tang, R.C. (1973) The microfibrillar orientation in cell wall layers of Virginia pine tracheids. Wood Sci. 5: 181-186.

Telewski, F.W. (1989) Structure and function of flexure wood in *Abies fraseri*. Tree Physiol 5(1): 113-121.

Timell, T.E. (1973) Studies on opposite wood in conifers Part I: Chemical composition. Wood Sci. Technol. 7(1): 1-5.

van Dam, J.E.G., van den Oever, M.J. A., Keijsers, E.R.P. (2004) Process for production of high density high performance binderless boards from whole coconut husk. Ind. Crop Prod. 20(1): 97-101.

Ververis C., Georghiou, K., Christodoulakis, N., Santas, P., Santas, R. (2004) Fiber dimensions, lignin and cellulose content of various plant materials and their suitability for paper production. Ind. Crop Prod. 19(3): 245-254.

Wardrop, A.B. (1951) Cell wall organization and the properties of the xylem. I. Cell wall organization and the variation of breaking load in tension of the xylem in conifer stems. Australian J. Sci. Res. B-4: 391-414.

Wilson, E.H. (1913) A naturalist in western China. Doubleday, New York.

Xu, P., Donaldson, L., Walker, J., Evans, R., Downes, G. (2004) Effects of density and microfibril orientation on the vertical variation of low-stiffness wood in radiata pine butt logs. Holzforschung. 58(6): 673-677.

Yamaguchi, A., Shimizu, K., Fujii, T. (1994) Chemical characterization of twenty

Japanese hardwoods in relation to the effect of autohydrolysis. Mokuzai Gakkaishi. 40(11): 1208-1213.

Yamauchi, H., Shoho, S., Yang, P., Kawai, S., Sasaki, H. (1997) Manufacture of cylindrical LVL by spiral-winding method I: Effect of interlocked-plies on the tensile Young's modulus. Mokuzai Gakkaishi 43: 747-753. [In Japanese]

Yu, H., Liu, R., Shen, D., Wu, Z., Huang, Y. (2008) Arrangement of cellulose microfibrils in the wheat straw cell wall. Carbohydr Polym 72: 122-127.

Zhai, S., Li, D., Pan, B., Sugiyama, J., Itoh, T. (2012) Tensile strength of windmill palm (*Trachycarpus fortunei*) fiber bundles and its structural implications. J. Mater. Sci. 47(2): 949-959.

Zhai, S., Horikawa, Y., Imai, T., Sugiyama, J. (2013) Cell wall characterization of windmill palm (*Trachycarpus fortunei*) fibers and its functional implications. IAWA J. 34(1): 20-33.

Zimmermann, M. H., Tomlinson, P. B. (1965) Anatomy of the palm *Raphis excelsa* I. Mature vegetative axis. J. Arnold. Arb. 46: 160-178.

Chapter 5

Cell wall ultrasturcture of fibers in palm leaf-sheath fibrovascular bundles

5.1 Introduction

In softwood and hardwood, the secondary cell wall of tracheids and fibers is composed of a three-layered structure, S_1, S_2 and S_3. In contrast, the woody monocots, such as bamboo and rattan, show a typical polylamellate structure (Parameswaran & Liese 1980; Bhat *et al*. 1990). Abdul Khalil *et al*. (2006, 2008) mentioned that the cell wall structure of fibers from coconut coir, oil palm frond and empty fruit bunch consisted of primary layer (P) and secondary layers (S_1, S_2 and S_3). They thought cell wall structure of these species is similar to that of the wood cell wall reported by Harada and Côte (1967). According to our former research (Zhai *et al*. 2013), the cell wall structure of leaf sheath fibers from the windmill palm showed neither a three-layered structure, nor a polylamellate structure, but a two-layered structure (S_1 and S_2) in the secondary wall. The present research was aimed to confirm that the two-layered structure in the secondary wall is common feature among different palm fibers, which are located outside of palm stem including palm leaf and fruits fibers. Author surveyed leaf sheath fibers of 20 different palm species. The cell wall characteristics of all fibers were investigated by both polarized light microscopy (PLM) and transmission electron microscopy (TEM).

5.2 Polarized light microscopic observation of leaf fibers in different palm species

A leaf fiber bundle of palm is composed of a fiber cap and vascular tissue with variations in shape and localization. The fibers in the fiber cap have fairly thick cell wall. The double rings of birefringence were always found in the transverse sections of palm

leaf fiber walls between crossed Nicols.

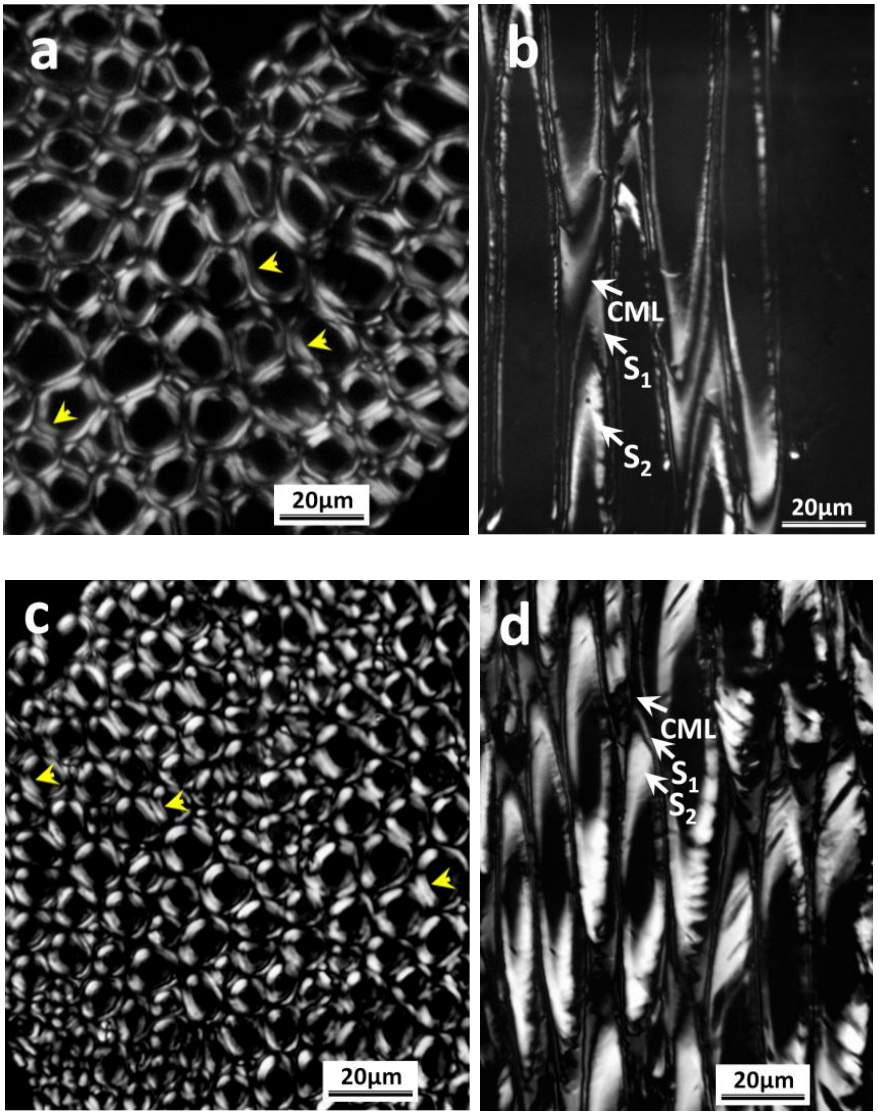

Figure 5.1 Polarized light micrographs of a transverse (a, c) and longitudinally oblique section (b, d) of fibers in leaf vascular bundles from coconut palm (*Cocos nucifera*, a & b) and oil palm (*Elaeis guineensis*, c & d). **a & c**: Arrowheads point out the double birefringence of the secondary wall indicating the presence of two layers in fibers. The S_1 layer near middle lamellae always shows a birefringence stronger than S_2 near the lumen. **b & d**: The 'black zone' in between S_1 and S_2 layers might be an overlapping area of microfibrils with different helices orientation, namely s-helix of S_1 layer and z-helix of S_2 layer. S_1, S_2: outer and inner layers of the secondary wall. CML: compound middle lamellae.

Figure 5.1 show examples from coconut palm (*Cocos nucifera*) and oil palm (*Elaeis guineensis*) leaf fibers. The double rings of birefringence indicated that the secondary wall of the leaf fibers was consisted of at least two layers, an outer (S_1) and inner one (S_2). It was noted that the S_1 near the middle lamellae showed a birefringence stronger than the S_2 near the lumen (Fig. 5.1 a & c).

Based on the performances of the birefringence, the microfibrils in the S_1 should have a flatter orientation to the fiber axis compared to those in the S_2. Figure 5.1 b & d shows a longitudinally oblique section of the coconut and oil palm fibers. The 'black zone' in between S_1 and S_2 layers might be an overlapping area of microfibrils with different helices orientation, namely s-helix of S_1 layer and z-helix of S_2 layer. This fact was confirmed in the leaf fibers from all palm species examined in the present research.

5.3 Cell wall structure of the leaf fibers in different palm species

The electron microscopic observations were mainly restricted to the fiber walls within the vascular bundles. Figure 5.2 presents the cell wall structure of leaf fibers in different palm species. The outermost layer adjacent to the middle lamella (ML) appears thin and electron-dense, corresponding to the primary wall (P). Some primary walls in fibers were clearly presented in the cell corner (CC), but others were difficult to distinguish from middle lamella, which were named as compound middle lamellae (CML). The secondary wall was consisted of only two layers in all palm leaf fibers, which are the outer (S_1) and inner layer (S_2). An S_3 layer in the leaf fibers was absent in all electron micrographs among different palm species.

The average thickness of S_1 and S_2 in palm leaf fibers is illustrated in Figure 5.3 in comparison with that of wood cells. From the former publications (Parameswaran & Liese 1980; Bhat *et al*. 1990), it is noted that bamboo and rattan fibers have multiple layers of the secondary wall. Therefore, it was difficult to compare the thickness of each layer with palm leaf fibers. The thickness of S_1 layer in leaf fibers from the different palm species ranged from 0.31 to 0.90 μm, with a mean value of 0.57 μm. The S_1 layer of leaf fibers from different species was thicker than that of tracheids/fibers in wood. Furthermore, the ratio of S_1 to the whole cell wall thickness in palm fibers was higher

than that of wood cells. In case of S_2 layer, its thickness ranged from 0.44 to 3.43 μm, with a mean value of 1.86 μm. Compared with the thickness of S_2 layer in tracheid from *Picea abies* (3.99 μm) and fibers from *Fagus crenata* (4.32 μm), the S_2 layer of palm fibers was remarkably thinner than wood cells. Interestingly, coconut leaf fibers had an S_1 (0.40 ± 0.04 μm) and S_2 (0.44 ± 0.23 μm) layers with similar thickness, same features can be found in EM photos from other publications (Abdul Khalil *et al*. 2006), while Abdul Khalil *et al*. believed the presence of S_3 layer in coconut coir fibers.

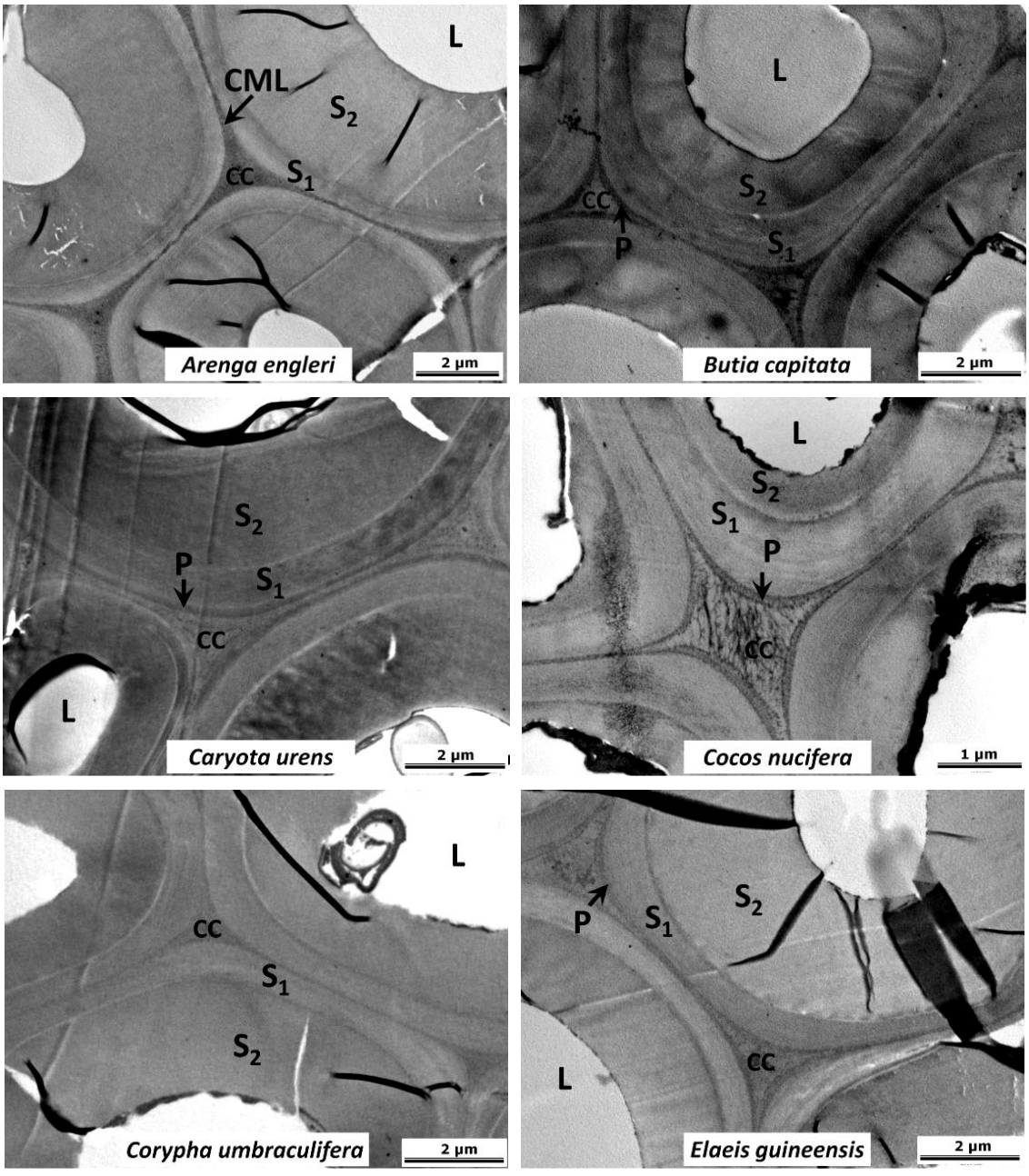

Figure 5.2 Electron micrographs of the leaf fibers from different palm species.

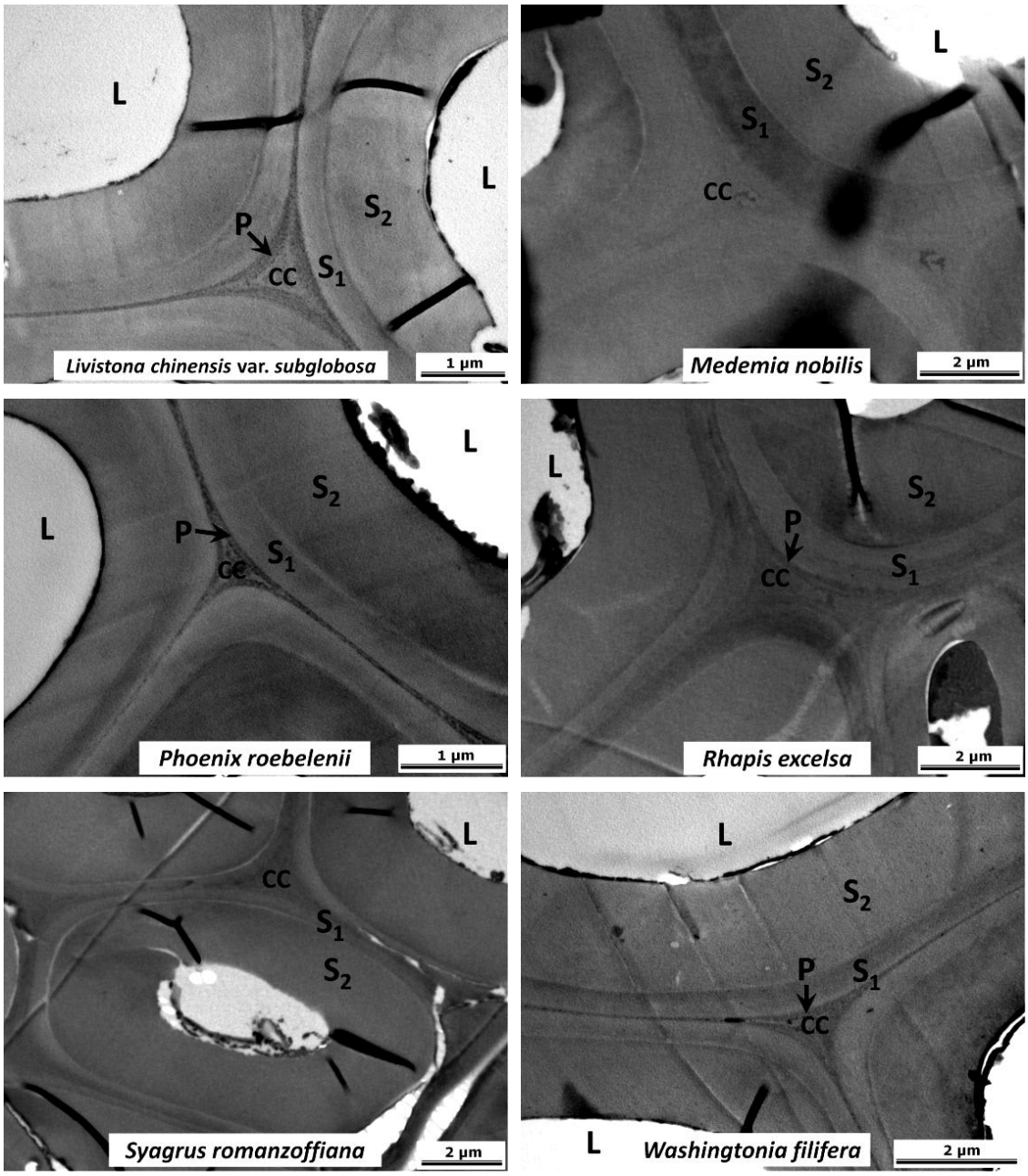

Figure 5.2 (Continued) Electron micrographs of the leaf fibers from different palm species. CC: cell corner; CML: compound middle lamellae; L: lumen; P: primary wall; S_1, S_2: outer and inner layers of the secondary wall.

Palm species - fiber	thickness (μm) S_1 (μm)	±SD	S_2 (μm)	±SD
Butia capitata	0.65	0.07	1.45	0.19
Cocos nucifera	0.40	0.04	0.44	0.23
Syagrus romanzoffiana	0.31	0.07	2.26	0.38
Elaeis guineensis	0.47	0.09	1.88	0.39
Medemia nobilis	0.89	0.15	1.78	0.39
Phoenix dactylefera	0.49	0.12	2.77	0.82
Phoenix roebilenii	0.37	0.99	0.99	0.22
Phoenix rupicola	0.70	0.16	2.00	0.45
Arenga engleri	0.57	0.11	3.43	0.64
Arenga sp.	0.68	0.13	3.08	0.53
Caryota maxima	0.58	0.09	2.18	0.41
Caryota monostachya	0.58	0.06	1.82	0.39
Caryota urens	0.90	0.13	2.50	0.35
Corpha umbraculifera	0.67	0.12	2.13	0.47
Sabal umbraculifera	0.69	0.17	1.79	0.34
Washingtonia filifera	0.40	0.07	1.55	0.36
Livistona chinensis	0.57	0.09	1.20	0.23
Livistona chinensis var. *subglobosa*	0.38	0.08	1.10	0.12
Trachycarpus fortunei	0.51	0.18	0.89	0.18
Rhapis excelsa	0.62	0.13	1.86	0.35

Wood species	S_1 (μm)	S_2 (μm)	S_3 (μm)	Reference
Pinus densiflora - tracheid	0.31	1.93	0.17	Harada 1965a
Pinus radiata - tracheid	0.13	0.71	0.09	Donaldson & Frankland 2004
Picea abies - tracheid	0.30	3.99	0.04	Bodig & Jayne 1982
Fagus crenata - tracheid	0.24	0.99	0.17	Harada 1965b
Fagus crenata - fiber tracheid	0.51	4.32	0.10	
Fagus crenata - axial parenchyma	0.35	0.78	0.37	

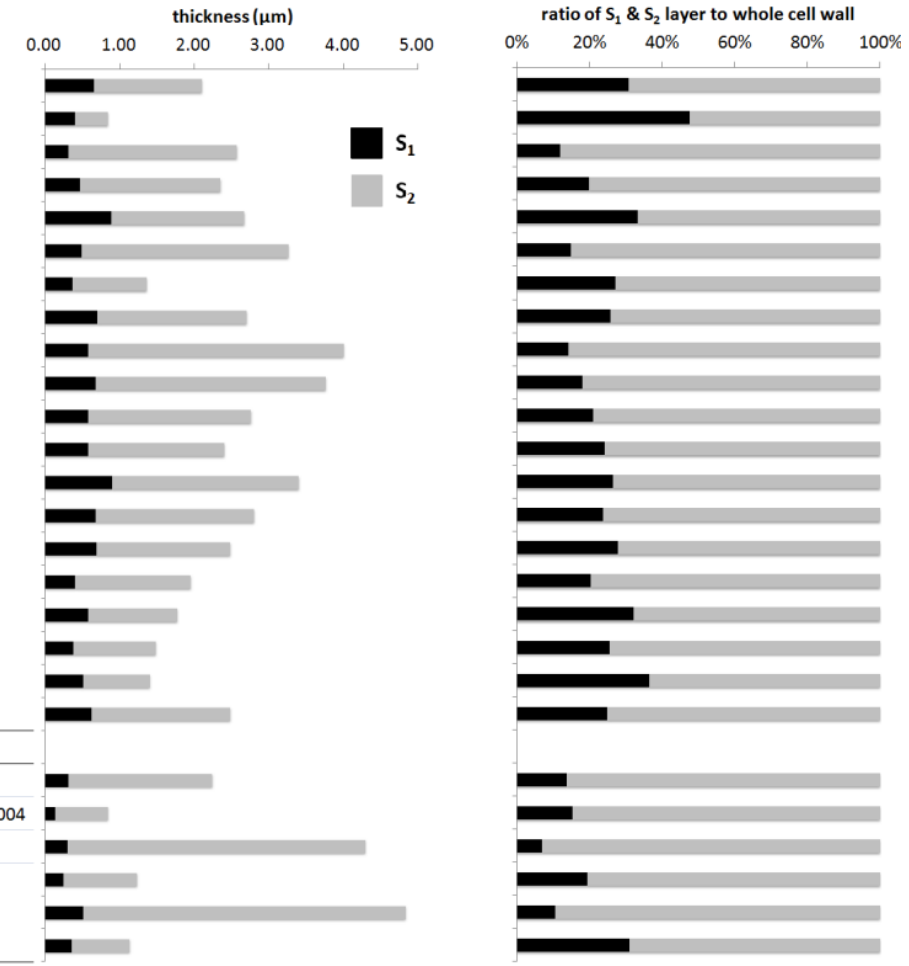

Figure 5.3 Illustration of cell wall thickness among different palm species, and its comparison with wood species. The order of palm species refers to the phylogenetic classification of palm family (Dransfield *et al*. 2008; Tomlinson *et al*. 2011).

5.4 Summary

After investigating the cell wall structure of leaf fibers from 20 different palm species by light and electron microscopy, it was confirmed that the secondary wall consisted of only two layers, S_1 and S_2. The occurrence of S_3 layer claimed in fibers from leaf part of coconut palm and oil palm (Abdul Khalil *et al*., 2006, 2008) was not confirmed in leaf fibers of 18 palm species examined in the present investigation. Therefore, it was concluded that the two-layered structure of S_1 and S_2 was the specific character in palm leaf fibers different from other monocotyledons (such as bamboo and rattan) and wood.

5.5 References

Abdul Khalil, H.P.S., Siti Alwani, M., Mohd Omar, A.K. (2006) Chemical composition, anatomy, lignin distribution, and cell wall strucuture of Malaysian plant waste fibers. Bioresources. 1: 220-232.

Abdul Khalil, H.P.S., Siti Alwani, M., Ridzuan, R., Kamarudin, H., Khairul, A. (2006) Chemical composition, morphological characteristics, and cell wall structure of Malaysian oil palm fibers. Polym. Plast. Technol. Eng. 47: 273-280.

Bhat, K.M., Liese, W., Schmitt, U. (1990) Structural variability of vascular bundles and cell wall in rattan stem. Wood Sci. Technol. 24: 211-224.

Dransfield, J., Uhl, N.W., Asmussen, C.B., Baker, W.J., Harley, M.M., Lewis, C.E. (2008) Genera Palmarum. The evolution and classification of palms. Kew Publishing, Royal Botanic Gardens, Kew, UK.

Harada, H., Côte, W.A. (1967) Cell wall organization in the pit border region of softwood tracheids. Holzforschung. 21: 81-85.

Parameswaran, N., Liese, W. (1980) Ultrastructural aspects of bamboo cells. Cellulose Chem. Technol. 14: 587-609.

Tomlinson, P.B., Horn, J.W., Fisher, J.B. (2011) The anatomy of palms. Oxford University press, New York.

Zhai, S., Horikawa, Y., Imai, T., Sugiyama, J. (2013) Cell wall characterization of windmill palm (*Trachycarpus fortunei*) fibers and its functional implications.

IAWA J. 34: 20-33.

Chapter 6

Tensile properties of windmill palm fibrovascular bundles and its structural implications

6.1 Introduction

Palmae (Arecaceae) is an important taxon of the monocotyledon and plays an essential role in the daily lives of millions of people in tropical and subtropical regions (Tomlinson 1961, 1990; Whitmore 1977; Essig & Dong 1987; Pei *et al*. 1991). The properties and commercial utilization of palms are dependent on their structural and mechanical characteristics. There are many publications on the oil palm (*Elaeis guineensis*), the wine palm (*Caryota urens*), and the coconut palm (*Cocos nucifera*), etc. (Hartley 1967; Dassanayake & Sivakadachcham 1972; Harries 1978; Satyanarayana *et al*. 1982; Sreenivasan *et al*. 1996; Sreekala *et al*. 1997, 2002; Hill & Abdul Khalil 2000; Matthes *et al*. 2001; Jacob *et al*. 2004; Abu-Sharkh *et al*. 2005). However, the windmill palm (*Trachycarpus fortunei*), which is the most common species in East Asia and is distributed throughout temperate and tropical zones, has yet to be thoroughly investigated. The recent work of Windsor-Collins *et al*. (2008) obtained data on the resistance to torsion versus the shape factor of petioles taken from *T. fortunei*. Insight has thus been gained into the mechanical behavior of the *T. fortunei* palm petioles. Windmill palm fibers have mainly been used for making thatch, marine rope, and traditional raincoats. According to the *Bencao gangmu*, a Ming Dynasty (1368–1644) meteria medica (Li 2008), people living long ago already knew that windmill palm fibers were well-suited for making rope that could be used in wet conditions for hundreds of years without showing signs of decay. Archeological excavations (Nanjing Municipal Museum 2006; Itoh *et al*. 2008) (Fig. 6.1) have indeed validated such claims.

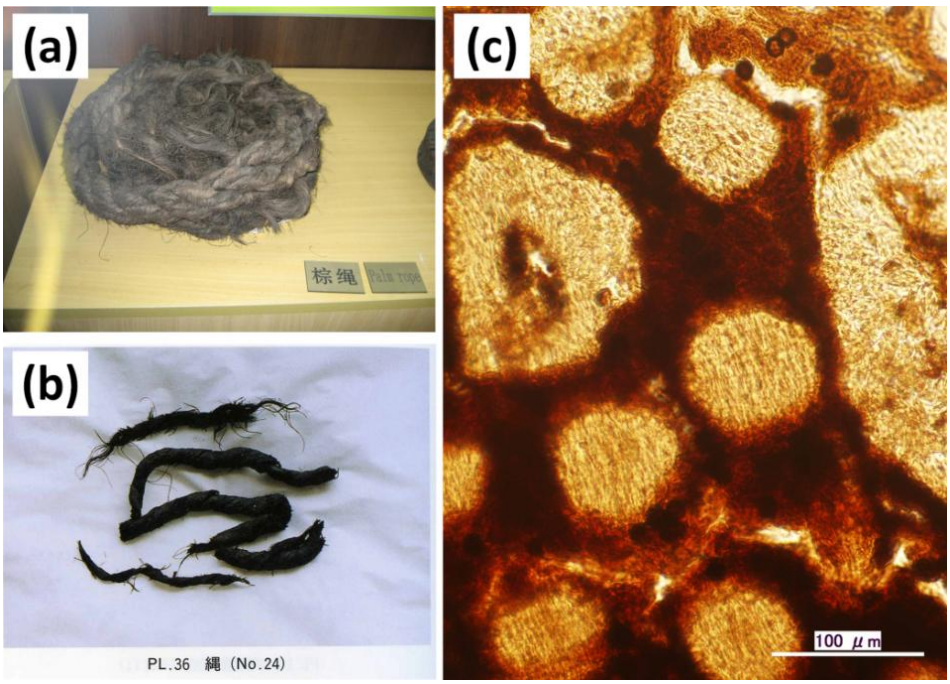

Figure 6.1 Objects excavated from archeological sites testifying to utilization of windmill palm fibers in ancient times: **(a)** windmill palm fiber rope more than 8 cm in diameter from a Ming Dynasty (1368-1644) shipyard site, **(b)** rope recovered from the seabed off Takashima Island, where the Yuan Dynasty (1279-1368) fleets of Kublai Khan sank, **(c)** cross section of Takashima Island rope fibers, identified as being windmill palm fibers (Zhai *et al*. 2012).

Although leaves originate from the stem, fibers for utilization are usually collected from the well-lignified leaves surrounding the windmill palm stem, rather than from the stem. The windmill palm stem is surrounded by many layers of leaves and the fibrovascular bundles in a leaf sheath are separated from each other when the parenchyma tissue disintegrates as the fibrovascular bundles mature and lignify (Fig. 6.2). The fibrovascular bundles in a leaf provide a good model for understanding the physical properties (or strength) of the windmill palm. On the contrary, it is absolutely impossible to measure the physical strength of intact fibrovascular bundles distributed in the palm stem. However, it can be estimated fairly precisely by measuring the physical properties (or strength) of fibrovascular bundles in the leaf sheath. Therefore, these estimations not only contribute to the utilization of the palm stem but also may lead to an understanding of the physical properties of the whole stem.

Figure 6.2 Photographs of windmill palm showing lignified fibrovascular bundles in leaf and stem: **(a)** windmill palm stem surrounded by many layers of leaf sheaths (at a height of 1.5 m), **(b)** one leaf sheath taken from a windmill palm, **(c)** windmill palm stem after all leaves have been pilled. (Zhai *et al*. 2012)

In general, the mechanical properties of plant fibers derive from such physical, chemical, and morphological characteristics as crystalline structure of cellulose, density, cellulose content, microfibril orientation, and fibrovascular bundle diameter. Satyanarayana *et al*. (1982) tested fibers from various parts of the coconut tree. Zhang *et al*. (1994) measured the tensile strength of some natural fibers such as jute and wood. Subsequently, Munawar *et al*. (2007) investigated physical and mechanical properties of fibers from several nonwoody plants. They compared tensile strength to fibrovascular bundle diameter. According to these papers, the tensile strength of fibrovascular bundles with a small diameter was larger than that of fibrovascular bundles with a larger diameter. Why do natural fibers show such a characteristic? If the characteristics of fibrovascular bundles are the same, the tensile strength of bundles of different diameters should be the same. Until now no clear answer to this question has been given. Meanwhile, the structure and mechanics of the fiber caps of different types of vascular bundles from the Mexican fan palm (*Washingtonia robusta*) were studied (Rüggeberg *et al*. 2008; 2009). It was found that gradients in stiffness appeared across the fiber caps in the center of the trunk, whereas stiffness remained high across the caps in the periphery of the trunk. This was attributed to the anatomy of the fiber caps of three different types of vascular bundles.

This chapter focuses on mechanical properties resulting from the internal structure of windmill palm fibers. The influence of anatomical structure variations and ultrastructure differences in windmill palm fibers are discussed. New evidence was obtained demonstrating why small fibrovascular bundles, as compared to large ones, show high tensile strength and high Young's modulus.

6.2 Structure of fibrovascular bundles

The difference in the diameters of the fibrovascular bundles from both transverse and longitudinal sections of the celloidine embedded samples was observed. The fibrovascular bundles in the middle layer were larger than those in the outer and inner layers (Figure 6.3).

A series of statistical data obtained using a digital optical microscope showed that the fibrovascular bundles in the middle layer had a mean diameter of 418.0 μm, while those of the bundles in the inner and outer layers were 202.1 and 342.5 μm, respectively. The divergence of diameter in fibrovascular bundles taken from different layers is shown in Fig. 6.4. Literature showed that Sisal aggregates (*Agava sisalana*) was 100–400 μm in diameter (Carr *et al*. 2006); the typical diameter of coir fibrovascular bundles from the coconut palm (*Cocos nucifera*) was about 200 μm (Martinschitz *et al*. 2008). Satyanarayana *et al*. (1982) measured the diameters of the coconut palm tree's fibrovascular bundles, and they also separated the fibrovascular bundles into three groups a thick group, a thin group and a middle group—which were located in one sheet of leaf sheath. According to their paper, the diameter of the thick group's fibrovascular bundles was 1100–1600 μm, while those of the thin and middle groups' fibrovascular bundles were 300–600 and 300–1000 μm. Comparing these data with our results, it can be noticed that fibrovascular bundles in the outer layer of our definition corresponded to the middle group, the middle layer to the thick group, and the inner layer to the thin group.

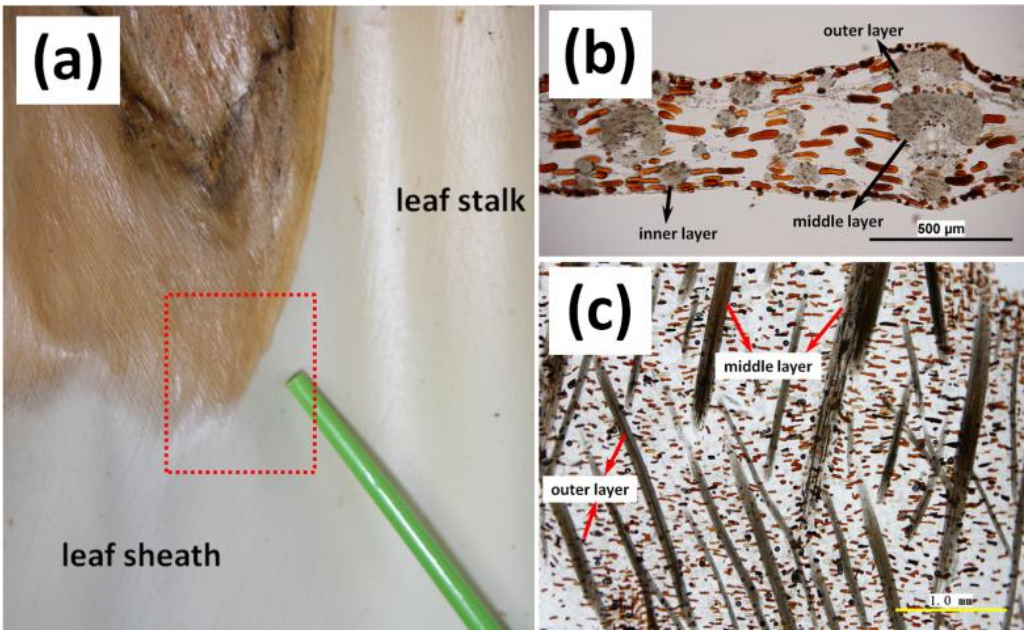

Figure 6.3 (modified images based on Fig. 3.1c, 3.6, 3.11) Layered arrangement of fibrovascular bundles in one sheet of leaf sheath: **(a)** sample of unlignified leaf sheath for celloidine embedding, **(b)** transverse section of leaf sheath, **(c)** longitudinal section of leaf sheath. (Zhai *et al*. 2012)

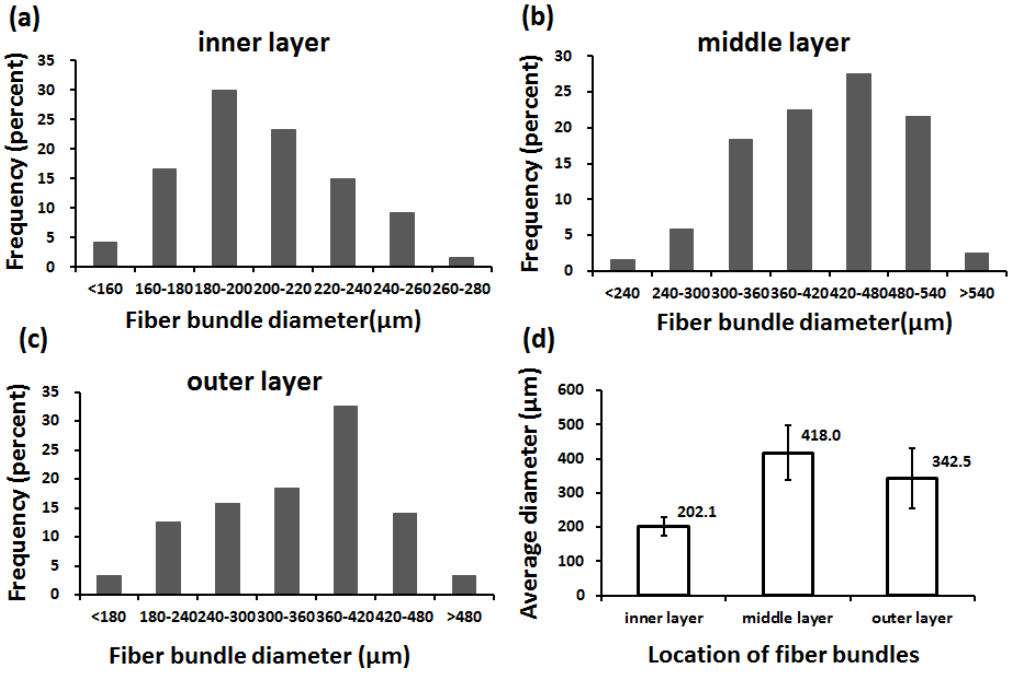

Figure 6.4 Diameter distributions of fibrovascular bundles among three layers in one sheet of leaf sheath. Fibrovascular bundles from inner layer **(a)**, middle layer **(b)** and outer layer **(c)** with remarkable difference in average diameter **(d)**. (Zhai *et al*. 2012)

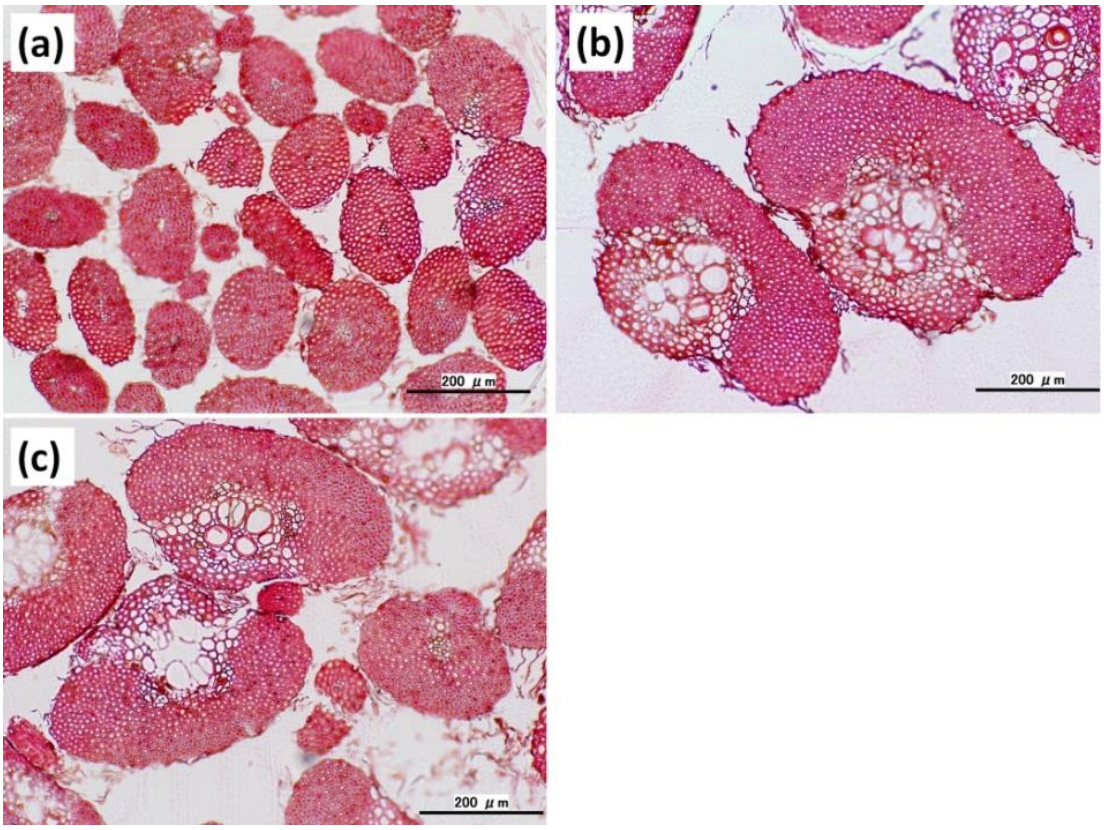

Figure 6.5 Transverse sections of fibrovascular bundles taken from inner **(a)**, middle **(b),** and outer layers **(c)** of one sheet of leaf sheath, showing vessels and phloem tissue accompanied by fibers in each fibrovascular bundle. (Zhai *et al*. 2012)

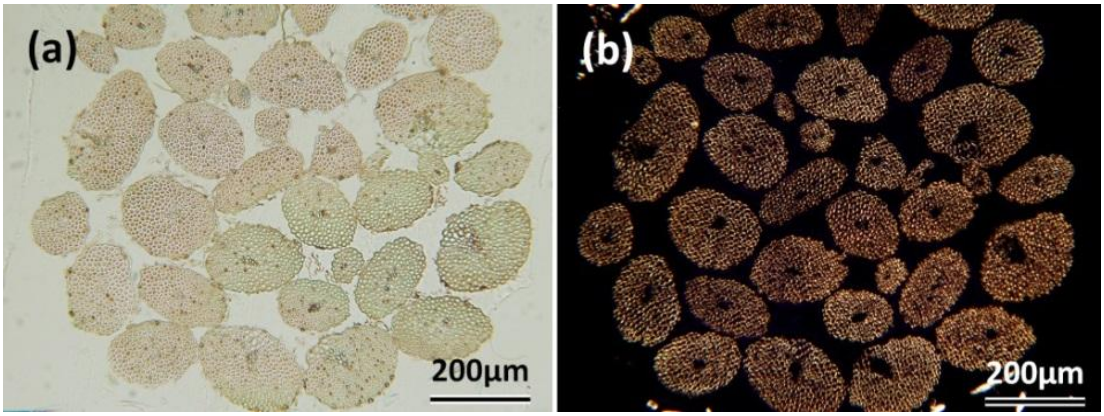

Figure 6.6 Transverse sectional image of fibrovascular bundles in the inner layer observed by transmitted- **(a)** and polarized-light **(b)**. The noticeable dark region near the center of each fibrovascular bundle in **(b)** is the area occupied by vessels and phloem tissue. (Zhai *et al*. 2012)

When focusing on one fibrovascular bundle, the transverse sections of the safranin-stained fibrovascular bundles clearly revealed lignified tissue. The fibrovascular bundles in the inner layer were almost completely composed of fibers (Fig. 6.5 a), while the fibrovascular bundles in the middle and outer layers showed clear vessels and phloem tissue occupying substantial amount of their transverse sectional area (Fig. 6.5 b, c). Figure 6.5 also shows that S_F was the largest in the middle layer, followed by the outer and inner layers. At the same time, S_V was also the largest in the middle layer followed by the outer and inner layers, although it was not easy to observe S_V in fibrovascular bundles from the inner layer.

Figure 6.6a shows a transverse sectional image of the fibrovascular bundles in the inner layer as observed by transmitted-light microscope. When the same fibrovascular bundles were observed under polarized-light, the amount of vessels and phloem tissue could be clearly seen as a dark region near the center of each individual fibrovascular bundle (Fig. 6.6b). It was clear that fibrovascular bundles consisted of a large number of fibers and a negligible amount of vessels and phloem tissue. The evidence indicates that no fibrovascular bundle consists only of fibers. Even fibrovascular bundles with a small diameter also have vessels and phloem tissue.

Table 6.1 Fiber characters in different layers of one sheet leaf sheath taken from windmill palm (Zhai *et al*. 2012)

Layers in leaf sheath	**Inner**	**Middle**	**Outside**
Area occupied by fibers (S_F) ($100\mu m^2$)	~193	~715	~589
Area occupied by vessels and phloem (S_V)($100\mu m^2$)	~13	~358	~279
Number of fibers in one bundle	~160	~840	~590
Fiber diameter (μm)	10.4 (±0.4)	9.5 (±0.5)	10.1 (±0.4)
Fiber wall thickness (μm)	2.2 (±0.16)	2.1(±0.25)	2.1(±0.16)

With this in mind, S_F and S_V in a fibrovascular bundle, the number of fibers in a bundle, fiber diameter, and fiber wall thickness were measured in each of the three layers of one leaf sheath. Table 6.1 shows that the mean fiber diameter and fiber wall thickness were similar in fibrovascular bundles taken from different layers of one leaf

sheath. In this case, the characteristics of a single fiber are almost the same among the different fibrovascular bundles.

6.3 Mechanical properties

After tensile strength was tested, typical stress–strain curves for fibrovascular bundles from different layers in one leaf sheath were obtained (Fig. 6.7). The curves showed a yielding, followed by plastic deformation until breakage from 30 to 60% strain for fibrovascular bundles. The line of breakage in the fibrovascular bundles mainly ran perpendicular to the direction of the tensile stress.

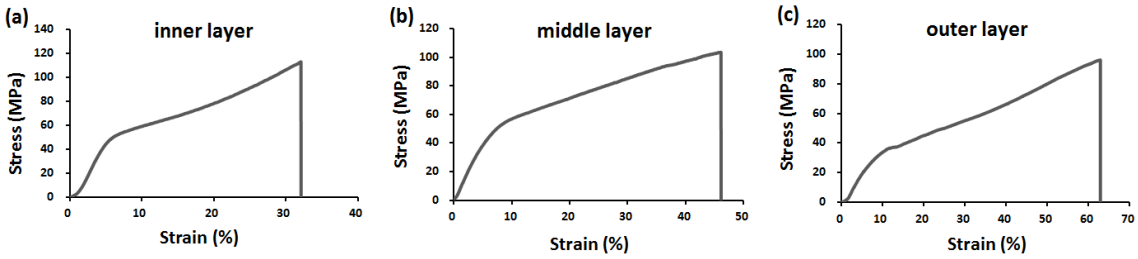

Figure 6.7 Typical stress-strain curves of fibrovascular bundles taken from the inner **(a)**, middle **(b)**, and outer **(c)** layers of one sheet of windmill palm leaf sheath. (Zhai *et al*. 2012)

Table 6.2 The mechanical properties of fibrovascular bundles in different layers of one sheet leaf sheath taken from windmill palm (*n*=70, test speed=1mm/min) (Zhai *et al*. 2012)

Layer	**Max. Load (kN)**			**Young's Modulus (MPa)**		
	Mean	S.D.	C.V. (%)	Mean	S.D.	C.V. (%)
Inner	3.45	0.83	24.18	1249.70	382.58	30.61
Middle	12.25	4.02	32.77	778.93	332.67	42.71
Outer	7.40	2.79	37.62	817.11	388.57	47.55
Layer	**Tensile strength (MPa)**			**BRK.% Strain (%)**		
	Mean	S.D.	C.V. (%)	Mean	S.D.	C.V. (%)
Inner	113.72	25.11	22.08	39.52	15.69	39.70
Middle	91.93	32.42	35.27	55.20	20.77	37.62
Outer	82.08	30.23	36.83	47.52	22.32	46.98

Table 6.2 presents the mechanical properties of fibrovascular bundles in the three different layers taken from one windmill palm leaf sheath. Although the diameter of the inner layer was the smallest among the three layers, the fibrovascular bundles from the inner layer showed higher tensile strength (113.72 MPa) and Young's modulus (1249.70 MPa) than did the fibrovascular bundles in the other layers. The plots of the mechanical properties of tensile strength and Young's modulus versus diameter of fibrovascular bundle from the windmill palm are shown in Figure 6.8. With these plots, the variation in mechanical properties can be evaluated. They show a decreasing trend in tensile strength and Young's modulus with an increasing trend in the diameter of the fibrovascular bundles in the three different layers and vice versa.

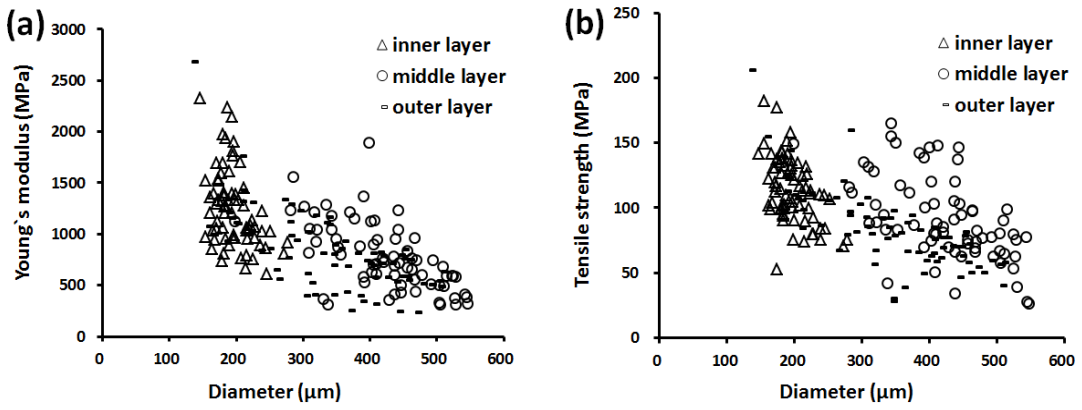

Figure 6.8 Relationship between diameter and Young`s modulus (a), and diameter and tensile strength (b) of windmill palm fibrovascular bundles. (Zhai *et al*. 2012)

Munawar *et al*. (2007) investigated the physical and mechanical properties of seven non-woody plant fibrovascular bundles such as abaca leaf fibers, pineapple leaf fibers, sisal leaf fibers, coconut husk fibers, and bast fibers of kenaf and ramie. The authors concluded that the tensile strength and Young's modulus showed a decreasing tendency with an increase in the diameter of the fibrovascular bundles. Some previous papers have also described a similar relationship between diameter and tensile strength as well as Young's modulus in flax fibers and jute fibers (Baley 2002; Zhang *et al*. 1994). However, no clear reasons were presented in these papers to explain these phenomena. A similar phenomenon in the fibrovascular bundles taken from the

windmill palm was confirmed in this study. Especially, the inner-layer fibrovascular bundles, which had the smallest diameters, showed the highest tensile strength among the three layers. If the fiber cell walls were thicker and the fiber diameters smaller in the inner layer than in the other layers, such a phenomenon as mentioned above could occur. However, as the results in Table 6.1 show, both fiber diameter and fiber cell wall thickness did not show any substantial differences in the three layers of fibrovascular bundles. Therefore, instead of anatomical features, more attention was paid to the different tissue types involved in a vascular bundle: that is, fibers, vessels, and phloem tissue.

The presence of fibers predominantly contributes to the mechanical strength of the fibrovascular bundles (or vascular bundles), while the presence of vessels and phloem tissue tends to reduce mechanical strength. Fibrovascular bundles in one sheet of leaf sheath taken from the windmill palm were divided into three layers according to their size, orientation, and location. As mentioned before, S_V was largest in the middle layer. It decreased dramatically in the inner layer of a mature leaf sheath. The vascular bundle in the inner layer of a leaf sheath did not show a substantial value of S_V.

However, the mean tensile strength and Young's modulus of the vascular bundles in the inner layer of a leaf sheath were the largest of the three different layers. Therefore, the only parameter that contributes to the mechanical properties of fibrovascular bundles was the ratio of S_V in one bundle. In the inner layer, S_V was about 1300 μm^2 and just 6–7% of one fibrovascular bundle's transverse sectional area (Table 6.1). However, S_F in the middle layer was 71500 μm^2, while S_V was 35800 μm^2. S_V increased to 33% of transverse sectional area. These findings strongly suggest that the tensile strength of a fibrovascular bundle increases in accordance with a decrease of S_V, which occurs with an increase in fibrovascular bundle diameter. Considering the structural and mechanical properties of the component cells in a fibrovascular bundle, it was found that S_V in a transverse sectional area of a fibrovascular bundle was an important factor affecting fibrovascular bundle tensile strength.

The tensile properties of various natural fibers, along with the results obtained here on windmill palm fibrovascular bundles, are summarized in Table 6.3 for better

comparison. The tensile strength and Young's modulus of windmill palm fibrovascular bundles are usual for natural fibers. The elongation at break percentage is much higher than that of the other plants referred to in Table 6.3. Composite materials having a too low elongation to break will be brittle. Therefore, the windmill palm will be a good natural resource for enhancing the strength and toughness of composite materials.

Table 6.3 Comparison of properties of windmill palm fibrovascular bundles with those of other natural fiber bundles ([a] Satyanarayana *et al*. 1982; [b] Rao *et al*. 2007; [c] Davies *et al*. 2007)

Origins	Diameter (μm)	Tensile strength (MPa)	Modulus (GPa)	BRK.%STN (%)
windmill palm leaf-sheath				
inner layer	202.1	113.72	1.25	39.5
middle layer	418.0	91.93	0.78	55.2
outer layer	342.5	82.08	0.82	47.5
Banana [b]	80-250	529-759	8-20	1-3.5
Elephant grass [b]	70-400	185	7.40	2.5
Sea-grass (*Zostera marina*) [b, c]	4.6	573±120	19.8±6.8	3.4±0.3
Flax [c]	17.8	1339±486	58±15	3.3±0.8
Hemp [c]	10-50	389	35	1.6
Jute [a, b, c]	25-200	393-773	26.5	1.5-1.8
Sisal [a, b]	7-47	350-700	9-21	3-7
coconut palm [a]				
Leaf sheath(inside top)	300-600	88.63	2.45	14.2
Leaf sheath(thick fibres)	1100-1600	115.24	4.54	4.0
Leaf sheath(middle fibres)	300-1000	91.97	3.59	6.2
Bark of the petiole	250-550	185.52	15.09	2.1
Root	100-650	157	6.2	3
Coir	100-450	131-175	4-6	15-40

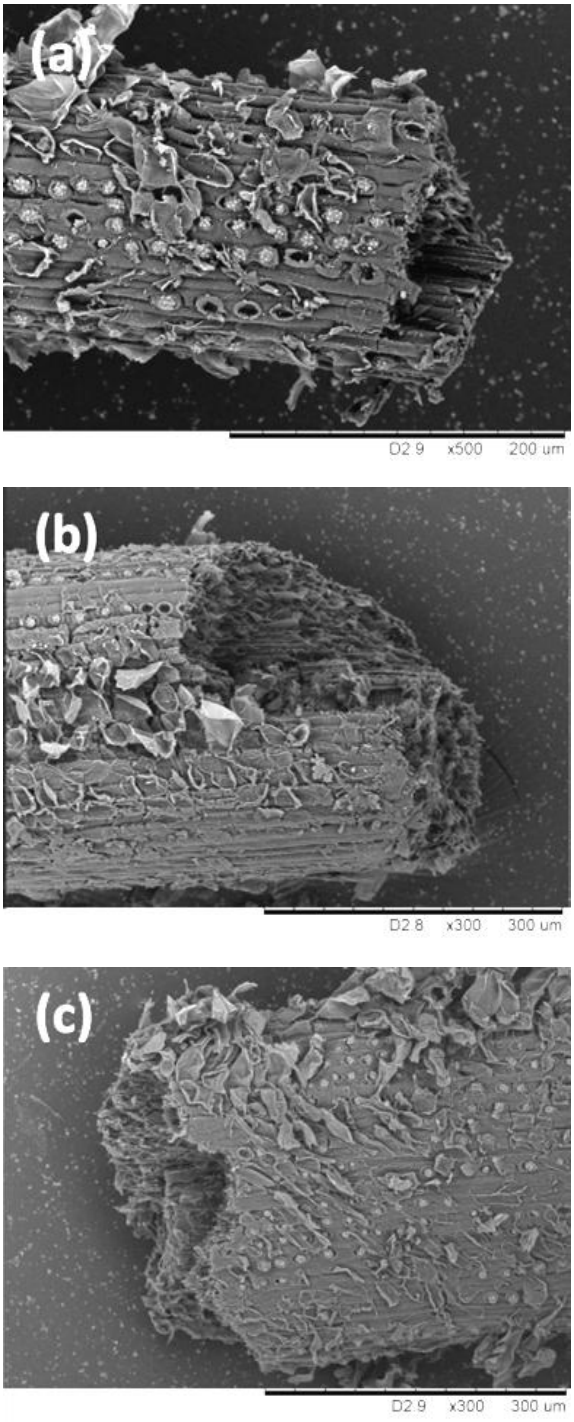

Figure 6.9 Fracture surface of fibrovascular bundles taken from inner **(a)**, middle **(b),** and outer layers **(c)** of one sheet of windmill palm leaf sheath. (Zhai *et al*. 2012)

To make sure there was zero or insignificant, slippage at normal conditions of tension, the fracture surface of broken fibrovascular bundles was observed under SEM.

In Figure 6.9, representative SEM micrographs of windmill palm fibrovascular bundles' fracture surface are presented. No epoxy resin penetrated the testing length of fibrovascular bundles—a condition that, as other researchers have mentioned (Yu *et al*. 2011),—may strengthen the mechanical properties of the fibrovascular bundles tested. The morphology of windmill palm fibrovascular bundles can also be characterized. The tubular cells are oriented parallel with the bundle axes. No specimens were found in which fibrovascular bundles were visibly pulled out in the proximity of the interface of fibrovascular bundles and epoxy resin. In the view of Martinschitz *et al*. (2008), the formation of curled triangular features is related to the fracture of individual helical cells, which indicates a specific fracture mechanism. Figure 6.10 shows the fracture surface with high magnification, the fracture of individual fiber can be clearly observed.

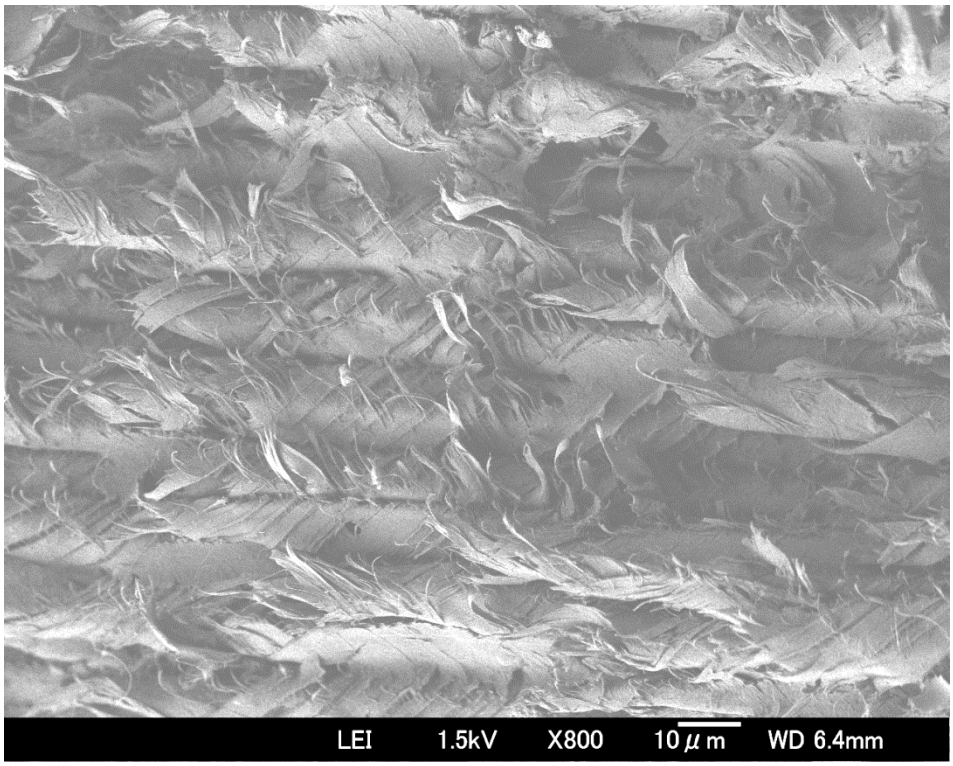

Figure 6.10 Fracture of individual fibers in one fibrovascular bundle from windmill palm leaf sheath under higher magnification.

6.4 Microfibril angle of windmill palm fibrovascular bundles and its bio-mechanics

Excluding S_V area and recalculating tensile strength only using the effective area (S_F) revealed that inner-layer fibrovascular bundles and middle-layer fibrovascular bundles have a similar degree of tensile strength. However, the tensile strength of the outer-layer fibrovascular bundles was lower, showing 127.3 MPa (Table 6.4). These data indicate that the structure of the outer-layer fibrovascular bundles might differ from that of the other two layers.

Table 6.4 Microfibril angles (MFA), relative crystallinity index (CrI) and recalculated data of fibrovascular bundles (Zhai *et al*. 2012)

Layers	MFA	CrI	$S_V/(S_V+S_F)$	Tensile strength* (MPa)
Inner	38.5	0.71	6%	171.2
Middle	37.8	0.73	33%	179.1
Outer	42.2	0.67	32%	127.3

* Excluding the S_V area and recalculating tensile strength using the effective area (S_F).

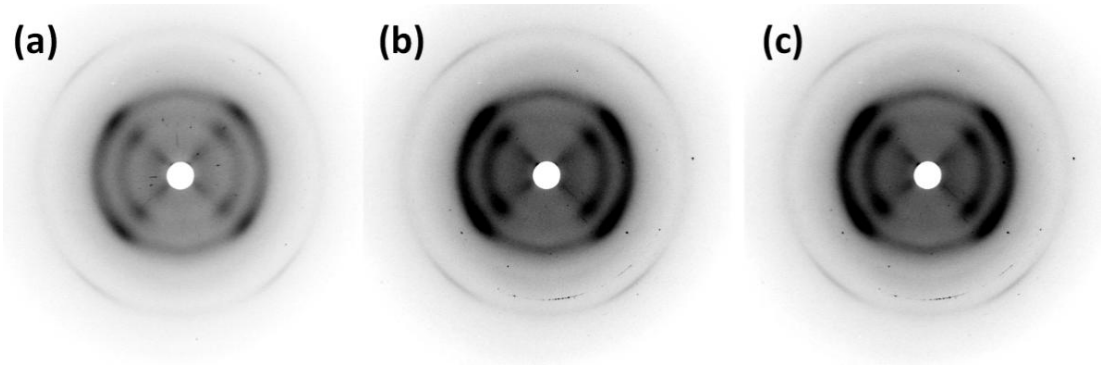

Figure 6.11 Result from WAXS on fibrovascular bundles taken from inner **(a)**, middle **(b),** and outer layers **(c)** of one sheet of windmill palm leaf sheath (Zhai *et al*. 2012).

Figure 6.11 shows the wide-angle X-ray scattering (WAXS) patterns of fibrovascular bundles in the different layers of one sheet of leaf sheath. Apparently it is difficult to detect a difference in MFA of the major cell wall layer. The data listed in Table 6.4 were obtained from profile analysis. Although there is no statistical data,

results of MFA showed opposite rank of recalculated tensile strength according to the position of fibrovascular bundles. The MFA data and tensile strength measurements for windmill palm fibrovascular bundles conformed to the same principle previously observed in wood by researchers; namely, the lower the microfibril angle, the higher the modulus of elasticity and tensile strength of both wood tissues and individual wood fibers (Cave & Hutt 1969; Reiterer *et al*. 1999; Burgert *et al*. 2002; Groom *et al*. 2002; Burgert & Fratzl 2009).

As seen in Table 6.4's list of mechanical properties, the outer layer had significantly smaller values in comparison to the other two layers. The difference is so large that the MFA could not be due only to poor mechanical properties. Other factors, such as matrix and/or cell wall architecture, also seemed to be responsible. In addition, the chemical constituents of fibrovascular bundles from the different layers of the windmill palm were measured. According to chemical analysis results, there was no significant difference in fibrovascular bundles from the different layers, which again supports the above contention that matrix and/or cell wall architecture are responsible for a fibrovascular bundle's mechanical properties.

It is interesting that the fibrovascular bundles in one sheet of leaf sheath showed different tensile strength and that MFA values also varied. A similar difference in the scales of seed-bearing pine cones was found by Dawson *et al*. (1997). A scale consists of two tissues, which differ greatly in their tensile stiffness. Pine cone scales move in response to changes in relative humidity, which results in the release of the cone's seeds. Researchers have concluded that the mechanism of the bending of the scales depends on the way in which the orientation of cellulose microfibrils controls the hygroscopic expansion of the cells. An arrangement of tissues and cells with cell walls of different orientations of cellulose fibrils can be utilized for adjusting mechanical properties and controlling specific movements of organs as shown for wood, pine cones, and wheat awns (Burgert & Fratzl 2009; Elbaum *et al.* 2007). Consequently, complex movements caused by the swelling or shrinking of cell walls are achieved by having cell wall architecture with well ordered cellulose fibrils. In the windmill palm, the varying MFA in one sheet of leaf sheath might be related to the biomechanical movements of organs,

such as development of a crossed structure and expansion of leaf sheaths.

6.5 Summary

Fibrovascular bundles taken from a mature windmill palm leaf sheath can be divided into three groups according to their size, orientation, and location in one sheet of leaf sheath: inner, middle, and outer layers. The diameter of fibrovascular bundles in the middle layer was the largest, while the diameter of those in the inner layer was the smallest. Tensile strength and Young's modulus showed a decreasing tendency with an increasing diameter of these fibrovascular bundles. S_V and S_F were measured by observing transmitted- and polarized-light photomicrographs of fibrovascular bundles from the three layers. The ratio of S_V versus transverse sectional area in the inner layer was just 6%, while that in the middle layer was 33%. These findings strongly suggest that the tensile strength of fibrovascular bundle increases in parallel with a decrease of S_V, while the presence of fibers predominantly contributes to mechanical strength. Therefore, the fibrovascular bundles in the inner layer were stronger that those in the middle layer.

Excluding S_V area and recalculating tensile strength using S_F revealed that the tensile strength of the outer-layer fibrovascular bundles was lower than that of the inner and middle layer fibrovascular bundles. The MFA data of the three layers followed the principle observed in wood; namely, that the lower the microfibril angle, the higher the tensile strength. Indeed, the varying MFA in one sheet of leaf sheath might be related to the biomechanical movements of leaf sheath in the windmill palm—a topic worthy of further exploration.

6.6 References

Abu-Sharkh, B., Rychlý, J., Matisová-Rychlá, L. (2005) Easy estimation of the progress of artificial weathering of palm fiber-polypropylene composites by chemiluminescence. J. Mater. Sci. 40(3): 613-619.

Baley, C. (2002) Analysis of the flax fibres tensile behaviour and analysis of the tensile stiffness increase. Composites Part A. 33(7): 939-948.

Burgert, I., Fratzl, P. (2009) Plants control the properties and actuation of their organs

through the orientation of cellulose fibrils in their cell walls. Integr. Comp. Biol. 49(1): 69-79.

Burgert, I., Keckes, J., Frühmann, K., Fratzl, P., Tschegg, S.E. (2002) A comparison of two techniques for wood fibre isolation - Evaluation by tensile tests on single fibres with different microfibril angle. Plant Biol. 4(1): 9-12.

Carr, D.J., Cruthers, N.M., Laing, R.M., Niven, B.E. (2006). Selected mechanical properties of sisal aggregates (*Agava sisalana*). J. Mater Sci. 41(2): 511-515.

Cave, I.D., Hutt, L. (1969) The longitudinal Young's modulus of *Pinus radiate*. Wood Sci. Technol. 3(1): 40-48.

Dassanayake, M.D., Sivakadachcham, B. (1972) The vascular skeleton of the leaf base of *Caryota urens*. Phytomorphology 22: 296-304.

Davies, P., Morvan, C., Sire, O., Baley, C. (2007) Structure and properties of fibres from sea-grass (*Zostera marina*). J. Mater. Sci. 42(13): 4850-4857.

Dawson, C., Vincent, J.F.V., Rocca, A.M.(1997) How pine cones open. Nature 390: 668.

Elbaum, R., Zaltzman, L., Burgert, I., Fratzl, P. (2007) The role of wheat awns in the seed dispersal unit. Science. 316(5826): 884-886.

Essig, F.B., Dong, Y. (1987) The Many Uses of *Trachycarpus fortunei* (Arecaceae) in China. Econ. Bot. 41(3): 411-417.

Groom, L., Mott, L., Shaler, S. (2002) Mechanical properties of individual southern pine fibers. Part I. Determination and variability of stress-strain curves with respect to tree height and juvenility. Wood Fiber Sci. 34(1): 14-27.

Harries, H.C. (1978) The evolution, dissemination and classification of *Cocos nucifera* L. Bot. Rev. 44(3): 265-319.

Hartley, C.W.S. (1967) The oil palm (*Elaeis guineensis* Jacq.). Longman Scientific and Technical, England.

Hill, C.A.S., Abdul Khalil, H.P.S. (2000) Effect of fiber treatments on mechanical properties of coir or oil palm fiber reinforced polyester composites. J. Appl. Polym. Sci. 78(9): 1685-1697.

Itoh, T., Mertz, M., Pan, B., Luo, J. (2008) Wood identification of excavated wooden artifacts in underwater site near Takashima island of Matsuura-city, second report

of the cultural properties of Matsuura-city. Report of emergency excavations following Kamizaki harbor repair works 2001 to 2002. Board of Education of Matsuura city, Nagasaki prefecture. [In Japanese]

Jacob, M., Thomas, S., Varughese, K.T. (2004) Mechanical properties of sisal/oil palm hybrid fiber reinforced natural rubber composites. Compos. Sci. Technol. 64(7-8): 955-965.

Li, S. (2008) Bencao gangmu (1578) – compendium of material medica. Science and Technology Publishing, Shanghai. [In Chinese]

Martinschitz, K.J., Boesecke, P., Garvey, C.J., Gindl, W., Keckes, J. (2008) Changes in microfibril angle in cyclically deformed dry coir fibers studied by in-situ synchrotron X-ray diffraction. J. Mater. Sci. 43(1): 350-356.

Matthes, M., Singh, R., Cheah, S.C., Karp, A. (2001) Variation in oil palm (*Elaeis guineensis* Jacq.) tissue culture-derived regenerants revealed by AFLPs with methylation-sensitive enzymes. Theor. Appl. Genet. 102: 971-979.

Munawar, S.S., Umemura, K., Kawai, S. (2007) Characterization of the morphological, physical, and mechanical properties of seven nonwood plant fiber bundles. J. Wood Sci. 53(2) : 108-113.

Nanjing Municipal Museum (2006) Ming dynasty Bao-chuan-chang Shipyard in Nanjing. Cultural Relics Publishing House, Beijing. [In Chinese]

Pei, S., Chen, S., Tong, S. (1991) Tomus 13(1): Angiospermae—Monocotyledoneae, Palme, Flora of Reipublicae Popularis Sinicae. Science Press, Beijing. [In Chinese]

Rao, K.M.M., Prasad, A.V.R., Babu, M.N.V.R., Rao, K.M., Gupta, A.V.S.S.K.S. (2007) Tensile properties of elephant grass fiber reinforced polyester composites. J. Mater. Sci. 42(9): 3266-3272.

Reiterer, A., Lichtenegger, H., Tschegg, S.E., Fratzl, P. (1999) Experimental evidence for a mechanical function of the cellulose microfibril angle in wood cell walls. Phil. Mag. A 79 (9): 2173-2184.

Rüggeberg, M., Speck, T., Paris, O., Lapierre, C., Pollet, B., Koch, G., Burgert, I. (2008) Stiffness gradients in vascular bundles of the palm *Washingtonia robusta*. Proc. R. Soc. B 275: 2221-2229.

Rüggeberg, M., Speck, T., Burgert, I. (2009) Structure–function relationships of different vascular bundle types in the stem of the Mexican fanpalm (*Washingtonia robusta*). New Phytologist 182: 443-450.

Satyanarayana, K.G., Pillai, C.K.S., Sukumaran, K., Pillai, S.G.K. (1982) Structure property studies of fibres from various parts of the coconut tree. J. Mater. Sci. 17(8): 2453-2462.

Sreekala, M.S., Kumaran, M.G., Thomas, S. (1997) Oil palm fibers: Morphology, chemical composition, surface modification, and mechanical properties. J. Appl. Polym Sci. 66(5): 821-835.

Sreekala, M.S., George, J., Kumaran, M.G., Thomas, S. (2002) The mechanical performance of hybrid phenol-formaldehyde-based composites reinforced with glass and oil palm fibres. Compos. Sci. Technol. 62(6): 339-353.

Sreenivasan, S., Bhama Iyer, P., Krishna Iyer, K.R. (1996) Influence of delignification and alkali treatment on the fine structure of coir fibres (*Cocos nucifera*). J. Mater. Sci. 31(3): 721-726.

Tomlinson, P.B. (1961) Anatomy of the monocotyledons. II. PALMAE. Oxford University Press, London.

Tomlinson, P.B. (1990) The structural biology of palms. Oxford University Press, USA.

Whitmore, T.C. (1977) Palms of Malaya. Oxford University Press, Oxford.

Windsor-Collins, A.G., Atherton, M.A., Collins, M.W., Cutler, D.F. (2008) Section properties of palm petioles, part 2: The relationship of petiole histology with the torsional rigidity of the palm, *Trachycarpus fortunei*. International Journal of Design & Nature and Ecodynamics 3(3): 190-202.

Yu, Y., Jiang, Z., Fei, B., Wang, G., Wang, H. (2011) An improved microtensile technique for mechanical characterization of short plant fibers: a case study on bamboo fibers. J. Mater. Sci. 46: 739-746.

Zhai, S., Li, D., Pan, B., Sugiyama, J., Itoh, T. (2012) Tensile strength of windmill palm (*Trachycarpus fortunei*) fiber bundles and its structural implications. J. Mater. Sci. 47(2): 949-959.

Zhang, M., Kishimoto, Y., Kawai, S., Sasaki, H. (1994) Relationship between tensile

strength of natural fibers and their sizes. Wood Res. Tech. Notes (Kyoto Univ.) 30: 32-39.

Chapter 7

Mechanical characteristics of fibrovascular bundles among different genus in palm

7.1 Introduction

The palm family (Arecaceae) consists of approximately 184 genera and about 2400 species. Most palm species are distributed in tropical and subtropical areas, particularly in tropical Asia and America, with some species in Africa (Pei *et al.* 1991; Dransfield *et al*. 2008). Some of the species have been cultivated as economically important agricultural products. Numerous palm species have been described in the literature, including coconut palm (*Cocos nucifera*), oil palm (*Elaeis guineensis*), nipa palm (*Nypa fruticans*), and others (Law *et al*. 2007; Munawar *et al*. 2007; Khalil *et al*. 2008; Tamunaidu & Saka 2011; Shinoj *et al*. 2011). However, many other common palm species are distributed throughout Asia and America, and play important roles in local areas. For instance, windmill palm (*Trachycarpus fortunei*) growing in Asia areas provides a rich source of fibrovascular bundles from the leaf-sheath parts and is known for its use in thatched roofs, sofas, mats, mattresses, marine ropes, and traditional working tools (Zhai *et al*. 2012; 2013). The Kitul palm (*Caryota urens*), growing in humid tropical Asia, is commonly cultivated in villages and is best known for the production of jaggery (a crude brown sugar) from the inflorescence in Sri Lanka. The Kitul palm provides a significant source of income for local economies (Ratnayake *et al*. 1990; de Zoysa 1992; Ashton *et al*. 1998). Furthermore, the *Corypha* palms provide raw material for palm-leaf manuscripts. Large collections of palm-leaf manuscripts are available in archives, museums, libraries, and Buddhist Gompas in India and Southeast Asia (Swarnakamal 1965; Dhawan 1995; Anupam 2002).

The widespread use of palms by humans has received much attention. The palm

family is known to have been important to past civilizations; palm remains are often excavated at archaeological sites (Morcote-Ríos & Bernal 2001; Li 2008; Tengberg 2012; Thomas *et al*. 2012).

Tomlinson *et al*. (1961; 1990; 2011) did comprehensive research on the comparative study of palm anatomy, especially on palm stem anatomy. Thomas and De Franceshi (2013) provided new descriptors for standardized description of palm stem. Some selected features of stem anatomy showed relation with the phylogenetic classification which allows specialists in archaeology and paleontology to better exploit palm fossils. Except the palm stems, the fibrovascular bundles in palm from leaf-sheath also have been widely used and many palm fiber-based products are excavated from archeological sites. For instance, the palm species mentioned before, windmill palm, Kitul palm and the *Corypha* palms, produce abundant of natural fiber resources. However, few publications have reported on the anatomical, chemical and mechanical characteristics of these fibrovascular bundles. This chapter presents the anatomical characteristics, mechanical properties, microfibril angles (MFAs), and Klason lignin contents of leaf-sheath fibrovascular bundles from 14 palm genera. This whole set of knowledge in palm leaf-sheath fibrovascular bundles could facilitate further understanding of palm fiber-based products and utilization of these widespread natural fiber resources in future.

7.2 Anatomical characteristics of palm fibrovascular bundles

The diameters of fibrovascular bundles from each palm species have remarkable differences (Fig. 7.1). The fibrovascular bundles from each palm species could be generally divided into 2 to 3 groups based on their diameters (Fig. 7.1). Tomlinson (1964) illustrated three main anatomical types of vascular bundle from coconut leaf sheath based on the size of vascular bundles. Type I vascular bundles are largest and situated abaxially; type II are intermediate diameter either pectinate with the type I strands and so occupy abaxial furrows between the ridges, or form an indistinct adaxial series; and type III are smallest and are distributed without apparent order throughout the ground tissue in coconut leaf base. These types were based on the size of

cross-sectional area in different vascular bundles. Zhai *et al*. (2012) also mentioned that the fibrovascular bundles from leaf-sheath of windmill palm can be divided into 3 groups. These groupings/classifications were based on the difference of diameters, orientations, and locations within one leaf in one palm species.

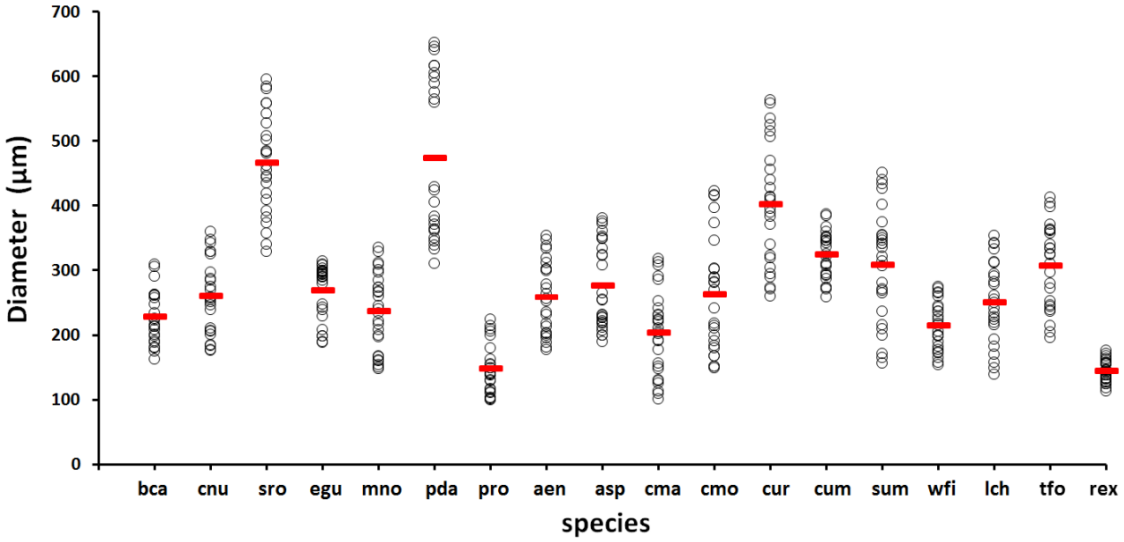

Figure 7.1 Statistic spread of the fibrovascular bundle's diameters among palm species. Open circles show original data, lines show mean diameters for the different palm species. The abbreviations presented in the figure refer to the Chapter 2.

There was a further discovery at present research to classify the fibrovascular bundles among different palm species. A fibrovascular bundle consisted equally of thick-walled sclerenchyma fibers and vascular tissue (xylem vessels and phloem tissues) (Fig. 7.2). If focusing on the largest and intermediate fibrovascular bundles, namely the type I and type II vascular bundles in Tomlinson's classification, it can be noted that the shape and localization of the vascular tissue on transverse sections of fibrovascular bundles varied among the different palm species. Figure 7.2 shows dominant (intermediate to large size in diameter) transverse-sectional images of the fibrovascular bundles for each palm species from 14 genera, taken with the same magnification.

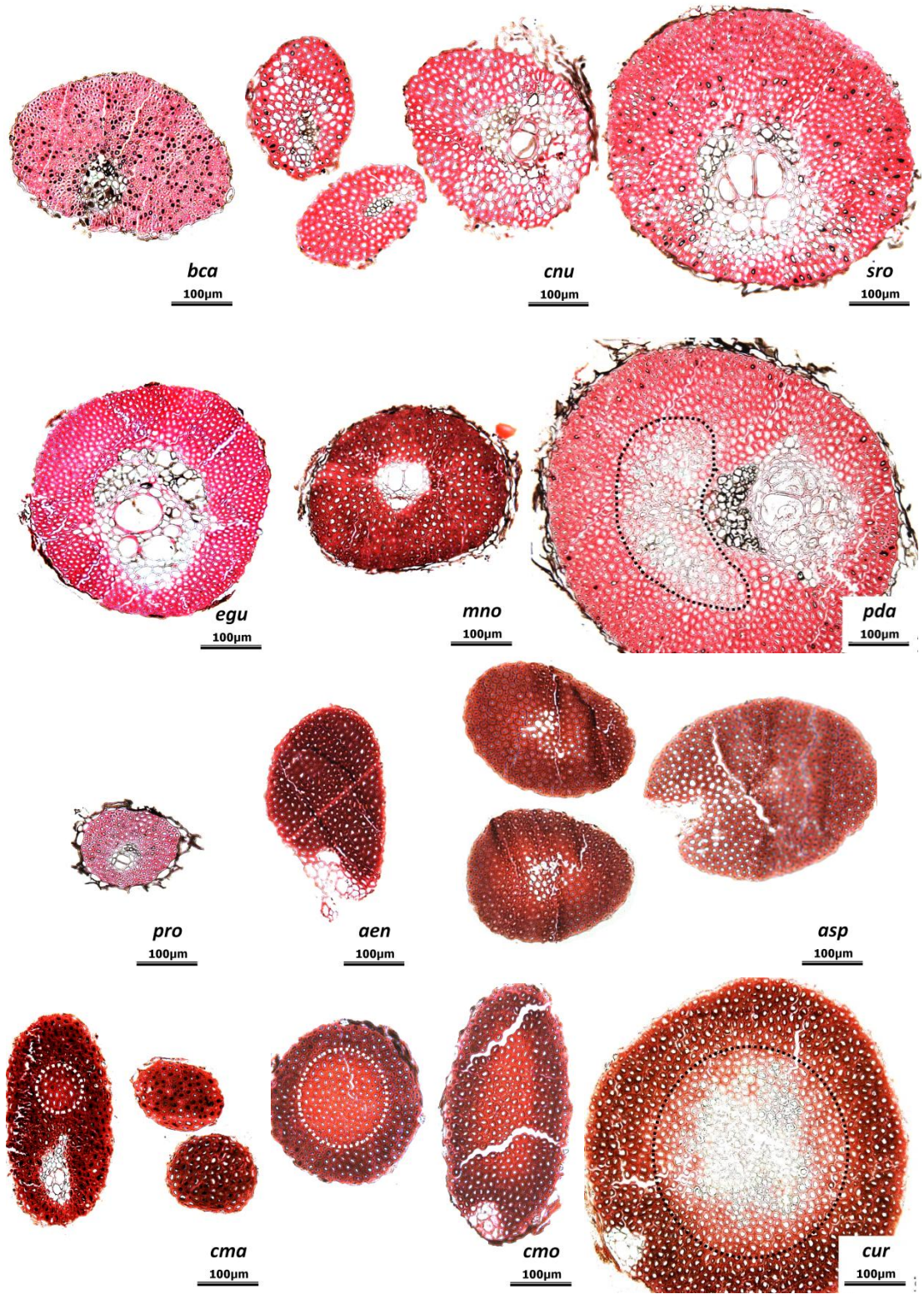

Figure 7.2 Transverse sectional images of leaf-sheath fibrovascular bundles among different palm species taken by light microscope with the same magnification. The dotted circles in *cma*, *cmo*, *cur* and *pda*, indicate the area of thin-walled fibers in fibrovascular bundles.

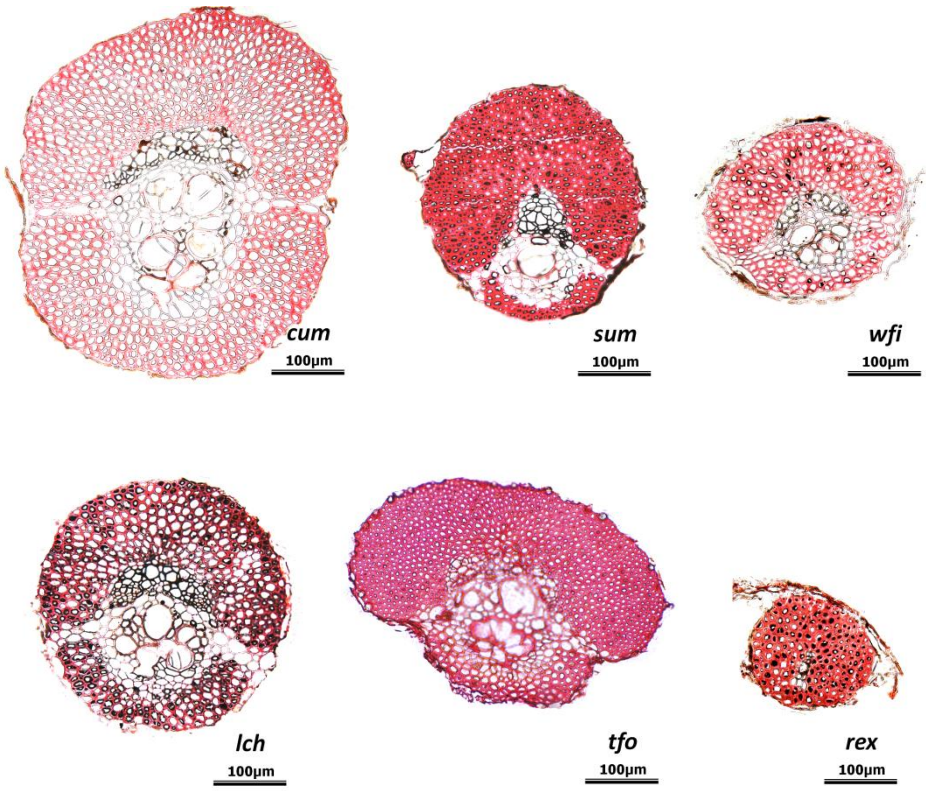

Figure 7.2 (continued).

On the basis of the anatomical differences in the vascular tissue, the palm fibrovascular bundles were classified into 3 types, A, B and C, as illustrated on the right side of Figure 7.3. The species with rounded vascular tissue located in the central region of the fibrovascular bundles were grouped into type A – vascular tissue rounded in the central region. The species in the genera *Arenga* and *Caryota* with rounded/angular vascular tissue located in the marginal region of a fibrovascular bundle were grouped into type B – vascular tissue angular in marginal region. In the remaining species, the vascular tissue was aliform in the central region; these species were grouped into type C – vascular tissue aliform in the central region (Fig. 7.3).

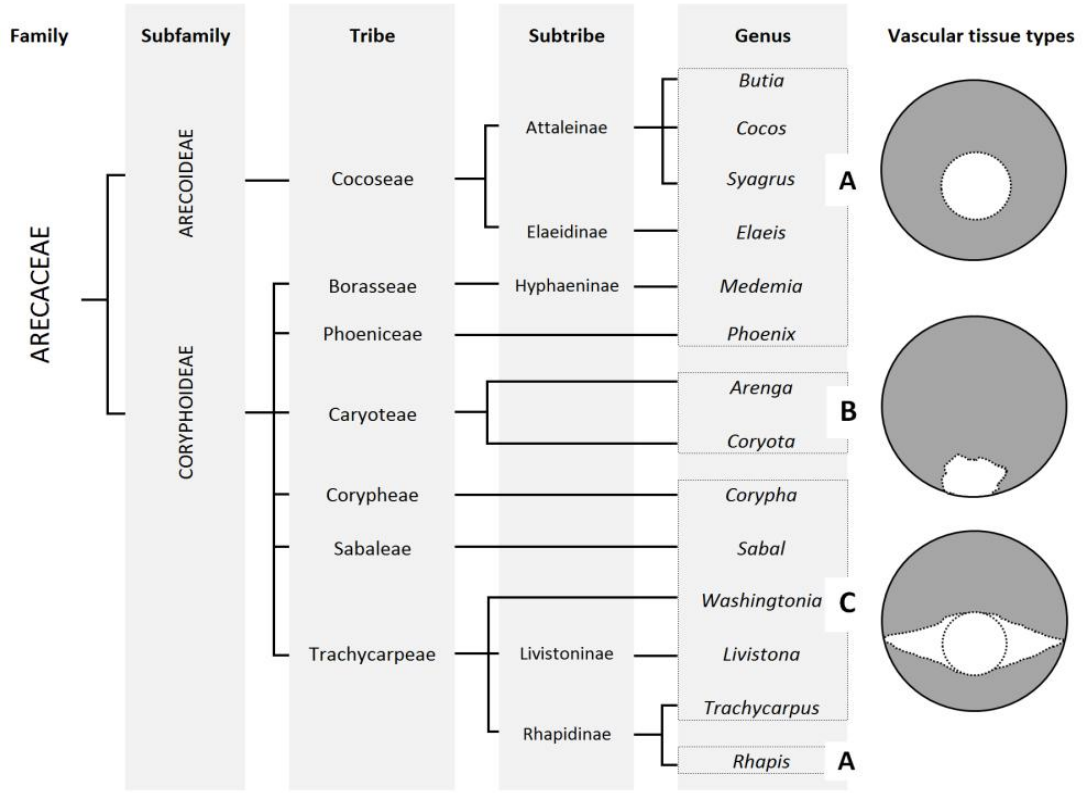

Figure 7.3 A diagram to show the phylogenetic classification of 14 genera in palm family (ARECACEAE), redrawn from Dransfield *et al*. (2008) and Tomlinson *et al*. (2011). A,B,C indicate three types of vascular tissues in fibrovascular bundles among 18 different palm species, where the grey area is occupied by sclerenchyma fibers and the white area by a vascular tissue.

These 3 types of fibrovascular bundles also showed close correlation with the phylogenetic classification of palm species (Fig. 7.3). The fibrovascular bundles from the tribes Cocoseae, Borasseae, and Phoeniceae were classified as type A, and those from the tribe Caryoteae were classified as Type B. With the exception of *R. excelsa*, the fibrovascular bundles from the tribes Trachycarpeae, Coryoheae, and Sabaleae were classified as type C. In general, the anatomical differences between different palm species within a genus are quantitative or so small as to be obscured by the variation exhibited by a single individual (Tomlinson 1961, 1964). The observations presented here provide the first account showing correlation between the current phylogenetic classification and the shape and localization of vascular tissues within different palm species, which might provide a method of identifying palm fibrovascular bundles.

Similar research has been done by Grosser and Liese (1971) for 52 bamboo species from 14 genera. It was found that according to the presence and location of fiber strands in one vascular bundle, one can distinguish different types of vascular bundles within bamboo culm. Together with our present results, these imply that anatomical characteristics beside morphological features may help for the classification of bamboo and palm genera into natural systematic units. Considering the large number of palm species that occur worldwide, the anatomical features of vascular tissue of fibrovascular bundles in other palms are worthy of investigation in future research.

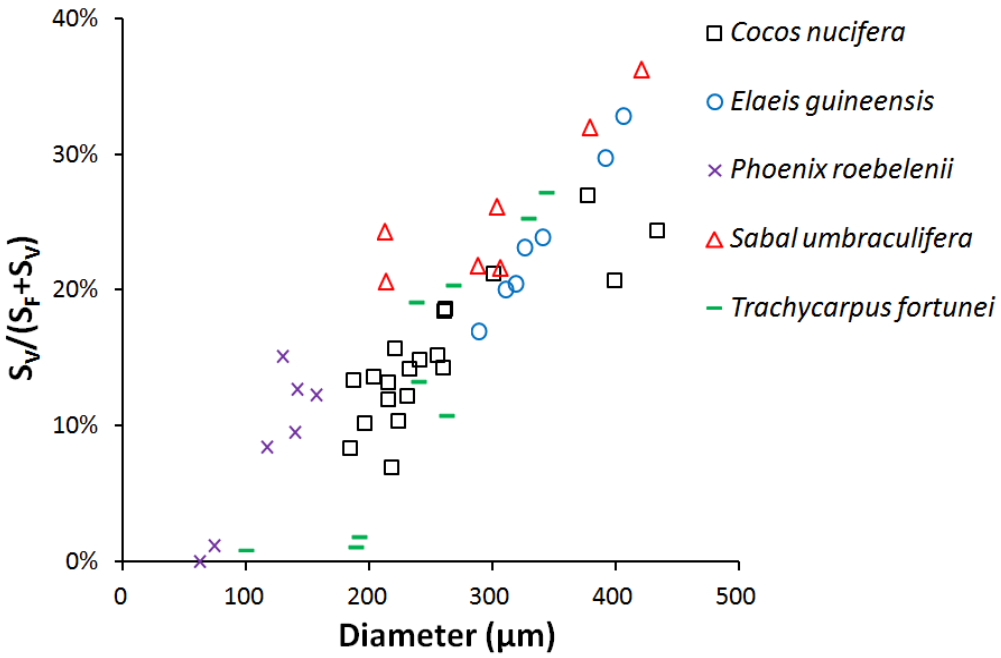

Figure 7.4 The ratio of vascular tissue area to whole transverse sectional area (= S_V/ S_F+S_V) against diameter of fibrovascular bundles from five palm species.

A remarkable feature of the palm species examined here is that the ratio of vascular tissue area to entire transverse sectional area increased markedly with increasing diameter of fibrovascular bundles. Figure 7.4 shows examples of the dynamic correlation in 5 palm species. This anatomical feature also has a strong correlation with the mechanical properties of fibrovascular bundles, as will be described in section 7.5.

Table 7.1 Fiber dimensions* and the derived values among different palm species ($P < 0.05$).

Species	Fiber length (mm)	Fiber diameter (µm)	Cell wall thickness (µm)	Slenderness ratio	Flexibility coefficient	Runkel ratio
Butia capitata	1.53 (±0.28)	11.7 (±1.8)	3.2 (±0.5)	132.8	45.0	1.28
Cocos nucifera	1.05 (±0.29)	16.7 (±3.2)	3.4 (±0.9)	63.7	59.2	0.73
Syagrus romanzoffiana	1.18 (±0.36)	16.2 (±2.7)	3.6 (±0.7)	72.8	54.8	0.87
Elaeis guineensis	0.95 (±0.26)	15.1 (±1.9)	3.2 (±0.5)	63.8	58.7	0.72
Medemia nobilis	0.92(±0.28)	13.5 (±1.7)	2.5 (±0.5)	69.7	63.1	0.62
Phoenix dactylifera	1.28 (±0.29)	17.0 (±3.3)	4.0 (±0.7)	77.9	52.4	0.96
Phoenix roebelenii	0.66 (±0.18)	11.6 (±1.5)	2.2 (±0.4)	57.9	61.2	0.66
Arenga engleri	1.66 (±0.24)	15.6 (±1.9)	4.2 (±0.5)	107.7	45.9	1.21
Arenga sp.	1.85 (±0.20)	13.8 (±1.6)	4.2 (±0.9)	136.3	39.5	1.72
Caryota maxima	1.12 (±0.30)	16.9 (±3.3)	3.8 (±1.6)	69.1	54.7	0.80
Caryota monostachya	1.76 (±0.48)	20.4 (±4.5)	4.0 (±1.0)	88.6	56.9	0.73
Caryota urens	1.45 (±0.24)	16.9 (±2.5)	4.4 (±0.8)	87.3	48.0	1.12
Corypha umbraculifera	1.11 (±0.32)	15.8 (±2.4)	2.3 (±0.7)	72.1	70.7	0.43
Sabal umbraculifera	0.89 (±0.27)	14.6 (±1.3)	2.5 (±0.4)	62.1	65.2	0.54
Washingtonia filifera	1.43 (±0.31)	14.9 (±3.3)	3.4 (±0.5)	98.5	53.4	0.91
Livistona chinensis	0.76 (±0.14)	15.5 (±1.7)	2.1 (±0.4)	49.7	72.3	0.39
Rhapis excelsa	0.74 (±0.14)	13.6 (±2.2)	3.2 (±0.5)	55.6	53.0	0.92

*Data are represented as mean and ± SD of 30 replications for each species.

Table 7.2 Mechanical properties[*], MFAs and Klason lignin contents of fibrovascular bundles from different palm species ($P < 0.05$).

Species	Diameter (µm)	Tensile strength (MPa)	Young's modulus (GPa)	BRK. Strain (%)	MFA (°)	Kalson lignin (%)
Butia capitata	228 (±42)	170 (±63)	2.5 (±1.6)	11 (±7)	17.6 (±3.9)	18.7 (±0.8)
Cocos nucifera	260 (±57)	63 (±32)	1.8 (±0.7)	9 (±6)	29.3 (±1.5)	25.6 (±1.1)
Syagrus romanzoffiana	466 (±79)	134 (±39)	1.3 (±0.8)	25 (±16)	13.4 (±1.8)	33.0 (±0.6)
Elaeis guineensis	269 (±42)	228 (±74)	2.2 (±1.1)	17 (±5)	21.1 (±13.1)	26.2 (±2.0)
Medemia nobilis	236 (±60)	83 (±31)	1.7 (±0.7)	24 (±12)	29.7 (±3.5)	34.7 (±2.2)[**]
Phoenix dactylifera	473 (±125)	147 (±76)	1.5 (±1.0)	25 (±15)	15.6	18.3 (±1.3)
Phoenix roebelenii	147 (±39)	162(±52)	2.1 (±0.9)	21 (±8)	23.5 (±1.4)	33.0 (±0.3)[**]
Arenga engleri	259 (±57)	202 (±78)	2.9 (±1.7)	13 (±8)	10.3 (±1.4)	29.6 (±3.2)
Arenga sp.	276 (±66)	76 (±27)	1.7 (±0.6)	8 (±4)	21.0 (±12.8)	37.8 (±0.7)
Caryota maxima	202 (±65)	128 (±48)	2.3 (±1.5)	40 (±25)	30.1 (±3.3)	38.2 (±0.3) [**]
Caryota monostachya	262 (±90)	99 (±38)	1.2 (±0.6)	40 (±17)	47.1 (±6.6)	34.8 (±0.3)
Caryota urens	402 (±94)	78 (±26)	1.2 (±0.6)	62 (±23)	34.8 (±2.2)	28.1 (±2.6)
Corypha umbraculifera	323 (±37)	57 (±29)	1.2 (±0.5)	10 (±6)	28.1 (±2.6)	30.4 (±1.9)[**]
Sabal umbraculifera	308 (±87)	111 (±36)	2.3 (±1.3)	13 (±8)	20.7 (±5.9)	25.8 (±0.7)
Washingtonia filifera	214 (±38)	170 (±58)	1.7 (±0.7)	21 (±7)	22.9 (±3.5)	35.2 (±0.9)
Livistona chinensis	250 (±63)	-	-	-	24.2 (±2.6)	31.6 (±0.8)
Rhapis excelsa	144 (±17)	109 (±36)	2.9 (±0.9)	11 (±4)	29.5 (±4.2)	33.9 (±1.0)

[*] Data of mechanical properties are represented as mean and ± SD of 30 replications for each species.

[**] The Klason lignin contents of these palm species include ash contents. These data were not used for discussion.

7.3 Anatomical characteristics of fibers in palm fibrovascular bundles

The large and intermediate fibrovascular bundles, namely type I and type II in Tomlinson's classification (1964), always have a large fiber strands with distinct vascular tissue area among different palm species. While, the fibrovascular bundles with small diameter, namely type III in Tomlinson's classification, are almost completely composed of fibers. Usually, the fibers of fibrovascular bundles in each palm species have similar characteristics in fiber length, diameter and cell-wall thickness (Table 7.1). However, a specific feature observed in 3 species of *Caryota* and in *P. dactylifera* was that the safranin staining in sclerenchyma fibers was uneven, as indicated by the white and black dotted circles in Figure 7.2. This feature could be caused by differences in cell-wall thickness. Examining the data listed in Table 7.1, the standard deviation of cell-wall thickness in *Caryota* fibers was approximately ± 1 μm, suggesting that the difference in color staining of fibrovascular bundles was affected by cell-wall thickness. The thin-walled fibers usually appeared at the central region of fibrovascular bundles; the presence of thin-walled fibers may decrease the mechanical strength of the fibrovascular bundles.

Furthermore, the anatomical characteristics of the sclerenchyma fibers from different palm fibrovascular bundles were surveyed using a maceration method. The length, diameter, and cell-wall thickness of fibers from the palm species are presented in Table 7.1. Fiber lengths varied from 0.66 to 1.85 mm. Fibers in the genera *Arenga* and *Caryota* were longer than those of other palm species, with an average value of 1.57 mm. The average fiber length of *P. roebelenii* and *T. fortune*i was < 0.7 mm, much shorter than that of the other palm species. Table 7.1 also shows the derived values (pulp-quality indices) of fibers from different palm species. Generally, it is essential in pulping and papermaking that slenderness ratio of fibers is more than 33 and/or Runkel ratio is low (<1) (Xu *et al*. 2006). Almost all palm species listed in Table 7.1 show acceptable value. On the basis of the flexibility coefficient, fibers of conifer and broad-leaved trees are classified into 4 groups: 1, highly elastic (>75); 2, elastic (50–75); 3, rigid (30–50); and 4, highly rigid (<30) (Bektas *et al*. 1999; Kiaei 2011).

The flexibility coefficients in *Arenga* spp. and *B. capitata* were <50; these fibers can be considered as rigid. The flexibility coefficients of the fibers from the other 15 palm specimens ranged between 50 and 75; these fibers are considered elastic.

7.4 Microfibril angles and Klason lignin contents

The MFAs of fibrovascular bundles among the palm species, as analyzed by X-ray diffraction, varied from 10.3º to 47.1º (mean = 25.4º) (Table 7.2). The MFAs of palm fibers were larger than those reported for other non-woody plant fibers including flax (*Linum* sp., 11º), jute (*Corchorus* sp., 8.1º), sisal (*Agave sisalana*, 10–22º), pine apple (*Anannus comosus*, 8–14º), and banana (*Musa sepientum*, 11º) (Satyanarayana *et al*. 1982; Baley 2002). The MFAs of palm species were also larger than those reported for wood fibers and tracheids (El-Osta *et al*. 1973; Yamamoto *et al*. 1993; Lichtenegger *et al*. 1999; Bonham & Barnett 2001).

The Klason lignin contents of fibrovascular bundles from the different palm species ranged from 18.38% to 37.8%, with a mean value of 29.6% (Table 7.2). These values are much higher than those reported for other non-woody plants, including flax (2.0%), jute (15.9%), sisal (12%), and banana (12%) (Baley 2002; Razera & Forllini 2003; Cordeiro *et al*. 2004; Megiatto *et al*. 2007). Lignin contents of the palm species were similar to those reported for conifers, including noble fir (*Abies procera*, 29.3%), western white pine (*Pinus monoticola*, 19.3%), and Douglas fir (*Pseudotsuga menziesii*, 27.2%). Palm fibrovascular bundles had relatively high lignin content compared to those reported for broad-leaved trees, including yellow birch (*Betula alleghaniensis*, 22.7%), quaking aspen (*Populus tremuloides*, 19.3%), and basswood (*Tilia Americana*, 20.0%)(Panshin *et al*. 1964).

7.5 Mechanical properties of palm fibrovascular bundles

Typical stress-strain (S-S) curves of fibrovascular bundles among the palm species are shown in Figure 7.5. The S-S curves varied among the species and showed a yield, followed by long-term plastic deformation until breakage from 8% to 62% strain. Specially, the species from *Caryota* genus showed much larger break strain than other species. These data (Fig. 7.5) indicate that palm fibrovascular bundles are strong and

tough, i.e., they could show passive elongation before breakage, and the long-term plastic deformation allows them to dissipate energy.

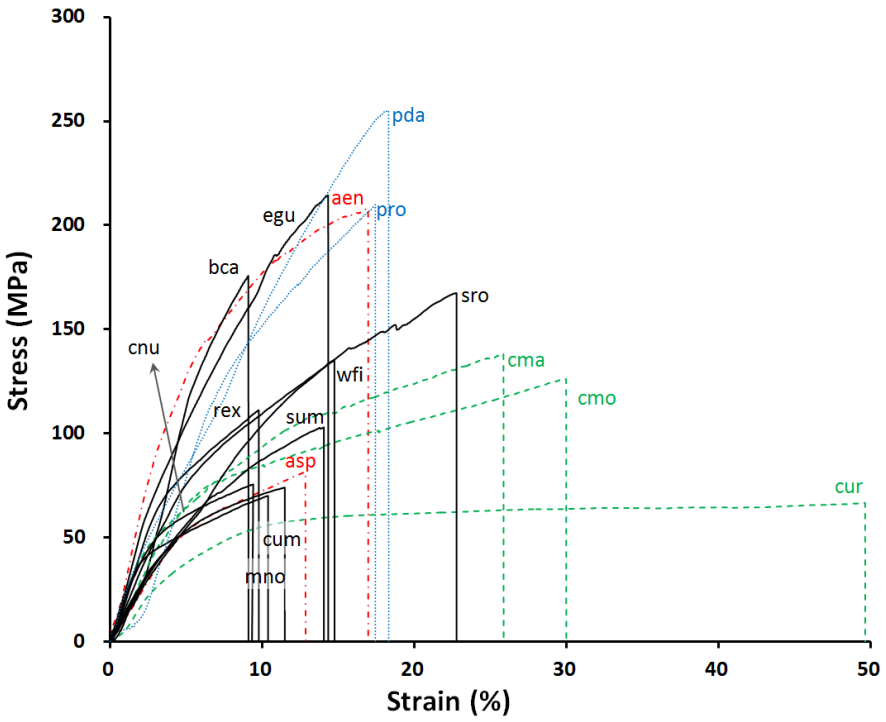

Figure 7.5 Typical stress-strain curves of fibrovascular bundles of different palm species, obtained at a crosshead speed of 1mm min^{-1} and using a gauge length of 10mm. Dash-dot line, dash line and dot line show stress-strain curves of species from *Arenga* (*aen*, *asp*), *Caryota* (*cma*, *cmo*, *cur*) and *Phoenix* (*pda*, *pro*) genus, respectively. Other species are in solid line..

Table 7.2 shows the mechanical properties of fibrovascular bundles of the various palm species. The tensile strengths of palm fibrovascular bundles were lower than those of other non-woody plants, including flax (1339 MPa), jute (466 MPa), seagrass (573 MPa), sisal (568–640 MPa), and cotton (287–597 MPa) (Satyanarayana *et al*. 1982; Baley 2002; Razera & Forllini 2003; Davies *et al*. 2007; Müsig 2010), but were higher than those of pine (40 MPa) and rubberwood (15 MPa) (Munawar *et al*. 2007). In addition, the breakage strain of palm fibrovascular bundles showed much higher values than those of non-woody plants, including flax (3.3%), jute (8.1%), seagrass (3.4%), sisal (3–7%), and banana (1.0–3.5%) (Satyanarayana *et al*. 1982; Baley 2002), also as shown in Figure 7.6 a.

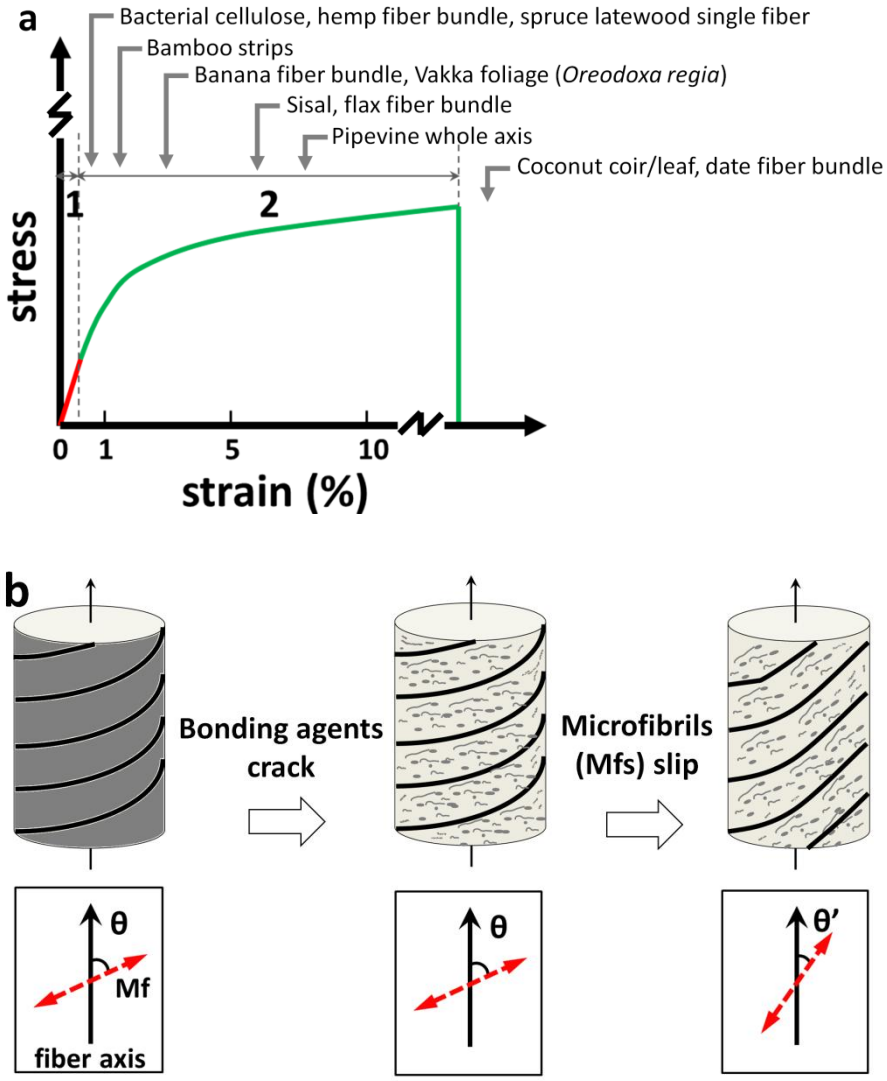

Figure 7.6 Illustration of elastic and plastic deformation behavior. **(a)** S-S curve shows elastic deformation region (1) and plastic deformation region (2) of different biomass materials. **(b)** Cell wall structural change during elastic and plastic deformation behavior.

The high lignin contents in combination with large MFAs account for the relatively low tensile strength, limited elastic deformation, and long-term plastic deformation of palm fibrovascular bundles. As illustrated in Figure 7.6 b, the bonding agents of cell wall, such as hemicellulose and lignin, firstly crack during tensile stress applying. Then, the microfibrils with large incline angle slip to each other. This will lead to a decrease to microfibril angle. In this case, the microfibril could maintain a higher stress because of less microfibril angle. Finally, the cellulose chains in microfibrils with large

deformation will break. The breakage also will lead to the whole fiber fracture. However, before break and during microfibrils slip to each other, the whole fiber cell wall systems absorb a lot of energy. This is the reason why palm fiber strong and though.

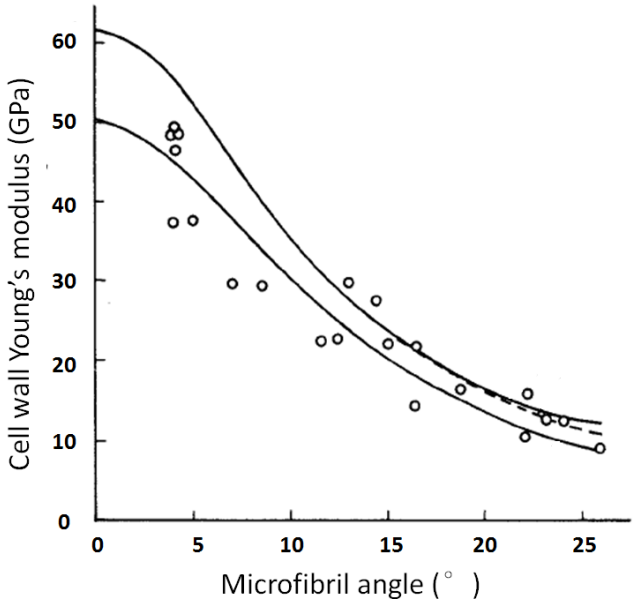

Figure 7.7 Relationships between cell wall Young's modulus and microfbril angle, modified from Norimoto *et al*. (1986).

Young's moduli in Table 7.2 of all palm fibrovascular bundles were lower than those of flax (58 GPa), jute (26.5 GPa), seagrass (19.8 GPa), and oak (11 GPa) (Satyanarayana *et al*. 1982; Baley 2002; Davies *et al*. 2007; Munawar *et al*. 2007). According to Norimoto *et al*. (1986), the specific dynamic Young's modulus depended remarkably on microfibril angle in S_2 layer of Hinoki wood (*Chamaecyparis obtusa*), but slightly on other factors (Fig. 7.7). In case the microfibril angle is around 30 to 40 degree, the cell wall Young's modulus tends to be 6 to 8 GPa according to Figure 7.7. By the following equation, we could speculate the tensile test result of fibers with 30 to 40 degree of microfibril angles.

$$E_{\text{palm fiber}} = E_{\text{cell wall of tracheid}} \times \rho_{\text{palm fiber density}} / \rho_{\text{conifer tracheid density}}$$

Which, $E_{\text{cell wall of tracheid}}$ is assumed around 6 to 8 GPa, $\rho_{\text{conifer tracheid density}}$ is around 1.46 to 1.47 g/cm^3, and $\rho_{\text{palm fiber density}}$ is around 0.22 to 0.62 g/cm^3 among different

species.

By this equation, the calculated Young's moduls of palm fibers, $E_{\text{palm fiber}}$, would be around 1 to 3 GPa, which showed a good agreement of the experimental results (Table 7.2).

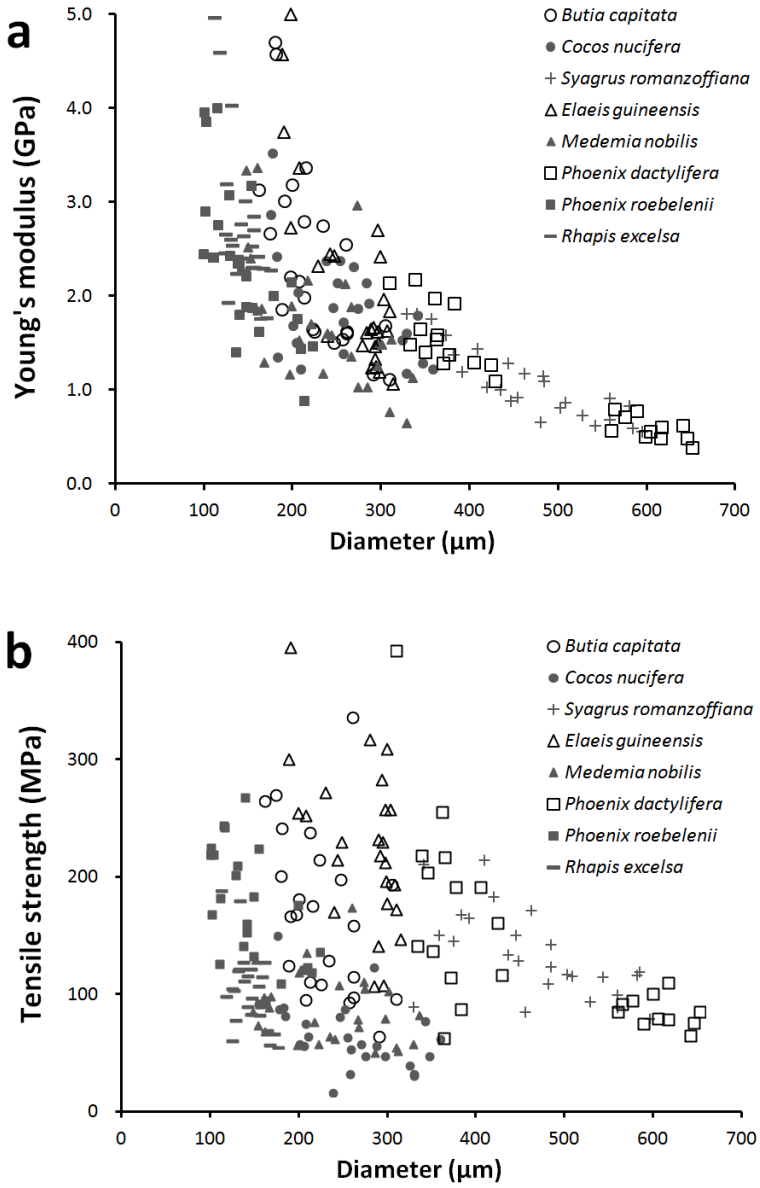

Figure 7.8 Relationships between diameter and mechanical properties for the fibrovascular bundles from different palm species. **(a)** Tensile strength plotted as a function of diameter in palm fibrovascular bundles. **(b)** Young's modulus plotted as a function of diameter in palm fibrovascular bundles.

It was noted that the diameter of fibrovascular bundles influenced the tensile strength and Young's modulus for all palm species. The general relationships between diameter and mechanical properties of fibrovascular bundles from 8 selected palm species are illustrated in Figure 7.8. It was striking phenomenon that as diameter increased, tensile strength and Young's modulus decreased. A similar phenomenon was found in fiber bundles from flax (Baley 2002), ramie, abaca leaf, and pineapple leaf (Munawar *et al*. 2007). Unfortunately, any reasonable explanation on this phenomenon has not been given by any papers. This phenomenon cannot be easily explained, because if the characteristics of fiber bundles are the same, the mechanical properties of fiber bundles of different diameters should also be the same. Our previous publication pointed out that the thick-walled sclerenchyma fibers predominantly contribute to the mechanical properties of fibrovascular bundles in windmill palm, while vascular tissues tend to reduce mechanical strength (Zhai *et al*. 2012). Considering the similar structural and mechanical properties of the individual fiber cells in a fibrovascular bundle, the ratio of vascular tissue to the entire transverse sectional area (sclerenchyma + vascular tissue) would be a key factor affecting mechanical properties of the fibrovascular bundles in palm species. In the present research, it was noted that this ratio increased markedly with increasing diameter of fibrovascular bundles (Fig. 7.4), indicating that the percentage of sclerenchyma fibers that affected mechanical properties decreased. These results demonstrated that the larger the diameter of fibrovascular bundles, the lower the mechanical strength, in all of the palm species examined.

7.6 Summary

This study on the anatomical characteristics of fibrovascular bundles from different palm species showed 3 types of fibrovascular bundles, based on the shape and localization of vascular tissues. These 3 types of fibrovascular bundles showed correlation with the phylogenetic classification of palm species.

The correlation between diameter and mechanical properties of fibrovascular bundles was further confirmed in all examined species. By observing the area occupied by sclerenchyma fibers and vascular tissue, it is noted that the proportion of the

transverse sectional area composed of vascular tissue increased markedly with increasing diameter of palm fibrovascular bundles. These findings explain why tensile strength and Young's modulus decreased with increasing diameter of fibrovascular bundles.

The large MFAs of palm fibers in combination with high lignin contents, result in limited elastic deformation, long-term plastic deformation, and relatively low tensile strength of palm fibrovascular bundles. However, it is difficult to find the major factors that contributed to the mechanical properties of palm fibrovascular bundles among different species. The mechanical properties are effected by fiber dimensions (fiber length, fiber diameter and cell wall thickness), vascular tissue area, fibrovascular bundle's diameter, MFAs, lignin contents, etc. among different palm species.

7.7 References

Anupam, S. (2002) Palm leaf manuscripts of the world: material, technology and conservation. Studies in Conservation. Suppl.1, 15-24. Maney Publishing.

Ashton, P.M.S., Gamage, S., Gunatilleke, I.A.U.N., Gunatilleke, C.V.S. (1998) Using Caribbean pine to establish a mixed plantation: testing effects of pine canopy removal on plantings of rain forest tree species. Forest Ecol. Manag. 106: 211-222.

Baley, C. (2002) Analysis of the flax fibres tensile behaviour and analysis of the tensile stiffness increase. Compos. Part A. 33: 939-948.

Bektas, I., Tutus, A., Eroglu, H. (1999) A study of the suitability of Calabrian pine (*Pinus brutiaten*) for pulp and paper manufacture. Turkish J. Agric. Forest. 23: 589-599.

Bonham, V.A., Barnett, J.R. (2001) Fibre length and microfibril angle in silver birch (*Betula pendula* Roth). Holzforschung. 55: 159-162.

Cordeiro, N., Belgacem, M.N., Torres, I.C., Moura, J.C.V.P. (2004) Chemical composition and pulping of banana pseudo-stems. Ind. Crop Prod. 19: 147-154.

Davies, P., Morvan, C., Sire, O., Baley, C. (2007) Structure and properties of fibres from sea-grass (*Zostera marina*). J Mater. Sci. Vol. 42(13): 4850-4857.

de Zoysa, N.D. (1992) Tapping patterns of the Kitul palm (*Caryota urens*) in the

Sinharaja area Sri Lanka. Principes. 36(1): 28-33.

Dhawan, S. (1995) Essential oil for prevention of mould growth on palm leaf manuscripts. In: Proceeding of the Third International Conference on Biodeterioration of Cultural Property. The Conservation Science Division, The Fine Arts Department, Bangkok, pp. 272-282.

Dransfield, J., Uhl, N.W., Asmussen, C.B., Baker, W.J., Harley, M.M., Lewis, C.E. (2008) Genera Palmarum. The evolution and classification of palms. Kew Publishing, Royal Botanic Gardens, Kew, UK.

El-Osta, M.L., Kellogg, R.M., Foschi, R.O., Butters, R.G. (1973) A direct X-ray technique for measuring microfibril angle. Wood and Fiber. 5: 118-128.

Grosser, D., Liese, W. (1971) On the anatomy of Asian bamboos, with special reference to their vascular bundles. Wood Sci. Technol. 5: 290-312.

Khalil, H.P.S.A., Azura, M.N., Issam, A.M., Said, M.R., Adawi, T.O.M. (2008) Oil palm empty fruit bunches (OPEFB) reinforced in new unsaturated polyester composites. J Reinf. Plast. Compos. 27(16-17): 1817-1826.

Kiaei, M. (2011) Basic density and fiber biometry properties of hornbeam wood in three different altitudes at age 12. Middle-east J. Sci. Res. 8: 663-668.

Law, K.N., Daud, W.R.W., Ghazali, A. (2007) Morphological and chemical nature of fiber stands of oil palm empty-fruit bunch (OPEFB). BioResources 2(3): 351-362.

Li, S. (2008) Bencao gangmu (1578) – compendium of materia medica. Science and Technology Publishing, Shanghai (in Chinese).

Lichtenegger, H., Retterer, A., Stanzl-Tschegg, S., Fratzl, P. (1999) Variation of cellulose microfibril angles in softwoods and hardwoods – a possible strategy of mechanical optimization. J. Struct. Biol. 128: 257-269.

Megiatto, J., Hoareau, W., Gardrat, C., Frollini, E., Castellan, A. (2007) Sisal fibers: Surface chemical modification using reagent obtained from a renewable source; characterization of hemicellulose and lignin as model study. J. Agric. Food Chem. 55: 8576-8584.

Morcote-Ríos, G., Bernal, R. (2001) Remains of palms (Palmae) at archaeological sites in the New World: A review. Bot. Rev. 67(3): 309-350.

Munawar, S.S., Umemura, K., Kawai, S. (2007) Characterization of the morphological, physical, and mechanical properties of seven nonwood plant fiber bundles. J. Wood Sci. 53: 108-113.

Müsig, J. (2010) Industrial applications of natural fibers: Structure, properties and technical applications. John Wiley & Sonsm Ltd. United Kingdom.

Norimoto, M., Tanaka, F., Ohogama, T., Ikimune, R. (1986) Specific dynamic Young's modulus and internal friction of wood in the longitudinal direction. Wood Res. 22: 53-65.

Panshin, A.J., de Zeeuw, C., Brown, H.P. (1964) Textbook of wood technology. Volume I – Structure, identification, uses, and properties of the commercial woods of the United States (2nd edition). McGraw-Hill, Inc. USA.

Pei, S., Chen, S., Tong, S. (1991) Tomun 13(1): Angiospermae-Monocotyledoneae, Palme, Flora of Reipublicae Popularis Sinicae. Science Press, Beijing. [In Chinese]

Ratnayake, P.D.K.C., Gunatilleke, C.V.S., Gunatilleke, I.A.U.N. (1990) *Caryota urens* L. (Palmae): An indigenous multiple purpose tree species in the wet lowlands of Sri Lanka. Regional Workshop on Multipurpose Tree Species, IFS/ Winrock Int., Los Banos, Philippines.

Razera, I.A.T., Forllini, E. (2003) Composites based on jute fibers and phenolic matrices: properties of fibers and composites. J. Appl. Polymer Sci. 91(2): 1077-1085.

Satyanarayana K.G., Pillai, C.K.S., Sukumaran, K., Pillai, S.G.K., Rohatgi, P.K., Kalyanivijayan. (1982) Structure property studies of fibres from various parts of the coconut tree. J. Mater. Sci. 17: 2453-2462.

Shinoj, S., Visvanathan, R., Panigrahi, S., Kochubabu, M. (2011) Oil palm fiber (OPF) and its composites: A review. Ind. Crop. Prod. 33: 7-22.

Swarnakamal, B. (1965) Conservation of palm-leaf manuscripts. Baroda Museum and Picture Gallery, Bull. 19: 59-65.

Tamunaidu, P., Saka, S. (2011) Chemical characterization of various parts of nipa palm (*Nypa fruticans*). Ind. Crop. Prod. 34: 1423-1428.

Tengberg, M. (2012) Beginnings and early history of date palm garden cultivation in the

Middle East. J. Arid Environ. 86: 139-147.

Thomas, R., De Franceshi, D. (2013) Palm stem anatomy and computer – aided identification: The Coryphoideae (ARECACEAE). Am. J. Bot. 100(2): 289-313.

Thomas, R., Tengberg, M., Moulhérat, C., Marcon, V., Besenval, R. (2012) Analysis of a protohistoric net from Shahi Yump, Baluchistan (Pakistan). Archaeol. Anthropol. Sci. 4: 15-23.

Tomlinson, P.B. (1961) Anatomy of the monocotyledons. Ⅱ. PALMAE. Oxford University Press, London.

Tomlinson, P.B. (1964) The vascular skeleton of coconut leaf base. Phytomorphology. 14: 218-230.

Tomlinson, P.B. (1990) The structural biology of palms. Clarendon Press, Oxford.

Tomlinson, P.B., Horn, J.W., Fisher, J.B. (2011) The anatomy of palms. Oxford University press, New York.

Xu, F., Zhong, X.C., Sun, R.C., Lu, Q. (2006) Anatomy, ultrastructure and lignin distribution in cell wall of *Caragana korshinskii*. Ind. Crop. Prod. 24: 186-193.

Yamamoto, H., Okuyama, T., Yoshida, M. (1993) Method of determining the mean microfibril angle of wood over a wide range by the improved Cave's method. Mokuzai Gakkaishi. 39: 375-381.

Zhai, S., Li, D., Pan, B., Sugiyama, J., Itoh, T. (2012) Tensile strength of windmill palm (*Trachycarpus fortunei*) fiber bundles and its structural impactions. J. Mater. Sci. 47: 949-959.

Zhai, S., Horikawa, Y., Imai, T., Sugiyama, J. (2013) Cell wall characterization of windmill palm (*Trachycarpus fortunei*) fibers and its functional implications. IAWA J. 34(1): 20-33.

Conclusion

The Palmae distributes worldwide and is one of the biggest groups together with bamboo and rattan among monocotyledon. Many palm species, for instance windmill palm, oil palm and coconut palm, are important plants for the daily life of human beings. In daily life, palm fibers have been widely used to make different products such as ropes with excellent durability/stability, *Tawashi* (a type of traditional-style brush used in Japan) and *Houki* (brooms). These fibers are from leaf sheath of palms.

According to the measurement, the height of leaf sheath almost had no change from top to bottom of the stem. The circumference length of leaf sheath was the same with circumference length of palm stem. The bottom part showed living tissue, while the top part a sheet or assembly of mature fiber bundles only. In between top and bottom, there was a transition area with light brown color where parenchyma tissues already died and still attached to vascular bundles loosely. When observing the vascular bundles embedded in the living tissue of leaf sheath closer, vascular bundles with crossed structure was visualized. The evidence was further confirmed by the microscopic observation of the longitudinal section parallel to a living tissue. It is noted that crossed structure of mature leaf sheath originated from it developmental stage. The transformation of chemical contents in leaf sheath along the axial direction including transition area was found by FTIR analysis. As fibers becoming matured and separated, the contents of cellulose and hemicellulose tended to decrease gradually, while lignin increased.

The cell wall structure of windmill palm fibers appeared different from that of common fibers/tracheids of hardwoods and softwoods, and even from bamboo and rattan. In case of the windmill palm fiber, the secondary wall comprises just two layers (outer and inner ones) with a crossed orientation of cellulose microfibrils in a single cell wall. The ratio of the S_1 to the whole cell wall thickness of the windmill palm fibers was much higher than that of fibers/tracheids in softwood and hardwood. The MFA of the S_1 layer of the windmill palm fibers was smaller and MFA of S_2 was larger compared to

that of normal wood fibers and tracheids. Further, the fibrovascular bundles of windmill palm showed a high lignin content. These evidences could help to explain the high durability and large elastic extension of windmill palm fibers. After investigating the cell wall structure of leaf fibers from 20 different palm species by light and electron microscopy, it was confirmed that the secondary wall consisted of only two layers, S_1 and S_2. The occurrence of S_3 layer claimed in fibers from leaf part of coconut palm and oil palm (Abdul Khalil *et al*., 2006, 2008) was not confirmed in leaf fibers of 18 palm species examined in the present investigation. Therefore, it was concluded that the two-layered structure of S_1 and S_2 was the unique and specific character in palm leaf fibers being different from other monocotyledons (such as bamboo and rattan) and wood.

Fibrovascular bundles taken from a mature windmill palm leaf sheath can be divided into three groups according to their size, orientation, and location in one sheet of leaf sheath: inner, middle, and outer layers. The diameter of fibrovascular bundles in the middle layer was the largest, while the diameter of those in the inner layer was the smallest. Tensile strength and Young's modulus showed a decreasing tendency with an increasing diameter of these fibrovascular bundles. S_V and S_F were measured by observing transmitted- and polarized-light photomicrographs of fibrovascular bundles from the three layers. The ratio of S_V versus transverse sectional area in the inner layer was just 6%, while that in the middle layer was 33%. These findings strongly suggest that the tensile strength of fibrovascular bundle increases in parallel with a decrease of S_V, while the presence of fibers predominantly contributes to mechanical strength. Therefore, the fibrovascular bundles in the inner layer were stronger that those in the middle layer.

The anatomical characteristics of fibrovascular bundles from 18 different palm species showed 3 types of fibrovascular bundles, based on the shape and localization of vascular tissues. These 3 types of fibrovascular bundles showed correlation with the phylogenetic classification of palm species. The correlation between diameter and mechanical properties of fibrovascular bundles was further confirmed in all 18 palm species. By observing the area occupied by sclerenchyma fibers and vascular tissue, it

was noted that the proportion of the transverse sectional area composed of vascular tissue increased markedly with increasing diameter of palm fibrovascular bundles. These findings explain why tensile strength and Young's modulus decreased with increasing diameter of fibrovascular bundles commonly to a number of palm species.

The large MFAs of palm fibers in combination with high lignin contents, result in limited elastic deformation, long-term plastic deformation, and relatively low tensile strength of palm fibrovascular bundles. However, it is difficult to find the major factors that contributed to the mechanical properties of palm fibrovascular bundles among different species. The mechanical properties are influenced by fiber dimensions (fiber length, fiber diameter and cell wall thickness), vascular tissue area, fibrovascular bundle's diameter, MFAs, lignin contents, etc. among different palm species.

Acknowledgments

This thesis represents a significant amount of work. It could not have been successfully completed without the help of many people.

I would sincerely like to thank my supervisor Professor Junji Sugiyama, for inspiring me with many ideas and information about my doctoral course. He helped me to set up my research outline and find my interests in scientific research. I really learned many from him. I am also deeply grateful to Professor Keiji Takabe and Professor Hiroyuki Yano, who gave me precise comments during thesis preparation.

I also want to thank Associate Professor Tomoya Imai, Assistant Professor Kei'ichi Baba and Suyako Tazuru for many valuable suggestions.

Dr. Yoshiki Horikawa helped me greatly on all of my research and taught me a lot of experimental techniques. Together with Dr. Misao Yokoyama and Rie Endo, their rigorous research attitude encouraged me. Specially thanks to them.

For all members in the Lab. Biomass Morphogenesis and Information and friends of me, they let me to enjoy these days in Kyoto, Japan. With their help in my life, I can carry out my research well and finish my doctoral course in three years.

I would like to thank Professor Shuichi Kawai, Kenji Umemura, Hiroyuki Yano, Kentaro Abe, Tuyoshi Yoshimura, Aya Yanagawa, Bunzo Mikami, Keiji Takabe and Arata Yoshinaga for helping me to carry out my experiments in their labs, Kyoto University.

My appreciation also extended to Professor Takao Itoh, Biao Pan and Dagang Li for my initial guidance to the scientific study and introduction to continue my PhD work in Kyoto University. Their guidance as well as kind suggestions always remind me to work hard in Japan.

I want to thank Kambayashi Scholarship Foundation for their generous financial support. With the research funding, I could focus on my experiments during these three years. And I also thank the G30 Program of Faculty of Agriculture, Kyoto University.

I also wish to thank my family, my grandparents, my parents and my relatives for

their love always being there with me. They are the most important mental support for me, no matter what kind people I will be. Their continual support and understanding has allowed me to pursue, explore and satisfy my various aspirations. Even from afar, they have been my constant source of strength to achieve my academic and personal goals.